FINITE ELEMENT ANALYSIS AND EXPERIMENTAL VALIDATION OF REINFORCED CONCRETE SINGLE-MAT SLABS SUBJECTED TO BLAST LOADS

A THESIS IN

Civil Engineering

Submitted to the Faculty of the University of
Missouri-Kansas City in partial fulfillment of
requirements for the degree of

MASTER OF SCIENCE

by

Akash Ashok Iwalekar

Bachelor of Civil Engineering (B.E.)

University of Mumbai – G. V. Acharya Institution of Technology

University of Missouri-Kansas City

2018

FINITE ELEMENT ANALYSIS AND EXPERIMENTAL VALIDATION OF REINFORCED CONCRETE SINGLE-MAT SLABS SUBJECTED TO BLAST LOADS

Akash Ashok Iwalekar, Candidate for the Master of Science Degree,

University of Missouri- Kansas City

ABSTRACT

The study carried out in this thesis is the investigation of the behavior of reinforced concrete slabs subjected to blast loading. A separate experimental study was performed involving twelve reinforced concrete (RC) slabs in a shock tube (Blast Load Simulator). Records from this experimental study were used for performing finite element analysis. Numerical simulation done in this research investigated the effect of using various bond-slip models in studying the behavior of these twelve RC slabs subjected to blast loading.

LS-DYNA®, a non-linear transient dynamic finite element analysis program, was used in this study. Finite element models for twelve slabs using the LS-DYNA® subjected to experimental blast loads were used to study the bond-slip behavior between steel reinforcing bars and concrete. High-strength concrete reinforced with high-strength steel slabs and normal-strength concrete reinforced with normal-strength steel slabs were the two material combinations used in this research. The primary objective of this study was the investigation of two bond interaction system between steel and concrete, available in LS-DYNA®, for the two material combinations under blast loading. The assumption of a perfect-bond between concrete and steel was the first bond interaction system studied, utilizing Constrained Lagrange in Solid Formulation. Beam bond

is another bond interaction system investigated using Beam in Solid formulation in the program. Furthermore, three functions were investigated in the beam bond interaction system along with the program generated beam bond function. Validation of these interaction systems, with experimental data, was the goal of the project.

Upon investigation of this research, comparison between results of the finite element analysis and the experimental validation of reinforced concrete single-mat slabs which were subjected to blast loading, assisted in the conclusion that the beam bond function proposed by Murcia-Delso Juan is the most consistent among all of the interaction systems. However, with slight modifications in the beam bond function proposed by Grassl, which is identical to the CEB-FIP model, gives the most accurate results for high strength materials in terms of peak deflection and residual deflection history. Most accurate prediction to experimental records in given by perfect bond formulation, and bond-slip fails to give accurate results for blast loading.

APPROVAL PAGE

The faculty listed below, appointed by the Dean of the School of Computing and Engineering, has examined the thesis titled "Finite Element Analysis and Experimental Validation of Reinforced Concrete Single-Mat Slabs Subjected to Blast Loads," presented by Akash Ashok Iwalekar, candidate for Master of Science in Civil Engineering, and certify, that in their opinion, it is worthy of acceptance.

Supervisory Committee

Thiagarajan Ganesh, Ph.D., P.E., Committee Chair
Department of Civil and Mechanical Engineering

Ceki Halmen, Ph.D., P.E.
Department of Civil and Mechanical Engineering

ZhiQiang Chen, Ph.D.
Department of Civil and Mechanical Engineering

TABLE OF CONTENTS

ABSTRACT……..iii

LIST OF ILLUSTRATIONS ix

LIST OF TABLES…….xv

CHAPTER 1. INTRODUCTION 1

1.1 An overview on Blast Effects on Structures 1

1.2 Significance of Studying Blast Effects on Reinforced Concrete Slabs 2

1.3 Proposed Solution 3

1.4 Thesis Organization 4

CHAPTER 2. LITERATURE SURVEY 6

CHAPTER 3. OBJECTIVE AND SCOPE 11

3.1 Problem Statement 11

3.2 Objectives 11

3.3 Tasks 12

CHAPTER 4. EXPERIMENTAL INVESTIGATION 15

4.1 Materials 16

4.2 Methods 18

4.3 Experimental Data 19

CHAPTER 5. NUMERICAL MODELING IN LS-DYNA® 20

5.1 Significance of Numerical Modeling in LS-DYNA® 20

5.2 Geometric Models 21

5.2.1 Meshing for Concrete Model 21

5.2.2 Meshing for Steel Model 23

5.2.3 Hourglass Control in LS-DYNA® 25

5.2.4 The Constrained Lagrange in Solid formulation 26

5.2.5 The Constrained Beam in Solid formulation 26
5.3 Boundary Conditions 30
5.4 Material Models in LS-DYNA® 31
5.4.1 The Concrete Damage Model Release 3 32
5.4.2 The Plastic Kinematic Model for Steel 36
5.5 Blast Load Application in LS-DYNA® 36
CHAPTER 6. NUMERICAL ANALUSIS RESULTS AND COMAPRISON WITH EXPERIMENTAL 38
6.1 Study NCOUP Parameter of Beam in Solid Formulation 39
6.1.1 NCOUP parametric study with JUAN function 39
6.1.2 NCOUP parametric study with CIB-FIP function 42
6.1.3 NCOUP parametric study with CIB-FIP-S3 function 46
6.2 High Strength Concrete with High Strength Steel Slabs (HSC-V) 49
6.2.1 Mesh size effect on Slab # 1 (HSC-V1-4in.) 50
6.2.2 Mesh size effect on Slab # 3 (HSC-V2-4in.) 52
6.2.3 Mesh size effect on Slab # 5 (HSC-V3-4in.) 54
6.2.4 Mesh size effect on Slab # 7 (HSC-V4-8in.) 56
6.2.5 Mesh size effect on Slab # 9 (HSC-V5-8in.) 58
6.2.6 Mesh Size Effect for Slab # 11 (HSC-V6-8in.) 61
6.3 Normal Strength Concrete with Normal Strength Steel Slabs (RSC-R) 62
6.3.1 Mesh size effect on Slab # 2 (RSC-R1-4in.) 63
6.3.2 Mesh Size Effect for Slab # 4 (RSC-R2-4in.) 65
6.3.3 Mesh Size Effect for Slab # 6 (RSC-R3-4in.) 67
6.3.4 Mesh Size Effect for Slab # 8 (RSC-R4-8in.) 70
6.3.5 Mesh Size Effect for Slab # 10 (RSC-R5-8in.) 72

6.3.6 Mesh Size Effect for Slab # 12 (RSC-R6-8in.) 74
CHAPTER 7. DISCUSSION OF RESULTS 77
7.1 High-Strength Concrete – Comparison of Model with 1 in. (25.4 mm.) Mesh to ½ in. (12.7 mm.) Mesh Model. 77
7.2 Normal-Strength Concrete – Comparison of Model with 1 in. (25.4 mm.) Mesh to ½ in. (12.7 mm.) Mesh Model. 79
7.3 Mesh Size Effects 82
CHAPTER 8. CONCLUSION AND FUTURE WORK 84
8.1 Future Scope of Work 85
APPENDIX A - PRESSURE AND IMPULSE DATA FOR 12 SLABS 86
APPENDIX B - PRESSURE AND IMPULSE PLOTS FOR 12 RC SLABS 87
APPENDIX C - SUMMARY TABLES 93
APPENDIX D – LS-DYNA INPUT 95
REFERENCES 107
VITA 111

LIST OF ILLUSTRATIONS

Figure 4.1-1: Single-mat reinforced concrete (rc) slab with 4 in. Type single layer reinforcement 17
Figure 4.1-2: Single-mat reinforced concrete (rc) slab with 8 in. Type single layer reinforcement 17
Figure 4.2-1: Blas load simulator (shock tube)..... 18
Figure 5.3-1: Single-mat reinforced concrete slab model with solid elements 1 in. (25.4 mm.) Mesh size 22
Figure 5.3-2: Single-mat reinforced concrete slab model with solid elements ½ in. (12.7 mm.) Mesh size 23
Figure 5.3-3: Single-mat reinforced concrete slab model with solid elements ¼ in. (6.35 mm.) Mesh size 23
Figure 5.3-4: Single layer reinforcement in 4 in. Type single-mat rc slab 25
Figure 5.3-5: Single layer reinforcement in 8 in. Type single-mat rc slab 25
Figure 5.4-1: Boundary conditions on the front and back face of slab..... 30
Figure 5.4-2: Boundary conditions on the top and bottom face of the slab..... 31
Figure 5.5-1: Pressure versus volumetric strain curve for equation of state form 8 with compaction for 11.6 ksi concrete..... 35
Figure 5.5-2: Pressure versus volumetric strain curve for equation of state form 8 with compaction for 5 ksi concrete..... 36
Figure 6.1-1: Deflection history of constrained beam-bond parameter with juan and cib-fip functions for cdr3 concrete model of 1 in. (24.4 mm.) Mesh model with constrained lagrange in solid and experimental deflection for slab#2-rsc-r1-4in. With boundary conditions of experiment setup. ..... **ERROR! BOOKMARK NOT DEFINED.**
Figure 6.1-2: Deflection history of constrained beam-bond parameter with juan and cib-fip functions for cdmr3 concrete material of 1 in. (24.4 mm.) Mesh model with constrained lagrange in solid and experimental deflection for slab#2-rsc-r1-4in. With all boundary conditions fixed..... **ERROR! BOOKMARK NOT DEFINED.**

Figure 6.2-1: Deflection comparison between ncoup parameter of constrained beam-bond parameter with juan function for cdr3 concrete model of 1 in. (24.4 mm.) Mesh model with experimental deflection for slab#4-rsc-r2-4in. 39
Figure 6.2-2: Deflection comparison between ncoup parameter of constrained beam-bond parameter with juan function for cdr3 concrete model of 1 in. (24.4 mm.) Mesh model with experimental deflection for slab#12-rsc-r2-8in. 40
Figure 6.2-3: Deflection comparison between ncoup parameter of beam-bond parameter with juan function for cdr3 concrete model of 1 in. (24.4 mm.) Mesh model with experimental deflection for slab#1-hsc-v2-4in. 41
Figure 6.2-4: Deflection comparison between ncoup parameter of constrained beam-bond parameter with juan function for cdr3 concrete model of 1 in. (24.4 mm.) Mesh model with experimental deflection for 41
Figure 6.2-5: Deflection comparison between ncoup parameter of constrained beam-bond parameter with ceb-fip function for cdr3 concrete model of 1 in. (24.4 mm.) Mesh model with experimental deflection for slab#12-rsc-r2-8in. 43
Figure 6.2-6: Deflection comparison between ncoup parameter of beam-bond parameter with cip-fip function for cdr3 concrete model of 1 in. (24.4 mm.) Mesh model with experimental deflection for slab#1-hsc-v2-4in. 44
Figure 6.2-7: Deflection comparison between ncoup parameter of constrained beam-bond parameter with ceb-fip function for cdr3 concrete model of 1 in. (24.4 mm.) Mesh model with experimental deflection forslab#11-hsc-v6-4in. 45
Figure 6.2-8: Deflection comparison between ncoup parameter of constrained beam-bond parameter with ceb-fip-s3 function for cdr3 concrete model of 1 in. (24.4 mm.) Mesh model with experimental deflection for slab#4-rsc-r2-4in. 46
Figure 6.2-9: Deflection comparison between ncoup parameter of constrained beam-bond parameter with ceb-fip-s3 function for cdr3 concrete model of 1 in. (24.4 mm.) Mesh model with experimental deflection for slab#12-rsc-r2-8in. 47
Figure 6.2-10: Deflection comparison between ncoup parameter of beam-bond parameter with cip-fip-s3 function for cdr3 concrete model of 1 in. (24.4 mm.) Mesh model with experimental deflection for slab#1-hsc-v2-4in. 48

Figure 6.2-11: Deflection comparison between ncoup parameter of constrained beam-bond parameter with ceb-fip-s3 function for cdr3 concrete model of 1 in. (24.4 mm.) Mesh model with experimental deflection forslab#11-hsc-v6-4in. 49
Figure 6.3-1 : Deflection comparison between 1 in. (25.4 mm.) And 0.5 in. (12.7 mm.) For constrained lagrange and beam in solid with no defined function and juan function with experimental deflection for slab#1– hsc-v1-4in. 50
Figure 6.3-2: Deflection comparison between 1 in. (25.4 mm.) And 0.5 in. (12.7 mm.) For ceb-fip and ceb-fip-s3 functions and experimental deflection for slab#1– hsc-v1-4in. 51
Figure 6.3-3: Deflection comparison between 1 in. (25.4 mm.) And 0.5 in. (12.7 mm.) For constrained lagrange and beam in solid with no defined function and juan function with experimental deflection for slab#3– hsc-v2-4in. 52
Figure 6.3-4: Deflection comparison between 1 in. (25.4 mm.) And 0.5 in. (12.7 mm.) For ceb-fip and ceb-fip-s3 functions and experimental deflection for slab#3– hsc-v2-4in. 53
Figure 6.3-5: Deflection comparison between 1 in. (25.4 mm.) And 0.5 in. (12.7 mm.) For constrained lagrange and beam in solid with no defined function and juan function with experimental deflection for slab#5– hsc-v3-4in. 54
Figure 6.3-6: Deflection comparison between 1 in. (25.4 mm.) And 0.5 in. (12.7 mm.) For ceb-fip and ceb-fip-s3 functions and experimental deflection for slab#5– hsc-v3-4in. 55
Figure 6.3-7: Deflection comparison between slab#1 vs. Slab#5 for ceb-fip and ceb-fip-s3 functions and experimental deflection for 1in. (25.4 mm) mesh size. 56
Figure 6.3-8: Deflection comparison between 1 in. (25.4 mm.) And 0.5 in. (12.7 mm.) For constrained lagrange and beam in solid with no defined function and juan function with experimental deflection for slab#7– hsc-v4-8in. 57
Figure 6.3-9: Deflection comparison between 1 in. (25.4 mm.) And 0.5 in. (12.7 mm.) For ceb-fip and ceb-fip-s3 functions and experimental deflection for slab#7– hsc-v4-8in. 57
Figure 6.3-10: Deflection comparison between 1 in. (25.4 mm.) And 0.5 in. (12.7 mm.) For constrained lagrange and beam in solid with no defined function and juan function with experimental deflection for slab#9– hsc-v5-8in. 58
Figure 6.3-11: Deflection comparison between 1 in. (25.4 mm.) And 0.5 in. (12.7 mm.) For ceb-fip and ceb-fip-s3 functions and experimental deflection for slab#9– hsc-v5-8in. 59

Figure 6.3-12: Deflection comparison between slab#7 vs. Slab#9 for ceb-fip and ceb-fip-s3 functions and experimental deflection for 1in. (25.4 mm) mesh size. 60
Figure 6.3-13: Deflection comparison between 1 in. (25.4 mm.) And 0.5 in. (12.7 mm.) For constrained lagrange and beam in solid with no defined function and juan function with experimental deflection for slab#11– hsc-v6-8in. 61
Figure 6.3-14: Deflection comparison between 1 in. (25.4 mm.) And 0.5 in. (12.7 mm.) For ceb-fip and ceb-fip-s3 functions and experimental deflection for slab#11– hsc-v6-8in. 62
Figure 6.4-1: Deflection comparison between 1 in. (25.4 mm.) And 0.5 in. (12.7 mm.) For constrained lagrange and beam in solid with no defined function and juan function with experimental deflection for slab#2– rsc-r1-4in. 63
Figure 6.4-2: Deflection comparison between 1 in. (25.4 mm.) And 0.5 in. (12.7 mm.) For ceb-fip and ceb-fip-s3 functions and experimental deflection for slab#1– rsc-r1-4in. 64
Figure 6.4-3: Deflection comparison between 1 in. (25.4 mm.) And 0.5 in. (12.7 mm.) For constrained lagrange and beam in solid with no defined function and juan function with experimental deflection for slab#4– rsc-r2-4in. 65
Figure 6.4-4: Deflection comparison between 1 in. (25.4 mm.) And 0.5 in. (12.7 mm.) For ceb-fip and ceb-fip-s3 functions and experimental deflection for slab#4– rsc-r2-4in. 66
Figure 6.4-5: Deflection comparison between 1 in. (25.4 mm.) And 0.5 in. (12.7 mm.) For constrained lagrange and beam in solid with no defined function and juan function with experimental deflection for slab#6– rsc-r3-4in. 67
Figure 6.4-6: Deflection comparison between 1 in. (25.4 mm.) And 0.5 in. (12.7 mm.) For ceb-fip and ceb-fip-s3 functions and experimental deflection for slab#6– rsc-r3-4in. 68
Figure 6.4-7:Deflection comparison between slab#2 vs. Slab#4 vs. Slab#6 for constrained lagrange and beam in solid with no defined function and juan function with experimental deflection for0.5 in. (12.7 mm.) Mesh size. 69
Figure 6.4-8 : Deflection comparison between 1 in. (25.4 mm.) And 0.5 in. (12.7 mm.) For constrained lagrange and beam in solid with no defined function and juan function with experimental deflection for slab#8– rsc-r4-8in. 70
Figure 6.4-9 : Deflection comparison between 1 in. (25.4 mm.) And 0.5 in. (12.7 mm.) For ceb-fip and ceb-fip-s3 functions and experimental deflection for slab#8– rsc-r4-8in. 71

Figure 6.4-10: Deflection comparison between 1 in. (25.4 mm.) And 0.5 in. (12.7 mm.) For constrained lagrange and beam in solid with no defined function and juan function with experimental deflection for slab#10– rsc-r5-8in. 72
Figure 6.4-11 : Deflection comparison between 1 in. (25.4 mm.) And 0.5 in. (12.7 mm.) For ceb-fip and ceb-fip-s3 functions and experimental deflection for slab#10– rsc-r5-8in. 73
Figure 6.4-12: Deflection comparison between 1 in. (25.4 mm.) And 0.5 in. (12.7 mm.) For constrained lagrange and beam in solid with no defined function and juan function with experimental deflection for slab#12– rsc-r6-8in. 74
Figure 6.4-13: Deflection comparison between 1 in. (25.4 mm.) And 0.5 in. (12.7 mm.) For ceb-fip and ceb-fip-s3 functions and experimental deflection for slab#12– rsc-r6-8in. 75
Figure 6.4-14: comparison between slab#2 vs. Slab#4 vs. Slab#6 for constrained lagrange and beam in solid with no defined function and juan function with experimental deflection for0.5 in. (12.7 mm.) Mesh size. 76
Figure B-8.1-1 : Average pressure-time history for slab # 1. 87
Figure B-8.1-2**:** Average pressure-time history for slab # 2. 87
Figure B-8.1-3: Average pressure-time history for slab # 3. 88
Figure B-8.1-4: Average pressure-time history for slab # 4. 88
Figure B-8.1-5: Average pressure-time history for slab # 5. 89
Figure B-8.1-6: Average pressure-time history for slab # 6. 89
Figure B-8.1-7: Average pressure-time history for slab # 7. 90
Figure B-8.1-8: Average pressure-time history for slab # 8. 90
Figure B-8.1-9: Average pressure-time history for slab # 9. 91
Figure B-8.1-10: Average pressure-time history for slab # 10. 91
Figure B-8.1-11: Average pressure-time history for slab # 11. 92
Figure B-8.1-12: Average pressure-time history for slab # 12. 92
Figure D - 8.1-1 : Input and output control parameters 95
Figure D- 8.1-2: iInput parameters for concrete damage model release 3 for high-strength concrete 96
Figure D - 8.1-3: Input parameters generated by concrete damage model release 3 for high- strength concrete. 97

Figure D - 8.1-4 : Input parameters for concrete damage model release 3for normal-strength concrete 98
Figure D - 8.1-5: Input parameters generated by concrete damage model release 3 for high-strength concrete 99
Figure D - 8.1-6: Input parameters for plastic-kinematic model for high-strength concrete..... 100
Figure D - 8.1-7: Input parameters for plastic-kinematic model for normal-strength concrete . 100
Figure D - 8.1-8: Input parameters for constrained lagrange in solid formulation..... 100
Figure D- 8.1-9: Input parameters for constrained beam in solid formulation with no user defined function. 100
Figure D - 8.1-10: Input parameters for constrained beam in solid formulation with user defined function. 101
Figure D - 8.1-11: Input function for ceb-fip function for high-strength concrete. 101
Figure D - 8.1-12 : Input function for ceb-fip function for normal-strength concrete..... 102
Figure D - 8.1-13 : Input function for ceb-fip-s3 function for high-strength concrete. 103
Figure D - 8.1-14: Input function for ceb-fip-s3 function for normal-strength concrete. 104
Figure D - 8.1-15: Input function for juan function for high-strength concrete. 105
Figure D - 8.1-16: Input function for juan function for normal-strength concrete. 106

LIST OF TABLES

Table 4-1: Experimental program schedule 15
Table 4-2 : Slab designation details foe experimental program. 16
Table 6-1: Ncoup parameter variation results for juan function 41
Table 6-2: Ncoup parameter variation results for CEB-FIP function 42
Table 6-3: Ncoup parameter variation results for CEB-FIP-s3 function 47
Table 6-4: Numerical simulation results for slab#1 HSC-V1-4in. 51
Table 6-5: Numerical simulation results for Slab#3, HSC-V2-4in. 52
Table 6-6: Numerical simulation results for Slab#5, HSC-V3-4in. 54
Table 6-7: Numerical simulation results for Slab#7, HSC-V4-8in. 57
Table 6-8: Numerical simulation results for Slab#9, HSC-V5-8in. 58
Table 6-9: Numerical simulation results for Slab#11, HSC-V6-8in. 61
Table 6-10: Numerical simulation results for Slab#2, RSC-R1-4in. 63
Table 6-11: Numerical simulation results for Slab#4, RSC-R2-4in. 65
Table 6-12: Numerical simulation results for Slab#6, RSC-R3-4in. 67
Table 6-13: Numerical simulation results for Slab#8, RSC-R4-8in. 70
Table 6-14: Numerical simulation results for Slab#10, RSC-R5-8in. 72
Table 6-15: Numerical simulation results for Slab#12, RSC-R6-8in. 74
Table 7-1: Analytical and experimental peak slab deflection summary for high strength slabs for 1 in. Mesh size. 77
Table 7-2: Analytical and experimental peak slab deflection summary for high strength slabs for 1/2 in. Mesh size. 78
Table 7-3: Percentage comparison of peak slab deflections with the experimental value for high strength slabs for 1in. Mesh size. 78
Table 7-4: Percentage comparison of peak slab deflections with the experimental value for high strength slabs for ½ in. Mesh size. 79
Table 7-5: Analytical and experimental peak slab deflection summary for regular strength slabs for 1 in. Mesh size. 80
Table 7-6: Analytical and experimental peak slab deflection summary for regular strength slabs for 1/2 in. Mesh size. 81

Table 7-7: Percentage change in peak slab deflection when the mesh size was reduced from 1 in. (25.4mm.) To ½ in. (12.7 mm.) For r strength slabs. 81
Table 7-8: Percentage comparison of peak slab deflections with the experimental value for regular strength slabs for ½ in. Mesh size..... 82
Table 7-9: Percentage change in peak slab deflection when the mesh size was reduced from 1 in. (25.4mm.) To ½ in. (12.7 mm.) For high strength slabs..... 83
Table 7-10: Percentage change in peak slab deflection when the mesh size was reduced from 1 in. (25.4mm.) To ½ in. (12.7 mm.) For regular strength slabs. 83
Table C- 0-1: Input parameters for concrete damage model release 3 93
Table C- 0-2: Input parameters for plastic kinematic model for steel rebar..... 94

ACKNOWLEDGEMENT

I would like to take this opportunity to thank all those people who helped me to complete this thesis.

It is with immense gratitude that I acknowledge the guidance and encouragement of my advisor, Dr. Thiagarajan Ganesh. Throughout the length of my education and research at University of Missouri – Kansas City, he has constantly supported me and has given me valuable insights which made the completion of this thesis possible.

I am grateful to Dr. Ceki Halmen and Dr. Zhiqiang Chen for serving as ~~the~~ members on the supervisory committee and for providing their valuable input and suggestions. I am thankful to the School of Computing and Engineering for providing the necessary facilities in order to pursue the research studies for this thesis.

I would like to express my deepest gratitude to my senior lab mates Hamad, Lorry and Jade. Their inspiring research work motivated me and was vital in developing my interest in performing research and provided me the opportunity to learn from them. I am thankful for them in keeping a peaceful and friendly environment in the lab which was motivating in performing my research. I owe my sincere thanks to my dear friends Raju, Soham, Maitrey, Plamond and Sanket for their moral support throughout my studies at UMKC. Their friendships were instrumental in my desire to achieve my goals.

I also wish to thank all my family members and friends for their support. Most importantly, I owe my loving thanks and sincere appreciation to my parents Ashok and Ashwini Iwalekar. Throughout my studies abroad they never failed in their encouragement, patience and understanding. To them I dedicate this thesis.

CHAPTER 1. INTRODUCTION

1.1 An overview on Blast Effects on Structures

In recent times, instances occur where civilian structures were under aggressive attack by means of blast or explosives. The attack on the World Trade Center on February 26th, 1993, in New York, and the bombing which destroyed the Alfred P. Murrah Building on April 19th, 1995, in Oklahoma City, are two primary examples of attacks that occurred during the past couple of decades. These attacks have led to the need for more blast resistant designs for civilian structures, as the reason that lives were lost in these attacks was due to the inability of these structures to resist blast loading. When considering blast loading, a new efficient design approach should be adopted in order to minimize the damage specifically to civilian structures. In past, military structures have been designed for blast loading. In recent history, government and civilian buildings have increasingly become potential threats to attacks. Therefore, design procedures and guidelines, which are easy to implement for civilian structures need to be designed and produced. DoD Minimum Antiterrorism Standards for Buildings, UFC 4-010-01, is one such design guideline, which has been established for stating the minimum level of protections against terrorist attacks for the Department of Defense structures [5]. Furthermore, these guidelines outline feasible ways to implement blast protection in military structures. It is imperative that adaptations for the application of blast mitigation methodology of civilian structures from military structures are be done. Blast-effect mitigation is the reduction in the severity of effects of an explosion on a structure resulting from having taken specific blast hardening measures in order to reduce or eliminate the effects of an explosion, according to the National Research Council [6]. In order to find the best alternative for the design of building components, such as wall panels, columns slabs,

beams etc., expensive research has been carried out. Structures like offices, research facilities, education institutions etc., which are occupied by large human populations and are more prone to aggressor attacks, such consideration state becomes critical.

1.2 Significance of Studying Blast Effects on Reinforced Concrete Slabs

The internal and external structure of buildings like walls and columns can get damaged due to an explosion, within or near the structure, leading to the partial disability or the complete failure of fire-safety and life-safety systems. Increasing the resistance of the structure to blast loading thereby strengthening the structure itself, can be one of the solutions. However, this adoption can prove to be expensive when it is implemented on a large scale. The study of the blast damage caused to the Alfred P. Murrah building during the Oklahoma City Bombing, done by Mlakar et al. [7], has evaluated the effect of the blast caused by the truck bomb on the buildings structural frame. Columns in the surrounding areas of the blast underwent major damage, and the blast induced pressures severely affected the floor slabs above and below the blast epicenter. This caused maximum displacement of 9.3 inches in an upward direction, between, above and below slabs which lead to the collapse of the slab. As reinforced concrete slabs are one of the most basic type of slabs designed today, their strengthening is required. Reinforced concrete wall panels designed for blast loading are one of the additional protective measures that act as a shield for the main structure. Studies of dynamic behavior of reinforced concrete slabs, under high blast loads of short duration, become necessary and is the motivation behind this study. Around the world, structural engineers use advanced analysis methods to ensure resistance to blast loading on their designed structures. For predicting blast loads and response of structures to blast loading, experimental studies, theoretical analysis and advanced numerical simulation can be used for the evaluation of behavior of civilian structure to blast loading.

1.3 Proposed Solution

In order to predict the effects of blast and the quantification of structural response to blast and its interaction with the structures, coming up with theories and experiments to test these theories are necessary. For estimating the response of a structure to an explosion, results obtained for these theories and experiments can be used. Even though the computational approach is far less expensive than the experimental approach, experimental studies are requiring for the validation of this computational approach. Numerous experiments are performed by various military organizations on military structures. The application of these experiments on civilian structures can and needs to be studied and investigated.

This study involves the numerical study of the reinforced concrete slab, an important component of any structural system. The comparison of the results of high strength and normal strength material from experiments done previously will be utilized and will then later be compared with the numerical study. Finite Element Method (FEM) is used to analyze the effectiveness of the strengthened slabs against blast loading. LS-DYNA®, a non-linear transient dynamic finite element analysis program code, is employed in this study. This program has various advantageous features of defining pressure-time histories generated in the blast event and later analyzing the model. Commercially available material models are used to define concrete and steel materials, which are Concrete Damage Model Release 3 for concrete and plastic kinematic model for steel. In order to define bond between the concrete and the steel, both perfect bonds employing Lagrange in solid, and bond slip under Beam in solid, are used for both material strengths [1]. Comparison of the two bond types is the focus of this study.

At the U.S. Army Engineering Research and Development Center in Vicksburg, MS, initial experiment investigation was carried out on twelve single-mat reinforced concrete RC

slab panels. The slabs consisted of two sets of panels; the first one consisted of High Strength Concrete reinforced with High Strength Steel Reinforcing bars (HSC-V) and the other one was of Normal Strength Concrete reinforced with Normal Strength Steel Reinforcing bars (NSC-R). The twelve sets of concrete had two different sets of reinforcement ratios, one set had #3 bars spaced at 4 inch (101.6 mm.) and the other set had #3 bars spaced at 8 inches (203.2 mm.). The twelve slabs were subjected to pressure conditions equivalent to those in a blast load which were generated using a Blast Load Simulator. The experimental data that was collected for this testing included measurement of the slab displacement, slab strain and slab damage/crack patterns. The displacement at mid-span was measured with lasers and accelerometers during the testing, using pressure versus time history at 6 locations on the slabs. Strains were measured at two locations using strain gages, photos and videos documented the locations and severity of damage crack patterns for each slab.

1.4 Thesis Organization

The thesis is organized as follows:

1. Chapter 1 introduces the subject of this thesis, which is about experimental validation of reinforced concrete single mat slabs subjected to blast loading and finite element analysis.
2. Chapter 2 includes the literature review for the study of this thesis.
3. Chapter 3 includes the scope and the objective of this thesis.
4. Chapter 4 describes experimental investigation. Dr. Ganesh Thiagarajan, the Principal Investigator for this project, conducted this experiment at U.S. Army Engineer Research and Development Center at Vicksburg, MS. That experiment is not a part of this thesis; therefore, it is described in detail. The information collected from this experiment includes the types of reinforced concrete panels, the equipment used for applying the blast pressures

and the various types of data collected. Numerical analysis is performed using the data obtained from this experiment.

5. Chapter 5 includes details of the reinforced concrete slabs numerical modeling, the geometry of the finite element models, the various mesh sizes adopted, the material models used for modeling the steel and the concrete from program are described in this chapter.
6. Chapter 6 includes the results obtained from the numerical simulations performed and the observations of such. The simulations are done using the LS-DYNA® program.
7. Chapter 7 includes the examination and deliberation of the results presented in Chapter 6.
8. Chapter 8 includes the conclusions that were drawn from this study and are based on the analysis of the test results. This chapter also includes details and recommendations for future work.

CHAPTER 2. LITERATURE SURVEY

In the research world, efforts have been made to improve the blast resistance of buildings. The primary focus has been to develop effective methods which can be easily implemented. The goal would be to produce design protective technologies which are readily available for both design and structural engineers.

A numerical analysis on the dynamic behavior of RC slabs under blast loading was performed by Hao and Zhongxian [9]. They discussed the influence of various structural and geometric parameters of RC slabs under blast loading in their study. Among their testing were the concrete strength, the reinforcement ratio and the dimension of the slab. They remarked that reinforced concrete (RC) slab resistance to blast loading increased with an increase in slab thickness.

To improve the blast resistance of buildings, Crawford and Lan [8] used different engineering techniques as solutions. They carried out studies of numerical modeling and testing of the effects of blasts and impacts. From their study, they recommended the use of high-fidelity physics-based (HFPB) finite element models. Their challenge was to develop a model which would provide a refined representation of the behavior during blast loading. HFPB models fulfilled this challenge and validation was stated as being significant. Ductility and plastic behavior, use of standard material in a non-standard way and shock relative behavior are the three primary design benchmarks described in their work.

The method of finite element analysis was used by Mosalam and Mosallam [10] to develop computational models of reinforced concrete slabs (RC) under blast loading. Non-linear transient analysis was carried out, by them, in order to investigate and compare the behavior between retrofitted RC slabs with carbon fiber reinforced (CFRP) polymer slabs to as-built RC

slabs when subjected to blast loading. The efficiency of CFRP polymer slabs was stated in this study noting a reduction of the displacement from 40% to 70%, in comparison to as-built slabs. Computational models were verified using experimental data.

Agardh [11] presented a study of FE model simulation on fiber reinforced concrete and the experimental results were focused on the behavior of these models under transient dynamic loads. The comparison of the experiments on conventional reinforced concrete slabs and steel fiber were carried out in this study with the blast experiments performed in a shock tube. Validation of these results were done using two codes: LS-DYNA® and ABAQUS®/explicit with Winfrith concrete model for LS-DYNA® and Constitutive model for brittle cracking in ABAQUS®/Explicit as concrete models. Accurate results were obtained for the use of parameters prediction of failure loads and for the displacement for low loads. The exclusion of the strain rate effect was recommended in this study by stating that the distance between the slabs and the charge was large, therefore causing the strain rate effect to be insignificant.

Due to the symmetry of the slabs Kuang [12] modeled only a quarter of three-dimensional FE model of RC slabs that were subjected to blast loading and carried out numerical simulation in LS-DYNA®. To model concrete material Johnson-Holmquist Concrete (H-J-C) [1] model was used in this study to account for the damage and strain rate effect and the erosion technique was used for modeling the spallation process. Effective prediction of the response of the reinforced concrete section was noted in comparison between the blast test results and the numerical simulation results.

For the purpose of analyzing responses of two-way reinforced concrete panels which were subjected to blast loading, El-Dakhakhni [13] used and studied the validity of Single-Degree-of-Freedom (SDOF) models which were developed in accordance to the guidelines of the

UFC 3-340-02 [6]. These RC panels had variations in dimensions, aspect and reinforcement ratios, and support conditions. Finite element analysis was carried out in LS-DYNA® utilizing the parameter generation capability of *MAT_CONCRETE_DAMAGE_REL3 (mat type 72R3) model for the concrete material and PLASTIC_KINEMATIC (mat type 003) for the steel material [1]. Razagpur (2006) had previously provided validation for these models. Results that were obtained from these numerical simulations were compared to results obtained for the nonlinear explicit finite-element (FE) analysis. Significant variations in the shear and deflection predictions were observed. This study identified the many limitations of the SDOF models over the FE analysis techniques. Above and beyond the SDOF model analysis parameters, the FE analysis method can include different failure modes such as shear, bar slippage, etc., as well as material strength enhancement due to strain rate effects. The results of this study noted the strong advantages of FE analysis over the SDOF model analysis.

Significant research has been carried out in the last couple of decades in order to accurately predict concrete material properties in finite element models developed for concrete structures. In order to replicate the exact behavior in the finite element model, sophisticated knowledge of the behavior of concrete structures is required. For this process, initial laboratory experiments were conducted with control over the structural parameters. Data from the experiments can then be used to calibrate the available computer models. A similar kind of methodology was adopted by Malvar and Schwer [14]. They characterized the parameters of 45.6 MPa unconfined compressive strength concrete model parameters from laboratory tests. They then implemented it with LS-DYNA® in commercial K & C concrete model [1]. The results obtained from this study recommended the use of a model parameter generation capability of Mat72R3 by using the unconfined compressive strength of the concrete as input.

Blast analysis was performed on 1.19m X 2.19m X 0.14m RC slabs by Tanapornaweekit [12] employing 500kg TNT testing in Woomera, South Australia. For predicting blast load properties, AIR3D and CONWEP computer programs were used. These predictions were compared to results obtained by pressure transducers in test. For the purpose of numerical simulation LS-DYNA® was used and the results obtained from the numerical simulations were compared to the experimental results. In the numerical simulation, to define the concrete material of the panel, *MAT_CONCRETE_DAMAGE_REL3 was used. This model takes account for three failure surfaces which are: Maximum shear failure surface, residual surface and initial yield surface. The advantage of this material model is that it has automatic parameter generation capability for the input compressive strength of the concrete [1]. For this study, the compressive strength of 40 MPa was used as input value, giving a total of 8 automatic parameters that were generated. Three failure surfaces were considered in this material model and they are governed by three equations which are discussed in this thesis. For the purpose of modeling the steel material, model *MAT_PLASTIC_KINAMATIC was utilized [1]. For defining the bond between the steel and concrete, a full bond between the two materials was assumed between nodes. The results of the numerical simulation in FE reported that the maximum deflection was 30mm and the maximum rebound deflection was 4 mm. This corresponds to the experimental difference of 17%. Experimental results for the maximum and the rebound deflection were 36mm and 5mm respectively.

The dynamic plastic damage model was adopted by Zhou and Kuznetsov [13] in order to study and compare both ordinary reinforced and high-strength steel fiber reinforced concrete slabs. This concert model is developed by taking reference form material models used in separate researcher which are not part of their project and with equations of concrete strength

derived from static and dynamic material testing and parameters such as deflection of damage, strain-rate effects and concrete strength envelope. The comparison gave understanding as to the numerical simulation for t > 2ms gives lower value to peak deflection results, for t < 2ms estimation of ultimate deflection is well with experimental records. This type of results is common for both RC and the high strength Steel Fiber Reinforced Concrete (SFRC) slabs.

Shetye [2] performed numerical analysis on single-mat reinforced concrete (RC) slabs in LS-DYNA® on 12 slabs. This study focused on the comparison of two commercially available concrete material models. Interaction between the steel and the concrete of RC slabs were modeled employing a perfect bond between them. Effect of mesh size model on finite element analysis and the outcome of two different reinforcement ratios were also investigated in this study. Increase in peak deflection, with decrease in mesh size for both concrete models, and on reduction on reinforcement ratio, led to increased deflection by twice the amount are results stated in this study with recommendation of Winfrith Concrete Model for both high and regular strength concrete.

Literature review here indicated different types of approaches adopted for investigating and analyzing blast mitigation techniques, which are evaluated using SDOF system or finite element analysis system in order to study the effect of dynamic loading of short duration on reinforced concrete slabs. This thesis including a similar combination of techniques which involves two different material strength, two different mesh sizes, two separate reinforcement ratios and two different bond interaction models between the steel and the concrete and compression of experimental records to numerical analysis study performed to investigate validation of numerical approach adopted.

CHAPTER 3. OBJECTIVE AND SCOPE

3.1 Problem Statement

To accurately predict the structural response to dynamic loading in finite element modeling is a difficult task. Hence, it is necessary to include the exact material description of material parameters through input parameters in model, which helps in capturing rapidly changing material behavior in dynamic loading. In order to obtain accurate material properties, the challenging task of comprehensive laboratory testing on materials needs to be performed. In order to counter this challenge, the use of commercially available material models was employed for this study, which accurately describe the response and behavior for developed FE slab models. Hence, it becomes necessary to validate the results obtained from numerical simulation, which employed commercial material models, to results obtained from experimental investigation.

3.2 Objectives

This thesis focuses on investigating blast loading on Reinforced Concrete (RC) one-way slabs having a single layer of reinforcement. This is achieved by performing Finite Element (FE) simulations which the results obtained from this simulation are then compared with experimental data. The scope of the thesis is outlined as follows to achieve this goal.

1. To perform numerical analysis and modeling in LS-DYNA® program, by using data from experimental investigation. This includes use of deflection-time history and pressure-time histories records.
2. In LS-DYNA® program, create slab models identical to experimental investigation with dimensions of 64 in. x 34 in. x 4in. (1652 mm. x 863 mm. x 101.6 mm.).

3. Mesh sizes of 1 in. (25.4 mm) having 4 elements through the slab thickness, ½ in. (12.7 mm.) having 8 elements through the slab thickness and ¼ in. (6.35 mm.) having 16 elements through the slab thickness, to be used in order to perform mesh analysis.
4. To use two different reinforcement ratios for each material combination, for investigating study the effect of reinforcement ratio.
5. Two types of material combinations to be considered based on concrete strength to be used, which involves normal strength concrete reinforced with normal strength steel and high strength concrete reinforced with high strength steel.
6. Using Plastic Kinematic Model to model the steel and Concrete Damage Model Release 3 to model the concrete in LS-DYNA® program.
7. Use Constrained Lagrange in Solid formulation to model prefect bond and Constrained Beam in Solid formulation for bond-slip modelling between steel and concrete.
8. Comparison is made between two types of bond relations molded in LS-DYNA® program are results are compared with experimental investigation to determine which bond formulation is accurate to predict outcome of analysis. Thus, validating bond relation between steel and concrete and avoiding expensive blast experiments is the goal of this study.

3.3 Tasks

Task 1: To utilize information of experimental investigation on twelve Reinforced Concrete (RC) slab panels performed earlier, which was not part on this study. This experimental investigation on twelve slabs had a combination of normal strength concrete with normal reinforced Concrete (RSC-R) and high strength concrete with high strength steel (HSC-V) slab panels, each with dimensions of 64 in. (1625 mm.) X 34in. (864 mm.) X 4 in. (101.6 mm.)

and consisted of single-mat reinforcement. This combination of normal strength concrete (5 ksi, 34.47 MPa) with normal strength steel (60 ksi, 413.68 MPa) and high strength concrete (15 ksi, 103.42 MPa) reinforced with high strength vanadium steel (83 ksi, 572.26 MPa) were loaded with blast pressure within a Shock Tube for experimental investigations. On six different regions on the slab, pressure and impulse histories were recorded and deflections were measured using a laser device which was placed at the center of the slab. The strain history was recorded employing strain gauges located at quarter points of the unloaded face of the slab.

Task 2: Material of concrete slabs were modelled using commercially available material models. Concrete Damage Model Release 3 is used for concrete while steel is modeled using Plastic Kinematic Model. The Bond between the concrete and steel were model using perfect bond relations and bond-slip mechanisms. Lagrange in solid formulation was used for modelling perfect bond whereas Beam in solid formulation was used for modeling bond-slip. In bond-slip formulation, three custom functions are used defining bond-slip law. CEB-FIP, CEB-FIP-S3 and function for bond-slip law proposed by Juan are used in this study. Mesh size analysis was also carried out to investigate its effect on FE analysis. These are explained in the following chapters. Verification of FE analysis results to experimental results was based on deflection history records of slab when subjected to blast pressures and impulses that the experimental specimen was subjected to.

Task 3: The effect of the reinforcement ratio was also investigated with two different reinforcement ratios, #3 bars spaced at 4in. c/c (101.6 mm.) in the longitudinal direction (reinforcement ratio = 0.68%) for first set of six slabs and #3 bars spaced at 8in. c/c in the longitudinal direction (reinforcement ratio = 0.46%) for the remaining six slabs for the main steel. These two set of models are referred to as 4in and 8in models respectively. The ratio of the

shrinkage of the steel is the same for all 12 slabs, #3 bars spaced at 8in. c/c in the longitudinal direction (reinforcement ratio = 0.46%).

The outcome of this study is used for recommendations for the custom function to be used for defining bond-slip low for both material strengths used in modeling for numerical formulation and are validated used experimental results, for blast loading in future.

CHAPTER 4. EXPERIMENTAL INVESTIGATION

An experimental research, which was conducted at the U.S. Army Engineer Research and Development Center at Vicksburg, MS, comprised of twelve reinforced concrete slabs (RC) with scale of 1/3 having clear span of 58 inch (1473.2 mm.). In this research, the slabs were fabricated at the facility itself. This faculty included a Blast Load Simulator, which was utilized for dynamically loading these twelve slabs. Table 4-1 shows the experimental program.

Table 4-1: Experimental program schedule

No.	Slab #	Slab Type	Date	Driver pressure	Explosion Type
1	Slab # 1	HSC - V1 - 4in.	12/13/2010	1150 psi	100% Air
2	Slab # 2	RSC - R1 - 4in.	12/14/2010	1150 psi	100% Air
3	Slab # 3	HSC - V2 - 4in.	12/15/2010	1150 psi	100% Air
4	Slab # 4	RSC - R2 - 4in.	12/16/2010	1150 psi	100% Air
5	Slab # 5	HSC - V3 -4 in.	12/17/2010	900 psi	100% Air
6	Slab # 6	RSC - R3 - 4in.	02/01/2011	900 psi	100% Air
7	Slab # 7	HSC - V4 - 8in.	02/03/2011	900 psi	100% Air
8	Slab # 8	RSC - R4 - 4in.	02/03/2011	700 psi	25% HE
9	Slab # 9	HSC - V5 - 8in.	02/04/2011	700 psi	25% HE
10	Slab # 10	RSC - R5 - 4in.	02/07/2011	750 psi	25% HE
11	Slab # 11	HSC - V6 - 8in.	02/08/2011	800 psi	25% HE
12	Slab # 12	RSC - R6 - 4in.	02/09/2011	725 psi	25% HE

4.1 Materials

Dr. Ganesh Thiagarajan was the Principal Investigator for this project when this experiment was conducted. High-strength materials were compared to conventional materials in this study. Resistance of both types of materials, under dynamic loads, were examined. The overall dimensions for the single-mat slab panels tested are 64 in. (1625 mm.) X 34in. (864 mm.) X 4 in. (101.6 mm.) which are 1/3 scale models. Based on strength two of material combinations which were used are designated as "HSC-V" for High-Strength material combination and "RSC-R" for Normal-Strength material combination. Table 4-1-1 gives detailed description of slab-designation.

Table 4-2 : Slab designation details foe Experimental Program.

Designation	Description	Material strength
HSC	High-strength concrete	15 ksi (103.42MPa)
RSC	Regular-strength concrete	5 ksi (34.47MPa)
V#	Vanadium steel rebar	83 ksi (572.26MPa)
R#	Grade 60 Conventional rebar	60 ksi (413.68MPa)
4 in.	Longitudinal bars spacing	-
8 in.	Longitudinal bars spacing	-

For the longitudinal bars, two different reinforcement spacing were used. The #3 bars spaced at 4 inches (101.6 mm.) was used for the first 6 slabs while for the remaining 6 slabs #3 bars were spaced at 8 inches (203.2 mm.). Figure 4-1 and 4-2 shows detailed layout for the two types of slabs based on the reinforcement spacing.

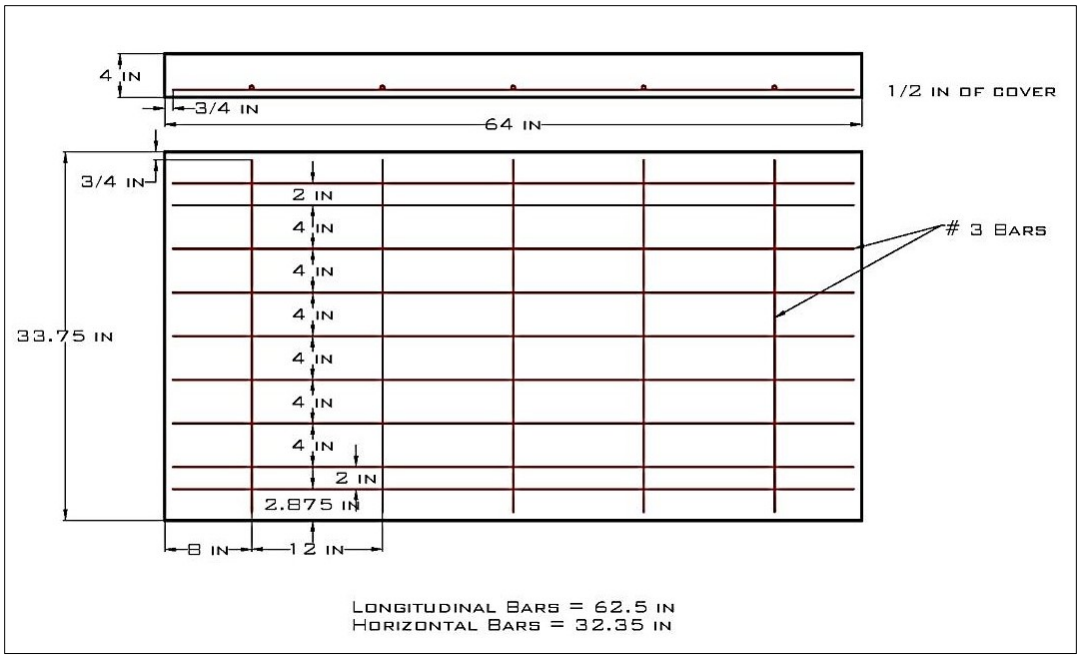

Figure 4.1-1: Single-Mat Reinforced Concrete (RC) Slab with 4 in. type single layer reinforcement

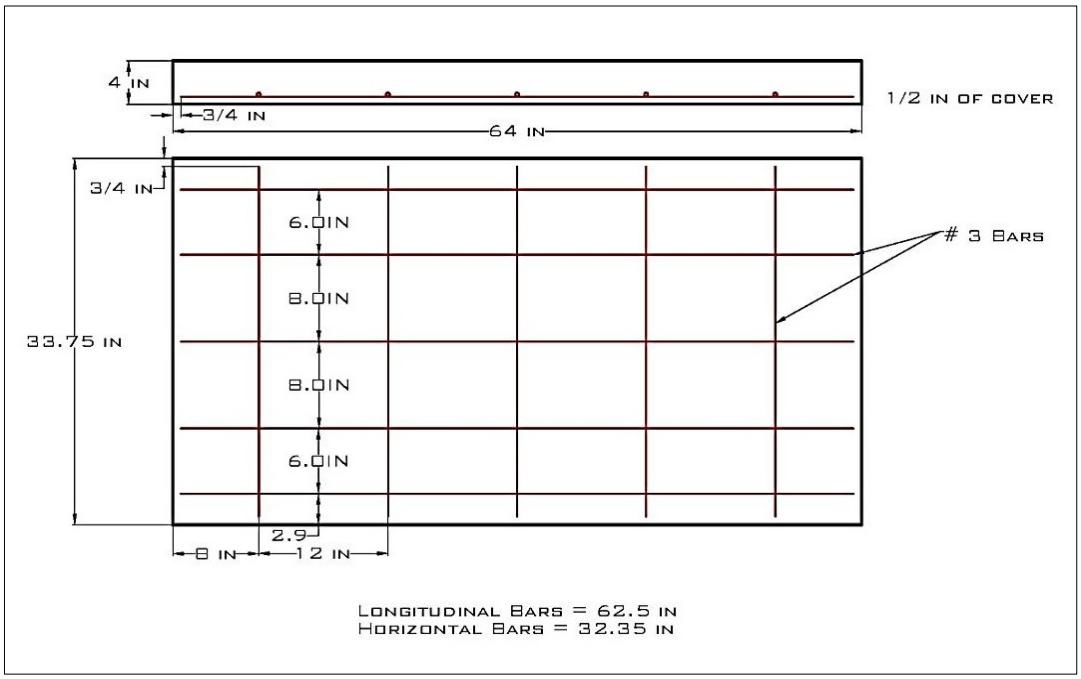

F

Figure 4.1-2: Single-Mat Reinforced Concrete (RC) Slab with 8 in. type single layer reinforcement

4.2 Methods

Shock tube and field test are the two most widely practiced methods for performing blast testing. Among these two, filed tests include security and safety issues combined with defining a separate prediction model for predicting measurements of blast pressures generated in study. A Blast Load Simulator (Shock Tube) is used in this study for performing blast load application on reinforced concrete slabs. The Advantages of recording both the positive and negative phases of pressure versus time variations has been utilized to accurately record blast loads. On six separate locations on the slabs, pressure data was recorded. Similarly, to record deflection on the back face of the slabs, laser deflection measurement device was employed, and high-speed video cameras were used for recording the behavior of the slabs under blast loads. Later, the raw data obtained from this experimental study was compiled into usable format. In this thesis, data obtained from this experimental study was used for finite element modeling. The next section describes the data collected for this experimental study.

Figure 4.2-1: Blast Load Simulator (Shock tube)

4.3 Experimental Data

Four important parameters are recorded for twelve 1/3 scale RC slabs from experimental investigation. These four parameters are as follows:

1. Pressure at six separate locations on the slab.
2. On the back-face, mid-span deflections.
3. On the back-face, strains at two-locations.
4. Crack patterns recorded as post-blast photos.

At six different locations, both positive and negative phases of pressure vs. time history data has been recorded on reinforced concrete slabs. Pressures gages, which were located inside of the blast load simulator on the loading frame, were used for recording the pressure vs. time history. With this experimental study, data of average peak pressures and impulse for twelve slab has been recorded (Appendix A). Appendix B includes pressure vs. time history plots for all twelve reinforced concrete slabs. For utilizing coordinates of pressure vs. time, history plots in numerical simulation spreadsheet in comma separate format is employed.

Blast pressures which were subjected to reinforced concrete slabs in this experimental study were pre-determined and the dynamic response of the slabs to the applied blast loading were recorded. The dynamic response of all twelve slabs under blast loading were recorded in two standards, strains measured with respect to time and center-span displacements for a short duration. For the purpose of validation of numerical models generated in this study, displacement-time history recorded using accelerometers and lasers are utilized.

CHAPTER 5. NUMERICAL MODELING IN LS-DYNA®

The study of numerical simulation is carried out in LS-DYNA®. For this numerical analysis a numerical model of Single-Mat RC slab was developed. This model was subjected to blast load to replicate the experiments performed. To achieve the primary objective of comparing different bond relations between steel and concrete against blast loading, results achieved form numerical simulations are compared to records of high-strength reinforced and normal-strength reinforced concrete slabs of experiments. This numerical study performs validation of different pre-defined bond relation between reinforcing steel and concrete materials of two different strengths. This chapter discusses significance of LS-DYNA® for numerical simulations, constitutive material model, ability to define bond relations by user between reinforcement steel and concrete, boundary conditions and blast load application.

5.1 Significance of Numerical Modeling in LS-DYNA®

LS-DYNA® is a highly non-linear finite element program, which uses explicit time integration for performing transient dynamic finite element analysis. This program provides various material models and elements formulation in its material and element library [1]. A single-mat reinforced concrete slab model was developed in LS-DYNA® and finite element analysis was carried out.

Accurate modeling of reinforced concrete in finite element analysis is a challenge, since material contains non-homogeneity and irregular composite bond behavior between concrete and steel under dynamic loading. Bond relation between steel and concrete should be defined appropriately in order to get a good response under applied loading. This bond can be defined in LS-DYNA® using predefined relations in program or using user defined bond relations. Program has pre-defined material models for steel and concrete. The definition of this

predefined material models requires basic properties of materials. Two different elements models are used from element library to define concrete and steel reinforcement of slab, for concrete solid element and for steel beam element are selected [1].

To define perfect bond relation *CONSTRAINED_LAGRANGE_IN_SOLID keyword is used employing concrete bond description by this keyword and merging nodes of elements of solid element and beam element. *CONSTRAINED_BEAM_IN_SOLID keyword is used to define this bond in a different way. In this keyword unlike *CONSTRAINED_LAGRANGE_IN_SOLID the user can define a relation between concrete and steel through custom functions. This feature has been employed in this study and three functions are been studied and compared with *CONSTRAINED_LAGRANGE_IN_SOLID. The detailed explanation of numerical modeling of two separate Single-mat RC slabs geometric models used in this study are described in the following sections.

5.2 Geometric Models

5.2.1 Meshing for Concrete Model

Pre-processor in LS-DYNA® is used for modeling purpose. Two different reinforcement spacing of Single-mat are modeled in this study. This is done by using two parts rectangular concrete block and the reinforcing steel bars. Dimensions for rectangular concrete block are 64 in. x 34 in. x 4in. (1652 mm. x 863 mm. x 101.6 mm.). With constant stress solid element formulation this concrete block is modeled employing the eight-noded hexahedron elements. Two different reinforcement section are developed using two sets of six slab models having three different mesh sizes. These uniform mesh sizes include 1 in. (25.4 mm) having 4 elements through slab thickness, ½ in. (12.7 mm.) having 8 elements through slab thickness and ¼ in. (6.35 mm.) having 16 elements through slab thickness. The node are connected to concrete block according to their respective mesh size. As seen in Figure 5.1 for 1 in. (25.4 mm) mesh size

consist of 8,704 solid elements and of 11,375 nodes. Figure 5.2 shows model with ½ in. (12.7 mm.) mesh size and consists of 69,632 solid elements and 80,109 nodes. Figure 5.3 shows the single-mat model with ¼ in. (6.35 mm.) mesh size and comprise of 557,056 solid elements and 598,553 nodes.

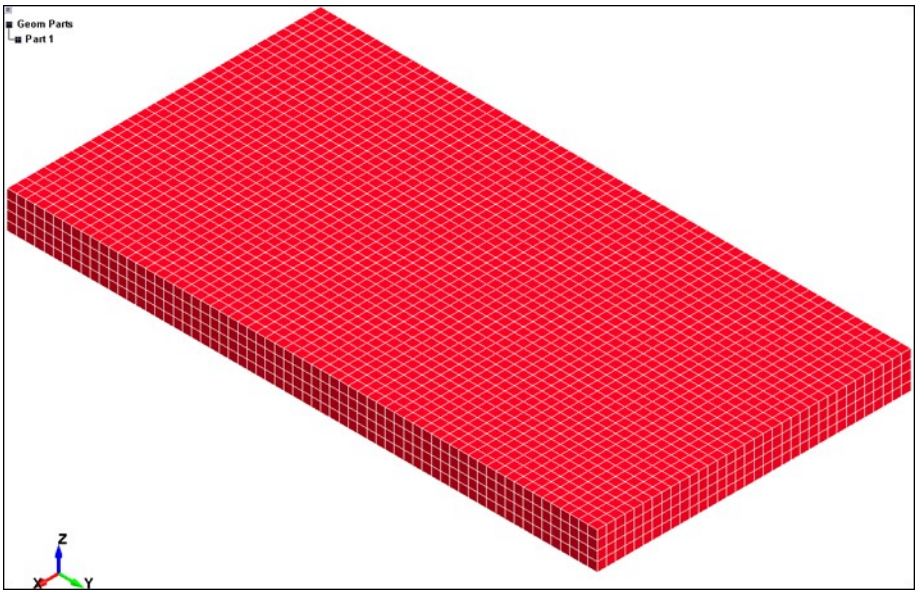

Figure 5.2-1: Single-Mat Reinforced Concrete slab model with Solid Elements 1 in. (25.4 mm.) mesh size

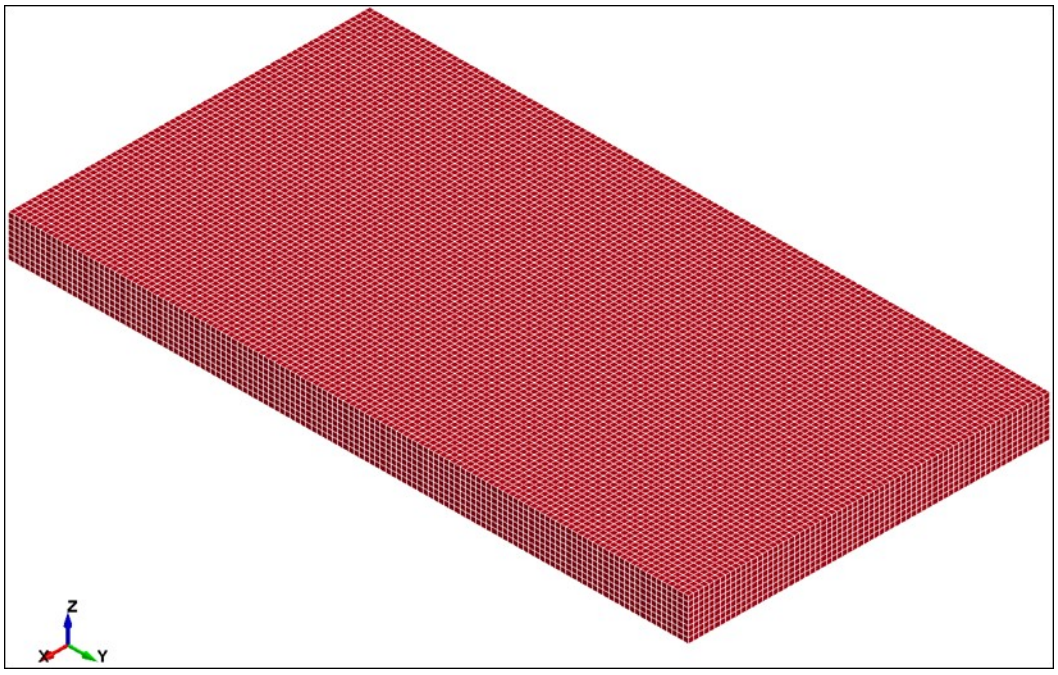

Figure 5.2-2: Single-Mat Reinforced Concrete slab model with Solid Elements ½ in. (12.7 mm.) mesh size

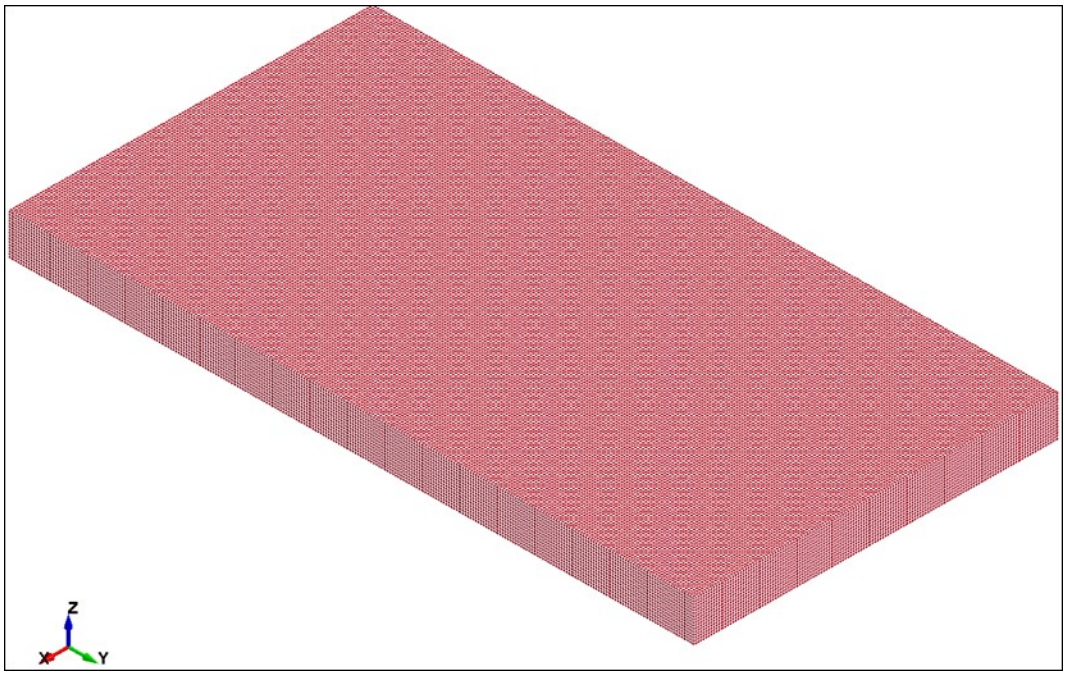

Figure 5.2-3: Single-Mat Reinforced Concrete slab model with Solid Elements ¼ in. (6.35 mm.) mesh size

5.2.2 Meshing for Steel Model

From 1 in. (25.4 mm.) concrete cover from back face of concrete slab has single layer steel reinforcement hence this model is Single-Mat RC slab. Hughes-Liu Beam elements are used to model steel reinforcements. These elements are employed with cross-section integrations formulation and has three different mesh sizes like concrete element described before. Two different main steel spacing 4 in. (101.6 mm.) and 8 in. (203.2 mm.) are used. For 4 in. (101.6 mm.) main steel spacing slabs have two end bars at 2 in. (50.8 mm.) spacing and shrinkage steel modeled at 12 in. (304.8 mm.) spacing on center. Similarly, for 8 in. (203.2 mm.) main steel spacing slabs have the two end bars at 6 in. (152.4 mm.) spacing and shrinkage steel modeled at 12 in. (304.8 mm.) spacing on centers. For 4 in. type model with 1 in. (25.4 mm) mesh size models contain 746 beam elements. Similarly, for ½ in. (12.7 mm.) mesh size consists of 1492 beam

elements and the model with ¼ in. (6.35 mm.) mesh size consists of 2983 elements. Slabs with reinforcement 8 in. (101.6 mm.) spacing on center with 1 in. (25.4 mm) mesh size models contain 490 beam elements in total. Similarly, for ½ in. (12.7 mm.) mesh size consists of 980 beam elements and the models with ¼ in. (6.35 mm.) mesh size consists of 1958 elements in total.

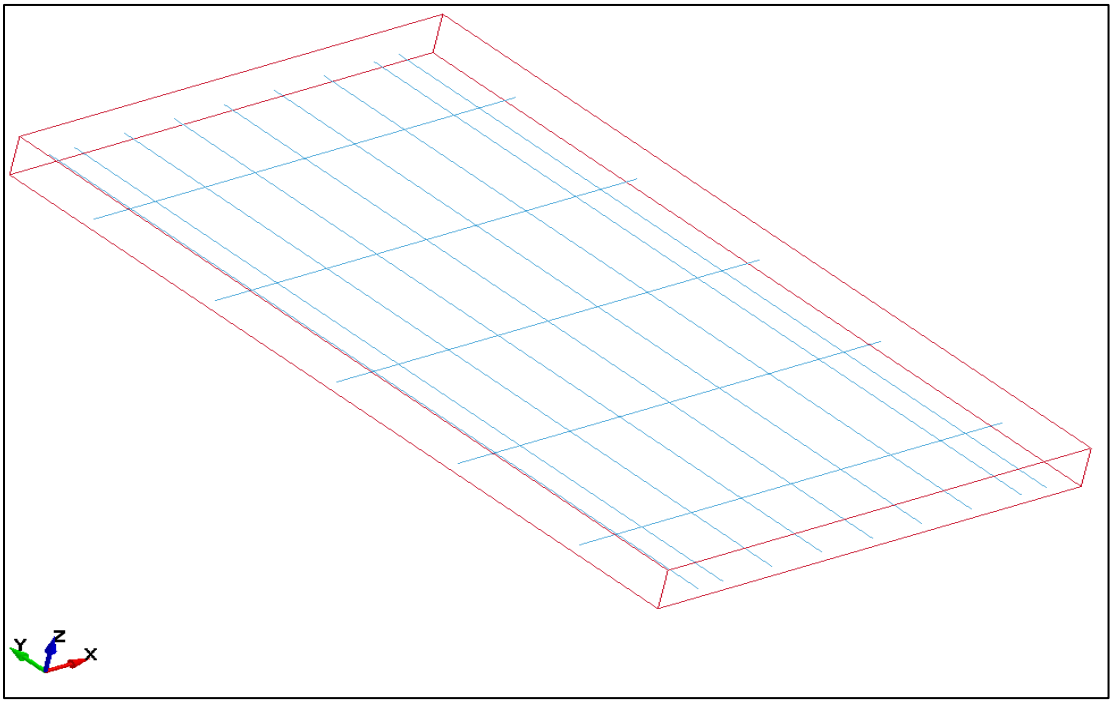

Figure 5.2-4: Single layer reinforcement in 4 in. type single-mat RC slab

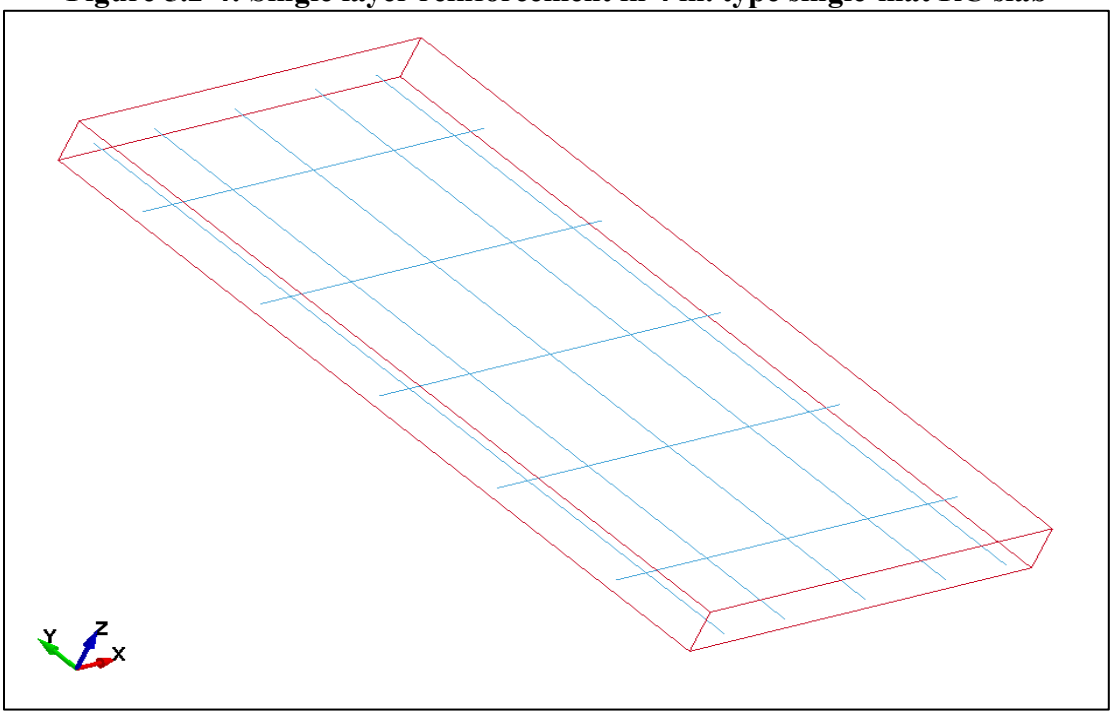

Figure 5.2-5: Single layer reinforcement in 8 in. type single-mat RC slab

5.2.3 Hourglass Control in LS-DYNA®

In order to avoid formation of zero energy modes LS-DYNA® recommends the use of small elastic stiffness or viscous damping capable of stopping undesirable hourglassing. Kosloff and Frazier (1974) [25] [26] developed algorithms which are employed in LS-DYNA®. For eight node element which is used in this study total of twelve hourglass points exists with one integration point. Force vector is employed to represent hourglass-resisting force and this force vector consists of constant QH defined by user. The value of this constant is set between 0.05 to 0.15 [22].

*CONTROL_HOURGLASS keyword is available in LS-DYNA® to implement hourglass control procedure. This keyword allows user to set type of hourglass viscosity through variable IHQ [1]. IHQ types 4 & 5 are recommended for hourglass viscosity for

stiffness type control. Hourglass co-efficient is set in *CONTROL_HOURGLASS keyword through variable QH [1]. This user defined value should be kept less than 1.5, as value exceeding 1.5 may lead to instability. Use of hourglass resistance may lead to loss of energy as work done by resistance of hourglass is neglected in energy equation. Hence, to validate the accuracy of simulation total energy of system throughout simulation must by analyzed which consist of friction energy, damping energy, internal energy, kinetic energy and hourglass energy. In internal energy includes work done in plastic deformations and elastic strain energy. Output files of MATSUM and GLSTAT consists data of energy loss due to dissipation of energy by hourglass forces reacting against formation of hourglass modes. For computation of hourglass energy and inclusion in energy balance is done under *CONTROL_ENERGY keyword variable HGEN by selection of type 2 [1]. In order to hourglass control work effectively, non-physical hourglass energy should be small relative to the peak internal energy (< 10% as rule of thumb) [23].

5.2.4 The Constrained Lagrange in Solid formulation

*CONSTRAINED_LAGRANGE_IN_SOLID (CLS) keyword is used to define the interface between steel and concrete. This interface is assumed to be a perfect bond. In this formulation of steel and concrete element nodes are independent of each other. Vasudevan [21] performed a study on CLS using the Double-mat Reinforced Concrete slab for two concrete material models Winfrith Concrete Model and Concrete Damage Model Release 3. Shetye [2] studied effects of CLS formulation for Single-mat model with same concrete material model used by Vasudevan and compared the both numerical results and experimental.

5.2.5 The Constrained Beam in Solid formulation

Keyword *CONSTRAIN_BEAM_IN_SOLID is alternative to *CONSTRAIN_LAGRANGE_IN_SOLID and its purpose is to sidestep certain limitations on the

CTYPE = 2 in *CONSTRAIN_LAGRANGE_IN_SOLID. *CONSTRAIN_BEAM_IN_SOLID constrains beam structures to move the Lagrangian solid/thick shell, which are employed as master components, as it also assumes perfect bond between steel and concrete.

The advantage of *CONSTRAIN_BEAM_IN_SOLID keyword is that the user can define their own function for bond slip in this keyword using AXFOR input. Function ID is entered in this input and LS-DYNA manual recommends using AXFOR = -10 were 10 is the function the ID [1]. Alternatively, program can generate its own bond slip function if user does not use their own function and parameter CDIR = 0 should be entered for this purpose. In this study both program generated function and three user-defined functions are compared for all slabs. For employing a user defined function in this keyword input CDIR = 1 is recommended [1]. NCOUP feature can be used for coupling multiple points in between the beam elements nodes. This thesis also studies this parameter's effect on all slip functions used. The following sections discusses three functions defined for slip between steel reinforcement and concrete.

5.2.5.1 CEB-FIP Function

Grassl [3] conducted research using bond-slip to define interaction between concrete and steel using the equations of the European CEB-FIP Model code [1] and compared it with perfect bond. A 3D finite element model was developed for this purpose is LS-DYNA using damage-plasticity constitutive *MAT_CONCRETE_DAMAGE_PLASTIC_MODEL (CDPME) for concrete [1]. Coincident slip approach is introduced by spring in between nodes of steel and concrete and tension stiffening effect was reproduced in bond-slip equation. For this purpose, three orthogonally oriented springs were used to model interaction between steel and concrete. These three springs inserted between the coincident nodes. One spring is aligned with average axial direction of two adjacent beam elements and other two springs are in lateral direction to the beam

axis. To define bond-slip law following equations are used in this study; first part ($s < s_{max}$) is identical to CEB-FIP model requirements, second part ($s \geq s_{max}$) considers *Tmax* remains constant after max slip is reached.

$$T_b = \begin{cases} Tmax\left(\frac{s}{s_{max}}\right)^{0.4} & \text{if } s < s_{max} \\ Tmax & \text{if } s \geq s_{max} \end{cases}$$

The first part of bond-slip function ($s < s_{max}$) is INDE to CEB-FIP Model, s_{max} is the slip at which bond value is reached and $Tmax = 2\sqrt{fc'}$ MPa. Hence, for high strength concrete 15 ksi (103.42 MPa) concrete, $Tmax = 2\sqrt{103.42}$ = 20.27 MPa (2940 psi) and for normal strength concrete 5 ksi (34.47 MPa), $Tmax = 2\sqrt{34.47}$ = 11.60 MPa (1700psi.).

5.2.5.2 CEB-FIP-S3 Function

A study conducted by Grassl [3] studied peak deflection and the residual deflection was neglected. Hence, the second part of bond-slip function ($s \geq s_{max}$) *Tmax* value remains constant. In order to properly define residual deflection a new parameter (S3) is introduced. The new function is defined as follows;

$$T_b = \begin{cases} Tmax\left(\frac{s}{s_{max}}\right)^{0.4} & \text{if } s < s_{max} \\ \frac{Tmax}{S3 - s_{max}}(S3\text{-}s_{max}) & \text{if } s_{max} < s < S3 \end{cases}$$

Here, for coding purpose S3 is defined as 5*s_{max}. Details of the function defined is given in Appendix D.

5.2.5.3 Juan Function

Juan [4] presented a new interface model to define bond-slip behavior between steel and concrete. This model introduced was an extension of already existing semi empirical cyclic bond stress vs. slip low stated in their study. Information of neighboring concrete and bar elements is not required in this model as slip at which peak is reached is completely dependent on the geometric property of the reinforcing bar. This allows the proposed model to be implemented for general-purpose finite element analysis. For validation of proposed model numerical analysis was carried out in ABAQUS software. The bond slip function is defined as follows;

$$T_b = \begin{cases} \dfrac{Tmax}{s_{max}} * s & \text{if } 0 \le s < 0.1\, s_{max} \\ Tmax\,[\,0.25 - 0.15\left(\dfrac{s - s_{max}}{0.9 s_{max}}\right)^4\,] & \text{if } 0.1\, s_{max} < s < s_{max} \\ 0.25\, Tmax & \text{if } s \ge s_{max} \end{cases}$$

Here $Tmax = 1.163\, fc'^{0.75}$ in MPa, hence for high strength concrete 15ksi (103.42 MPa), $Tmax = 1.163 * 15^{0.75}$ = 8.86 MPa (5470 psi) and for normal strength concrete 5ksi (34.47 MPa), $Tmax = 1.163 * 5^{0.75}$= 3.88 MPa (2398 psi), whereas s_{max} is given by 0.07db hence for #3 bar, 0.07* 0.375 = 0.026 in. (0.6604 mm.).

The comparison of these three bond-slip functions with the perfect-bond function is the primary focus of this thesis and the comparison to experimental results is presented in chapter 6.

5.3 Boundary Conditions

In order to replicate experimental conditions, boundary conditions applied on numerical model are described below:

i. Figure 5.4-1 shows the front face of the slab which was restrained for 3 in. in Z-direction after the distance of 3 in. from the top and bottom edge. Similar restraining conditions are applied at back face of the slab.

ii. A single line of nodes in the center of slab was restrained at both top and bottom faces in Y-direction as seen in the isometric view of the slab in Figure 5.4-2.

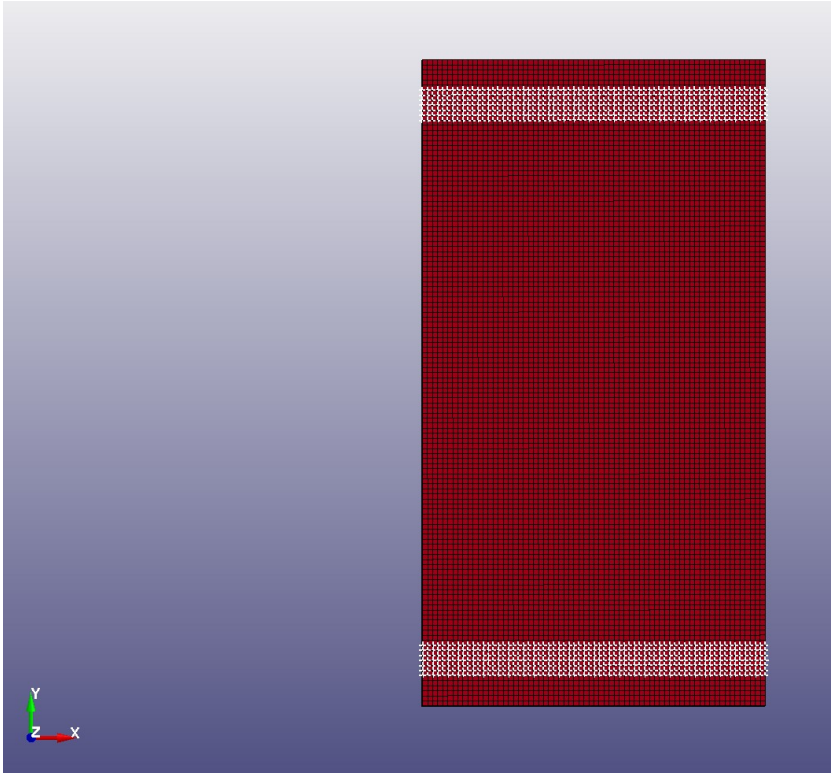

Figure 5.3-1: Boundary conditions on the front and back face of slab

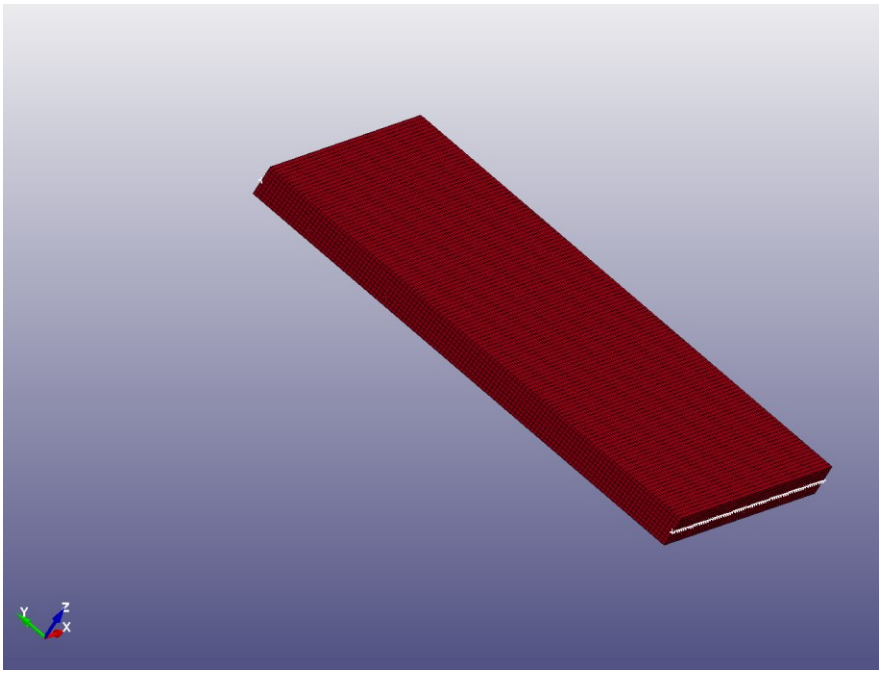

Figure 5.3-2: Boundary conditions on the top and bottom face of the slab

5.4 Material Models in LS-DYNA®

For modeling behavior of concrete in LS-DYNA®, 'simple input' concrete models are available. There simple input parameters are basic strengths obtained from test data. This 'simple input' methods take off the burden of performing too many comprehensive test to obtain various parameters. MAT_WINFRITH_CONCRETE (Mat 084 and Mat 085); MAT_PSEUDO_TENSOR (Mat 016), *MAT_CSCM_CONCRETE (Mat 159) and *MAT_CONCRETE_DAMAGE_REL3 (Mat 072R3), are some of various material models available in material library of LS-DYNA®. *MAT_CONCRETE_DAMAGE_REL3 (Mat 072R3) is used in this study due to availability of input parameter for both High-Strength (11ksi) and Normal-Strength (5ksi) concrete. Use of MAT_WINFRITH_CONCRETE was avoided as initial results obtained did not yield sensible results.

5.4.1 The Concrete Damage Model Release 3

The Concrete Damage Model Release 3 generates model parameter based on unconfined compressive strength of concrete and this is its most significant aspect of this material model. This is done by characterizing most of concrete properties including both plastic and elastic response critical to blast analysis [30]. Only 1 or 2 parameter input values are required to represent the complex material concrete and hence termed as a 'Simple input' model [14] [28]. Although internal parameter generation is available, user can also provide their input parameters which is recommended by Malvar and Schwer in their study [14] if laboratory test data for various parameters required are available. Once parameters are generated for unconfined compressive strength of concrete these generated parameters are written and stored in the LS-DYNA® message file where they can be modified later by the user. Similarly, 'Tabulated Compaction Equation-of-state' (EOS 8) is generated by program for pressure-volume strain response for the model. These parameters are also written and stored in the "messag" file [1]. These parameters obtained are studied and modified and again given as input in keyword file. This keyword file with modified parameters are analyzed using LS-DYNA® manager and LS-PrePost is employed to observe results.

5.4.1.1 The Three-Shear Failure Surfaces in Concrete Damage Model Release 3

The Karagozian and Case (K&C) – Concrete Damage Model Release 3 uses 3-shear failure surfaces, initial yield surface residual failure surface and maximum shear failure surface which makes it a three invariant material model along with incorporating with strain-rate and damage effects. Set of seven cards of model input parameters are required to be defined for this material model along with Equation-of-State for the pressure-volume strain response [1].

Three sets of parameters are used to define these three-failure surface. For maximum shear failure surface (a0, a1, a2), for residual failure surface (a0f, a1f, a2f) and for yield failure surface (a0y, a1y, a2y). Generally, a plot comprising stress difference and mean stress as two axes is used to demonstrate results of triaxial compression test, which is used to measure compressive shear strength. Following equation (10) represents equation of graph.

Von mises stress = (axial stress-lateral stress) =a0+((mean stress)/ (a1+(a2*mean stress)))

……. Equation (10)

Hence all 8 parameters in three fixed surfaces are defined as follows [13]

……. Equation (11)

$$\Delta\sigma_m = a0 + \frac{p}{a1 + a2 * \mathrm{p}}$$ (maximum failure surface)

$$\Delta\sigma_r = \frac{p}{a_{1f} + a_{2f} * \mathrm{p}}$$ (residual failure surface)

$$\Delta\sigma_y = a_{0y} + \frac{p}{a_{1y} + a_{2y} * \mathrm{p}}$$ (yield failure surface)

Here p is pressure in an element and $\Delta\sigma$ difference in principal stress in an element.

For a particular type of concrete, maximum shear failure surface parameter value is given as input for the variables a0, a1 and a2. The unconfined compressive strength fc' is provided as input in place of a0 with negative sign to represent compression if experimental data is not available. Using this value program automatically generates parameters for given model which are written and stored in "messag" file.

5.4.1.2 The tensile strength of concrete

Based upon unconfined compressive strength input of tensile strength of concrete can be designated. This is achieved by relationship described below which is based on CEB-FIP Model Code 1990 as used by Malvar and Schwer [11];

$$f_t = 1.58 * \left(\frac{fc'^2}{a_0}\right)^{\frac{1}{3}}$$

……...Equation (12)

According to equation 12 relation tensile strength for unconfined compressive strength of 11.6 ksi concrete is 7.832 ksi and for 5 ksi unconfined compressive strength, tensile strength is 4.62 ksi. Some tensile strength values are obtained using automatic parameter generation method for The Karagozian and Case (K&C) – Concrete Damage Model Release 3 model are written in 'messag' file.

5.4.1.3 Equation of State for Concrete Damage Model Release 3

In order to provide pressure and volume strains Concrete Damage Model release 3 employs an Equation of state. Study conducted by Malvar and Schwer [11] concluded that in comparison with laboratory data for 46.5 MPa, concrete response of Concrete Damage Model 3 gives less values in comparison to experimental records. Hence, in order to avoid variability in volumetric response for concrete (Equation of State), calibration of this material model is required for specific material. Thus, use of pressure-volume strain data is required for particular concrete material. The laboratory data available for 11.6 ksi concrete and 5 ksi concrete is shown in Figure 5.5-1 and 5.5-2 respectively and these values are default parameters are replaced with these values in 'messag' file [2]. The Equation of state thus obtained is provided as new input

in keyword file, in *EOS_TABULATED_COMPACTION keyword. Up to 10 points of pressure vs. volume can be entered in this keyword. In *PART card for pressure-volume data, EOSID=8 is recommended in LS-DYNA® keyword manual and this EOSID should be same as ID parameter for *EOS keyword [1]. Appendix D gives details of EOS in *PART form and Appendix C gives input parameters for the Concrete Damage Model Release3 for both types of concrete.

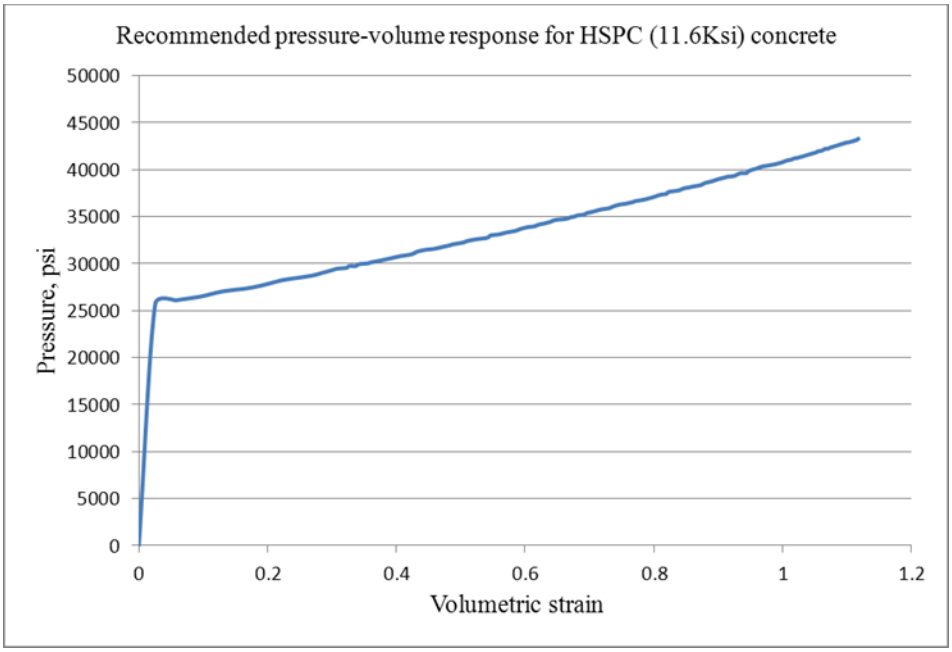

Figure 5.4-1: Pressure versus volumetric strain curve for Equation of state Form 8 with compaction for 11.6 Ksi concrete

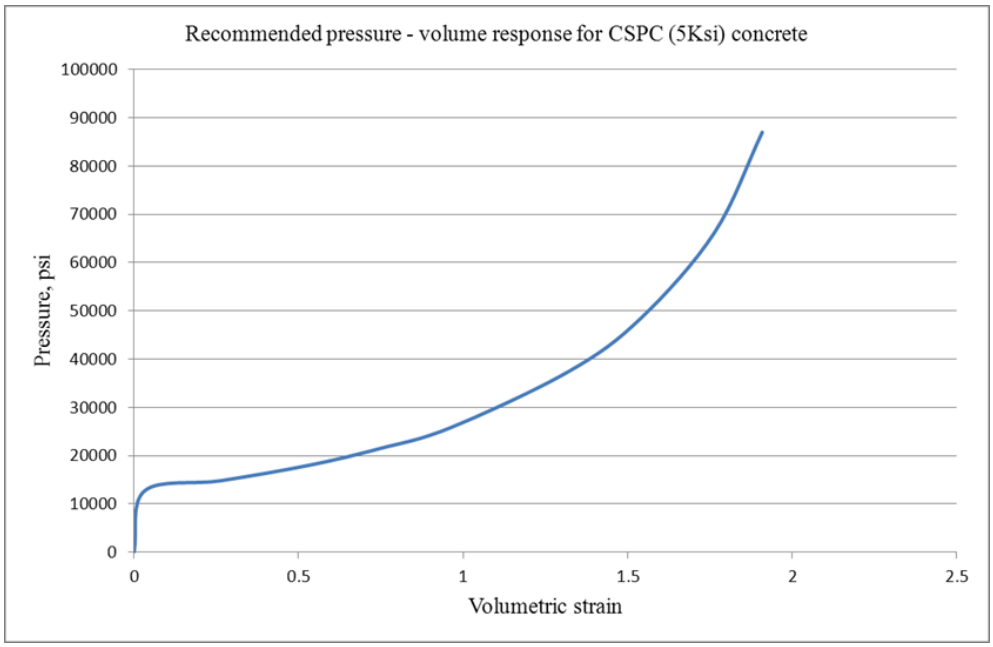

Figure 5.4-2: Pressure versus volumetric strain curve for Equation of state Form 8 with compaction for 5 Ksi concrete

5.4.2 The Plastic Kinematic Model for Steel

In this study in order to model steel reinforcement, the elastic-plastic Plastic Kinematic material model was selected. Krieg and Key developed this model, which contains options to include rate effects and at the same time is suitable for kinematic and isotropic hardening plasticity [1]. Hence, to specify Kinematic, Isotropic or combination of Kinematic and Isotropic hardening, parameter Beta is varied between $0 < \beta < 1$. Young's modulus, Tangent modulus, Yield strength, mass density and Poisson's ratio are other parameters to be specified for defining material properties of steel and this input parameter are tabulated in Appendix C for two types of steel.

5.5 Blast Load Application in LS-DYNA®

Blast wave is an explosion phenomenon in which sudden rise of energy in the atmosphere occurs which leads to change in pressure. This generated wave due to change in

pressure propagates in all direction emerging form source at very high speed. Nature of explosion and distance of point of consideration form source of explosion are factors which determine magnitude and shape of blast wave at desired point.

A shock tube is used to generate pressure which is equivalent to pressure generated by blast wave. Shock wave facilitates sudden rise in pressure above ambient pressure which later leads to gradual fall below ambient pressure which results in negative pressure wave. This can be used to define parameters of blast wave. Peak side-on positive overpressure P_{so}, with positive phase duration t_d and corresponding positive impulse I_o are parameter of blast waves to be used. negative phase of same parameter are denoted by P_{so}^-, t_d^- and I_o^- respectively.

In order to define blast wave in an accurate manner it is important to define these blast wave parameters in finite element analysis which replicates blast phenomenon of shock tube. To define the load curve and slab surface interaction in LS-DYNA®, *LOAD_SEGMENT_SET keyword is employed along with *DEFINE_CURVE which is used for pressure vs. time co-ordinates. Appendix B illustrates pressure versus time history with impulse values for all 12 slabs whereas figure B-1 to B-12 shows all load curves applied to the front face of respective slabs.

Thus, using various parameters and keywords of LS-DYNA®, numerical modeling of 12 reinforced concrete slabs are achieved. All simulation are completed using LS manager and later LS post processor is used for obtaining results of these simulations. Results which are important for this thesis, are mid-span deflection time histories for all bond relations between concrete and steel. Results from numerical simulations are presented in the following chapter.

CHAPTER 6. NUMERICAL ANALUSIS RESULTS AND COMAPRISON WITH EXPERIMENTAL

In this chapter experimental records are compared with numerical simulation results obtained from LS-DYNA®. The criterion used for comparison is peak deflection history. Numerical simulations were performed on twelve slabs of two different material strength, two separate reinforcement ratios and two types of bond relations are compared in this chapter.

Since Beam in Solid formulation is being investigated in this study, the parameters of this new keyword are compared, and four slabs consisting of different slab setups are studied for this purpose. Firstly, the effect of boundary conditions are investigated followed by a study of the effect of mesh analysis.

6.1 Study NCOUP Parameter of Beam in Solid Formulation

Effects of this parameter is studied on various Beam Bond functions. NCOUP parameters refers to Number of coupling points generated in one beam element. If set to 0, coupling only happens at beam nodes. Otherwise, coupling is done at both the beam nodes and those automatically generated coupling points. Following study is for the three functions used to defined Beam Bond slip, with variation in NCOUP parameter.

Four slabs are selected which bring all variation of material strengths and main steel spacing among 12 slabs of this study. Each function data is presented for these 4 slabs.

6.1.1 NCOUP parametric study with JUAN function

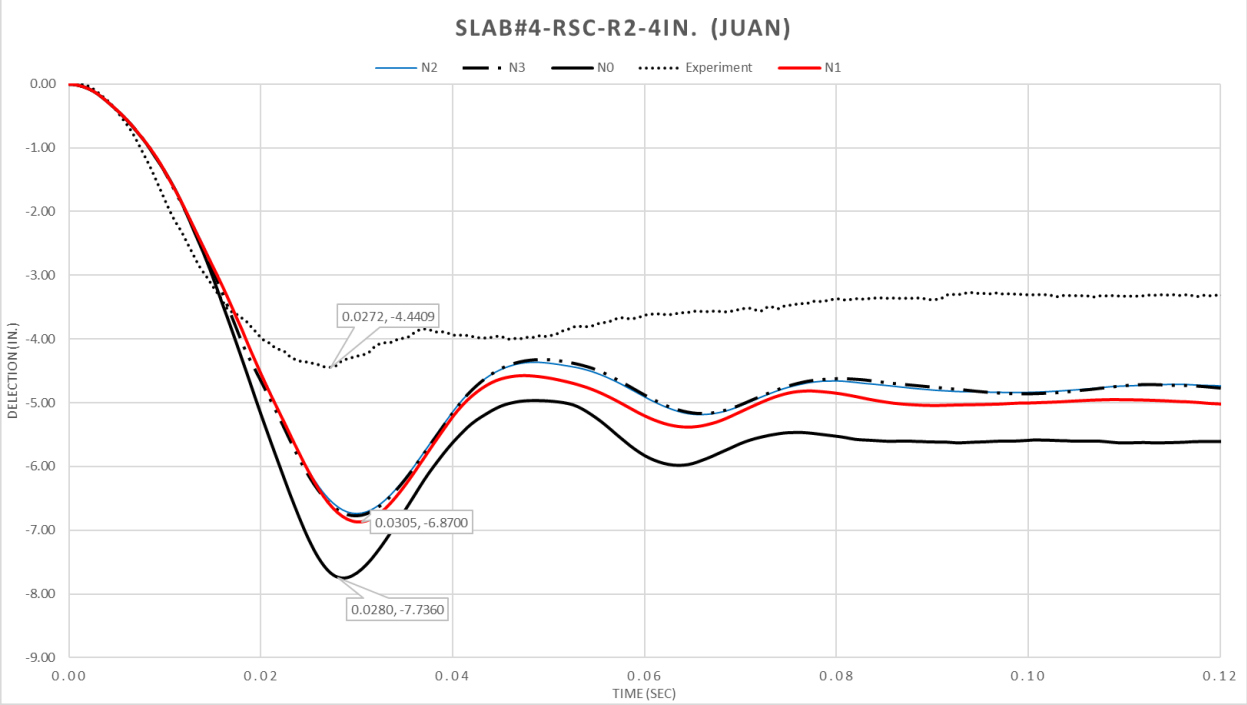

Figure 6.1-1: Deflection Comparison between NCOUP parameter of Constrained Beam-Bond Parameter with Juan function for CDR3 concrete model of 1 in. (24.4 mm.) mesh model with Experimental Deflection for Slab#4-RSC-R2-4in.

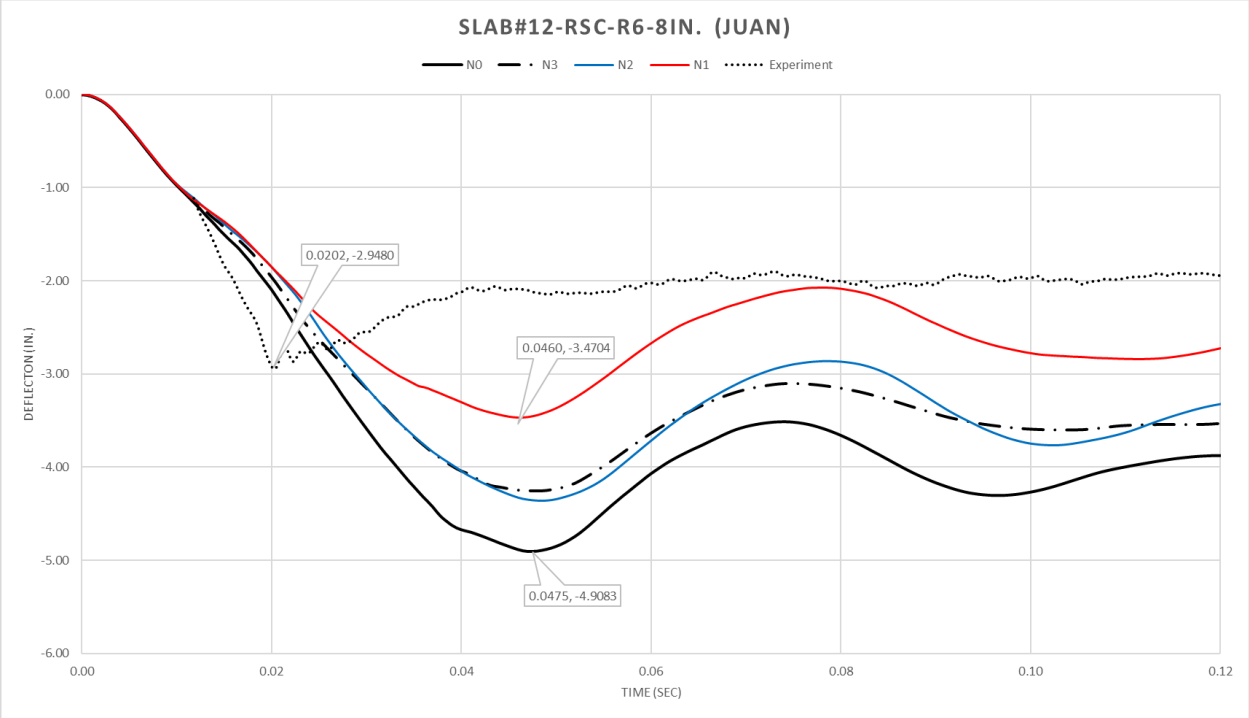

Figure 6.1-2: Deflection Comparison between NCOUP parameter of Constrained Beam-Bond Parameter with Juan function for CDR3 concrete model of 1 in. (24.4 mm.) mesh model with Experimental Deflection for Slab#12-RSC-R2-8in.

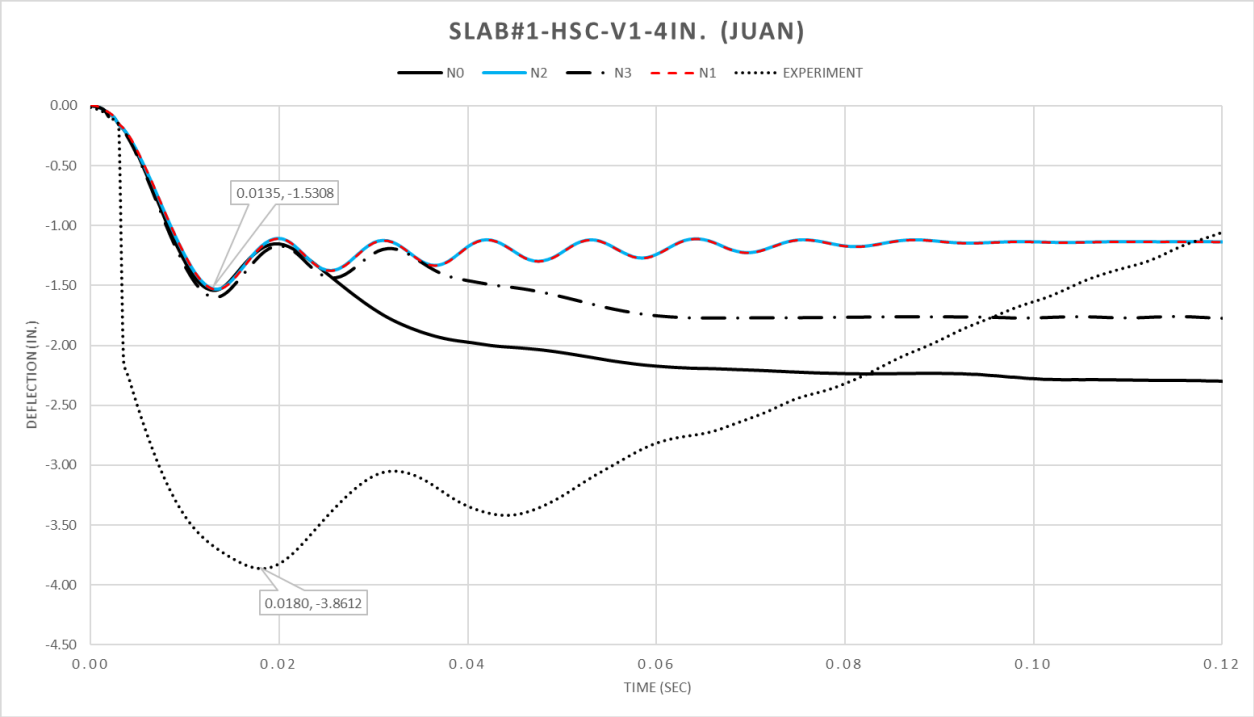

Figure 6.1-3: Deflection Comparison between NCOUP parameter of Beam-Bond Parameter with Juan function for CDR3 concrete model of 1 in. (24.4 mm.) mesh model with Experimental Deflection for Slab#1-HSC-V2-4in.

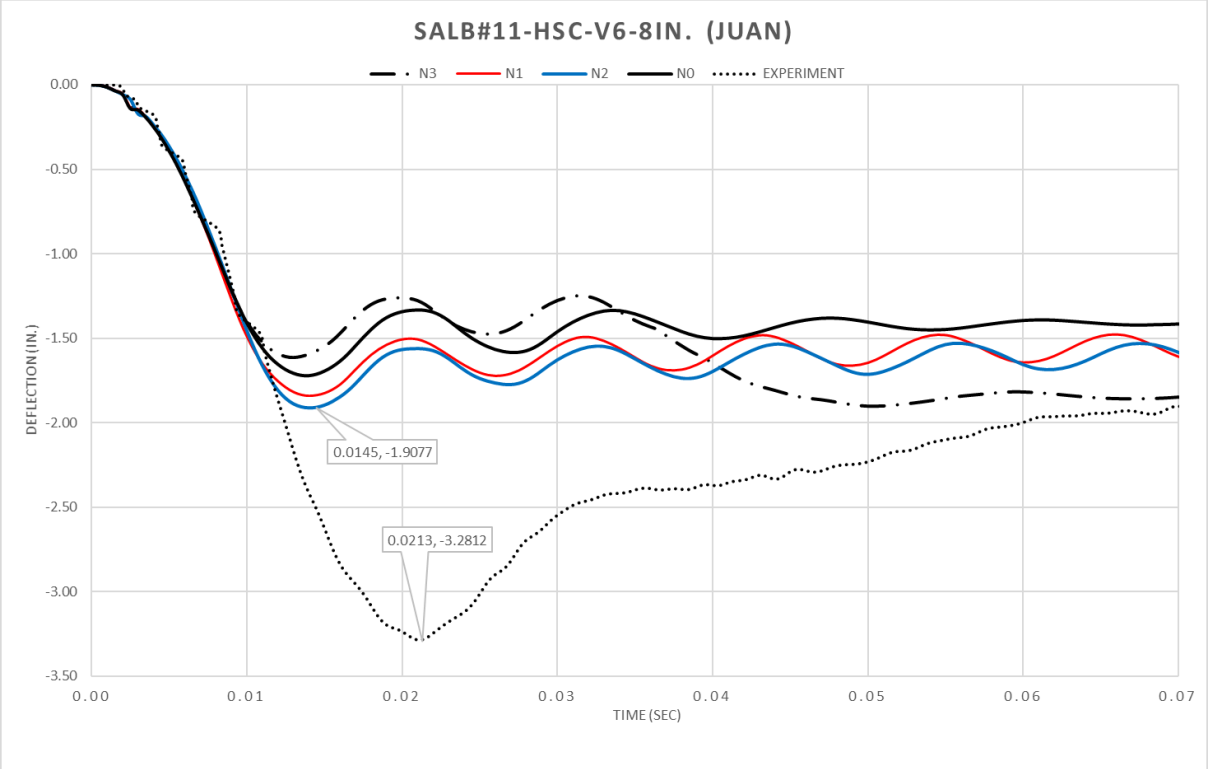

Figure 6.1-4: Deflection Comparison between NCOUP parameter of Constrained Beam-Bond Parameter with Juan function for CDR3 concrete model of 1 in. (24.4 mm.) mesh model with Experimental Deflection for Slab#11-HSC-V6-4in.

Juan Function (NCOUP)	Slab 1 HSC-V1-4IN		Slab 11 HSC-V6-IN		Slab 4 RSC-R2-4IN		Slab 4 RSC-R2-8IN	
	Expi.	N.S.	Expi.	N.S.	Expi.	N.S.	Expi.	N.S.
N0	3.85	1.54	3.28	1.73	4.43	7.75	2.94	4.9
N1		1.53		1.84		6.87		3.46
N2		1.53		1.91		6.74		4.36
N3		1.6		1.16		6.78		4.26

Expi : Experiment data, N.S. : Numerical Simulation results

Table 6-1:NCOUP parameter variation results for Juan function

6.1.2 NCOUP parametric study with CIB-FIP function

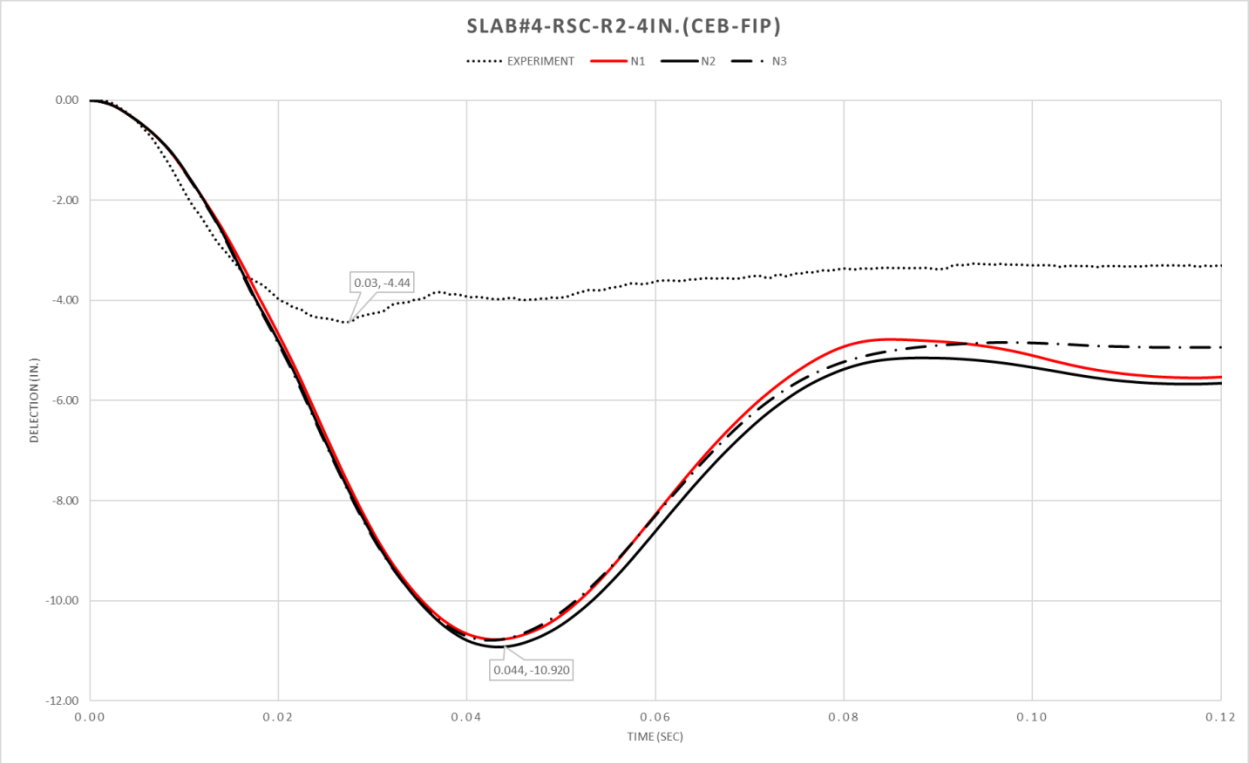

Figure 6-7: Deflection Comparison between NCOUP parameter of Constrained Beam-Bond Parameter with CEB-FIP function for CDR3 concrete model of 1 in. (24.4 mm.) mesh model with Experimental Deflection for Slab#4-RSC-R2-4in.

CEB-FIP Function (NCOUP)	Slab 1 HSC-V1-4IN		Slab 11 HSC-V6-IN		Slab 4 RSC-R2-4IN		Slab 4 RSC-R2-8IN	
	Expi.	N.S.	Expi.	N.S.	Expi.	N.S.	Expi.	N.S.
N1	3.85	6.75	3.28	1.01	4.43	10.8	2.94	4.20
N2		2.17		2.20		10.9		4.13
N3		2.41		3.84		10.8		3.67

Expi : Experiment data, N.S. : Numerical Simulation results

Table 6-2:NCOUP parameter variation results for CEB-FIP function

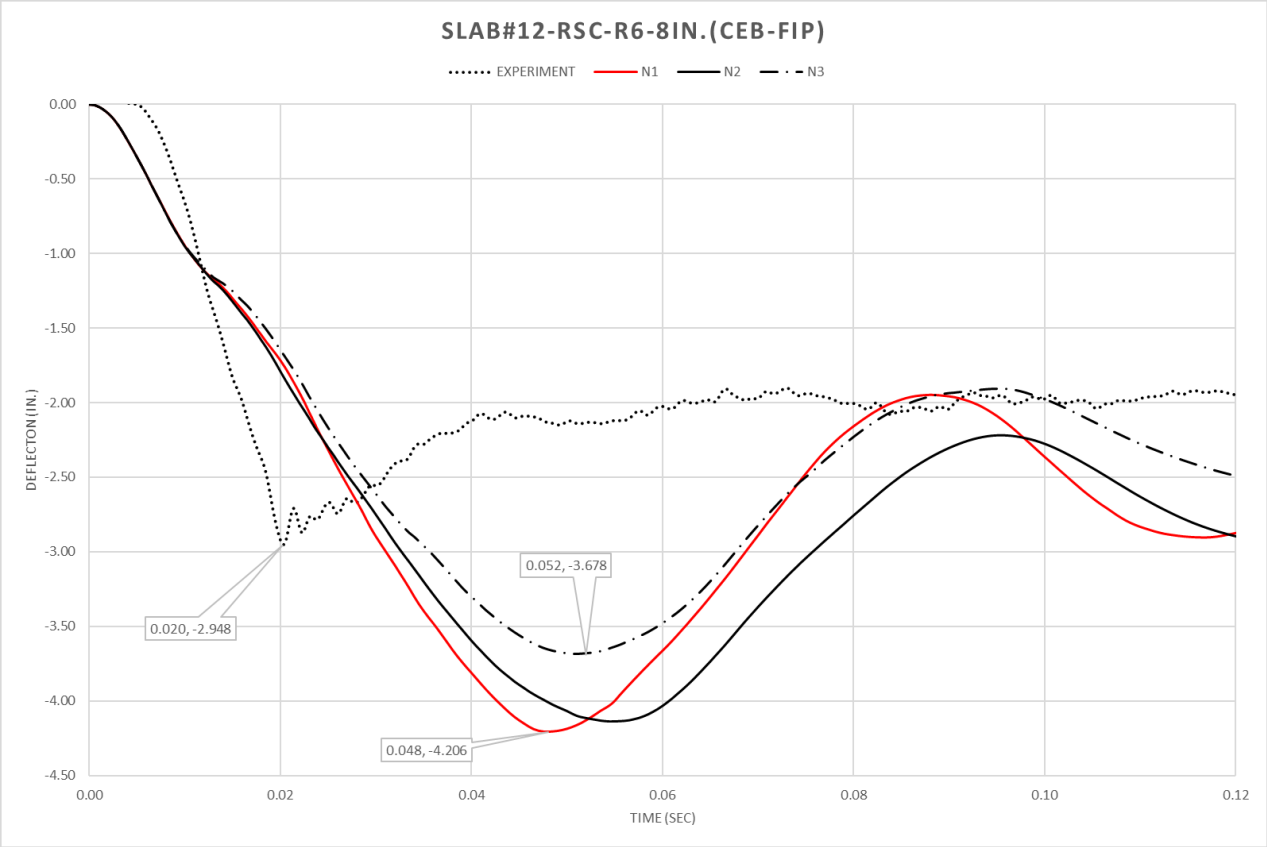

Figure 6.1-5: Deflection Comparison between NCOUP parameter of Constrained Beam-Bond Parameter with CEB-FIP function for CDR3 concrete model of 1 in. (24.4 mm.) mesh model with Experimental Deflection for Slab#12-RSC-R2-8in.

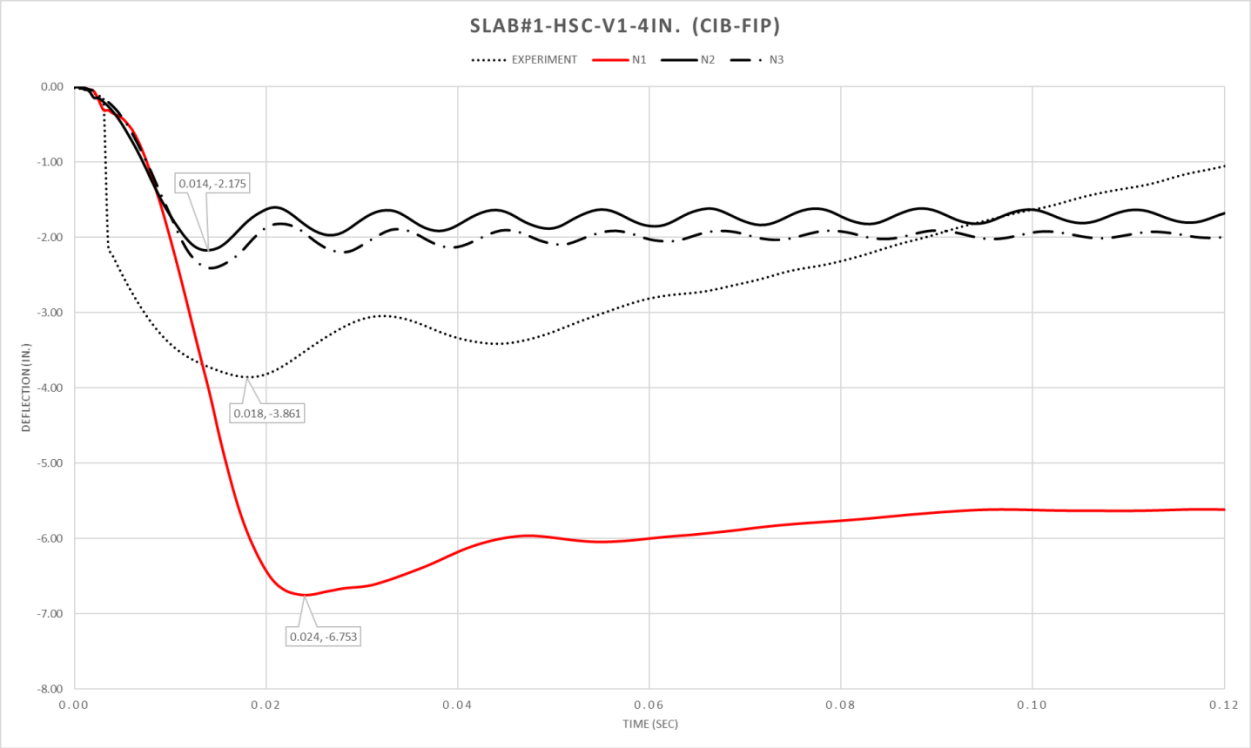

Figure 6.1-6: Deflection Comparison between NCOUP parameter of Beam-Bond Parameter with CIP-FIP function for CDR3 concrete model of 1 in. (24.4 mm.) mesh model with Experimental Deflection for Slab#1-HSC-V2-4in.

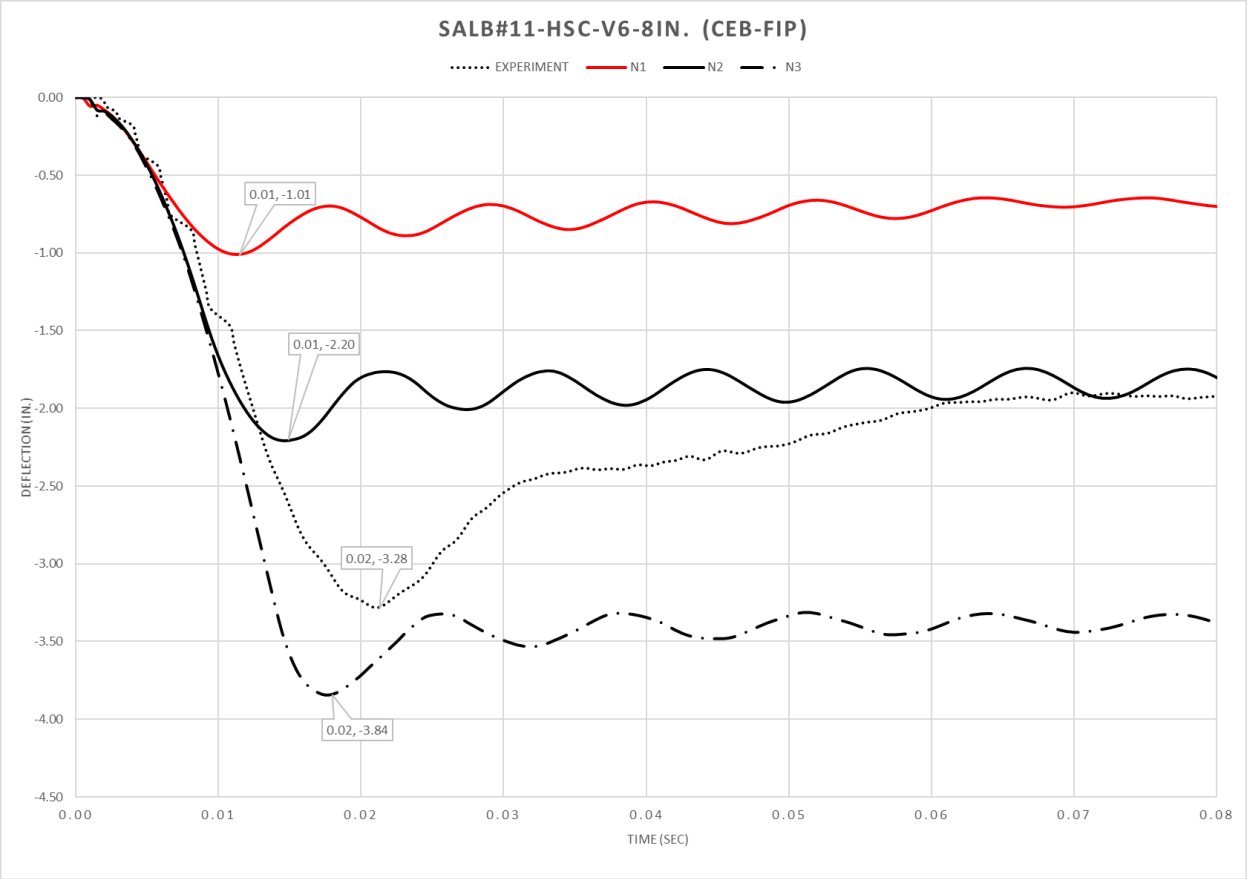

Figure 6.1-7: Deflection Comparison between NCOUP parameter of Constrained Beam-Bond Parameter with CEB-FIP function for CDR3 concrete model of 1 in. (24.4 mm.) mesh model with Experimental Deflection forSlab#11-HSC-V6-4in.

6.1.3 NCOUP parametric study with CIB-FIP-S3 function

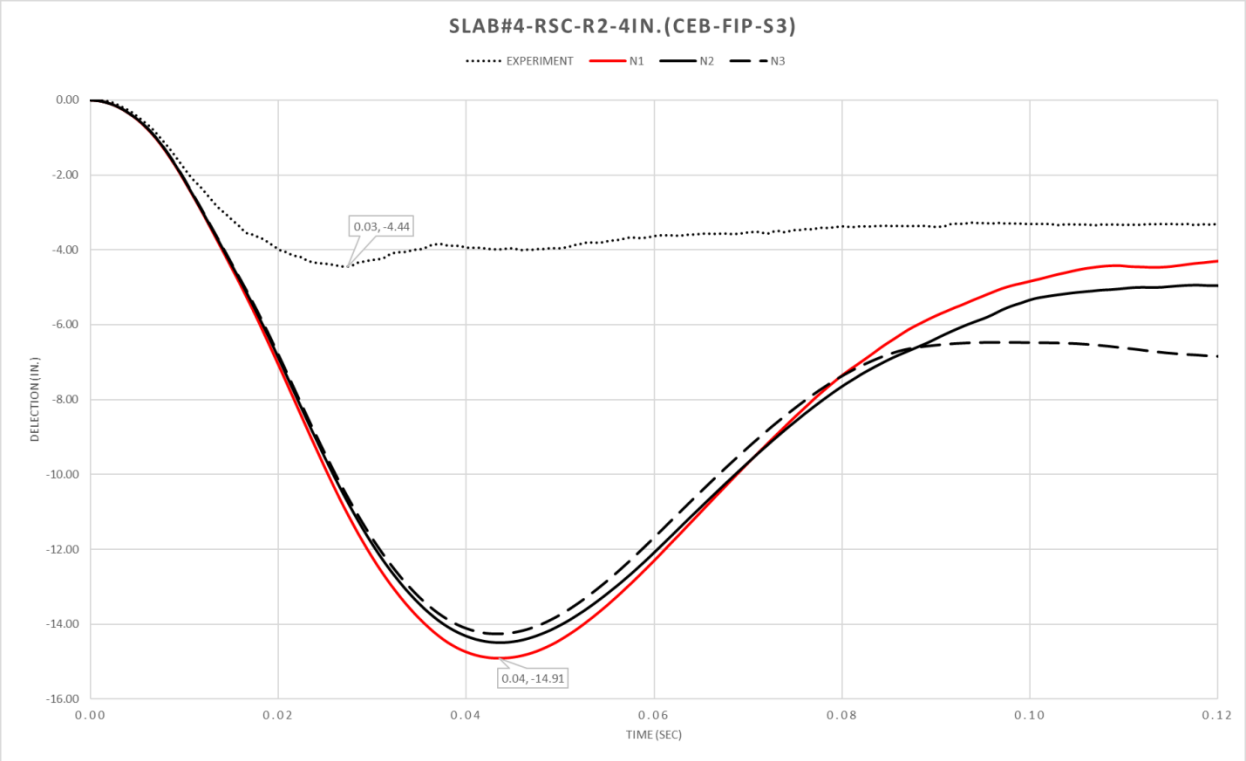

Figure 6.1-8: Deflection Comparison between NCOUP parameter of Constrained Beam-Bond Parameter with CEB-FIP-S3 function for CDR3 concrete model of 1 in. (24.4 mm.) mesh model with Experimental Deflection for Slab#4-RSC-R2-4in.

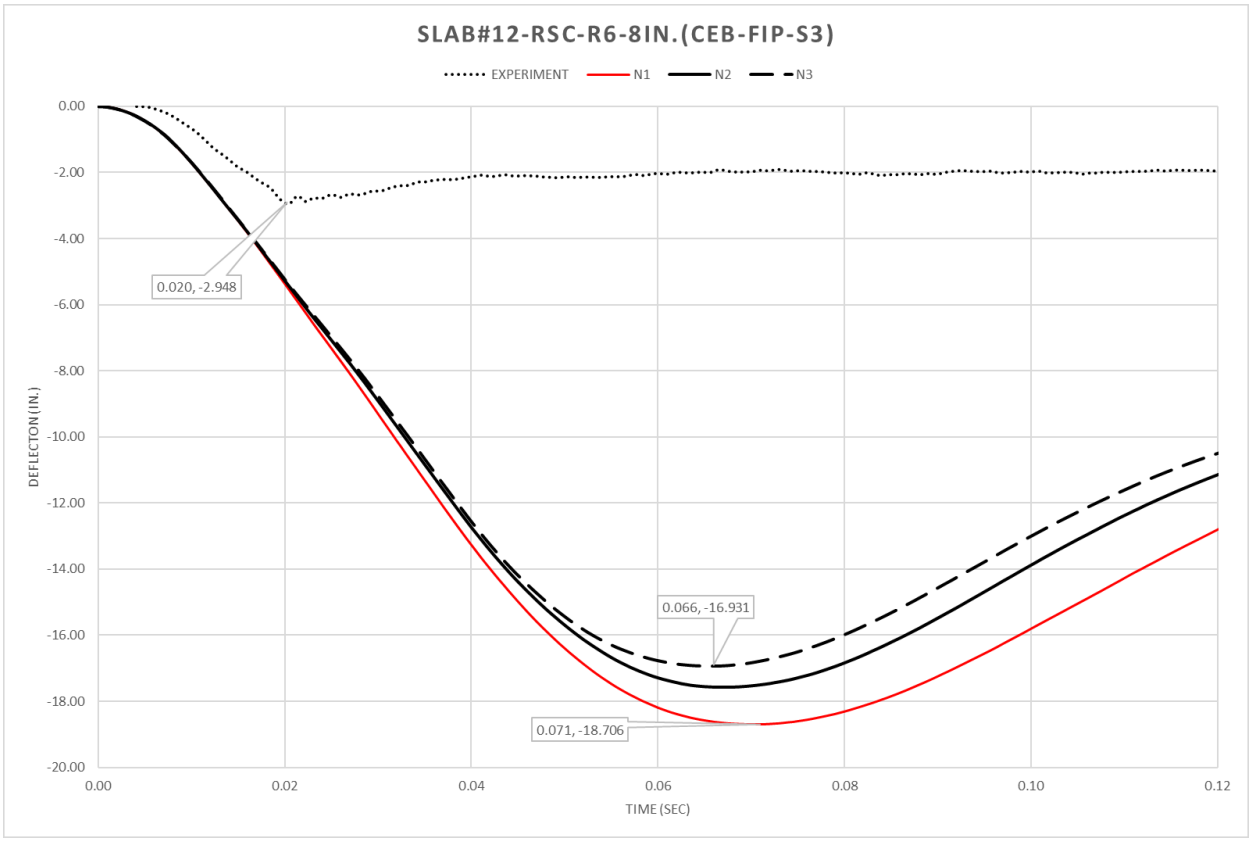

Figure 6.1-9: Deflection Comparison between NCOUP parameter of Constrained Beam-Bond Parameter with CEB-FIP-S3 function for CDR3 concrete model of 1 in. (24.4 mm.) mesh model with Experimental Deflection for Slab#12-RSC-R2-8in.

CEB-FIP-S3 Function (NCOUP)	Slab 1 HSC-V1-4IN		Slab 11 HSC-V6-IN		Slab 4 RSC-R2-4IN		Slab 4 RSC-R2-8IN	
	Expi.	N.S.	Expi.	N.S.	Expi.	N.S.	Expi.	N.S.
N1	3.85	3.03	3.28	2.63	4.43	14.9	2.94	18.7
N2		2.05		2.03		14.5		17.6
N3		3.26		2.00		14.2		19.8

Expi : Experiment data, N.S. : Numerical Simulation results

Table 6-3:NCOUP parameter variation results for CEB-FIP-S3 function

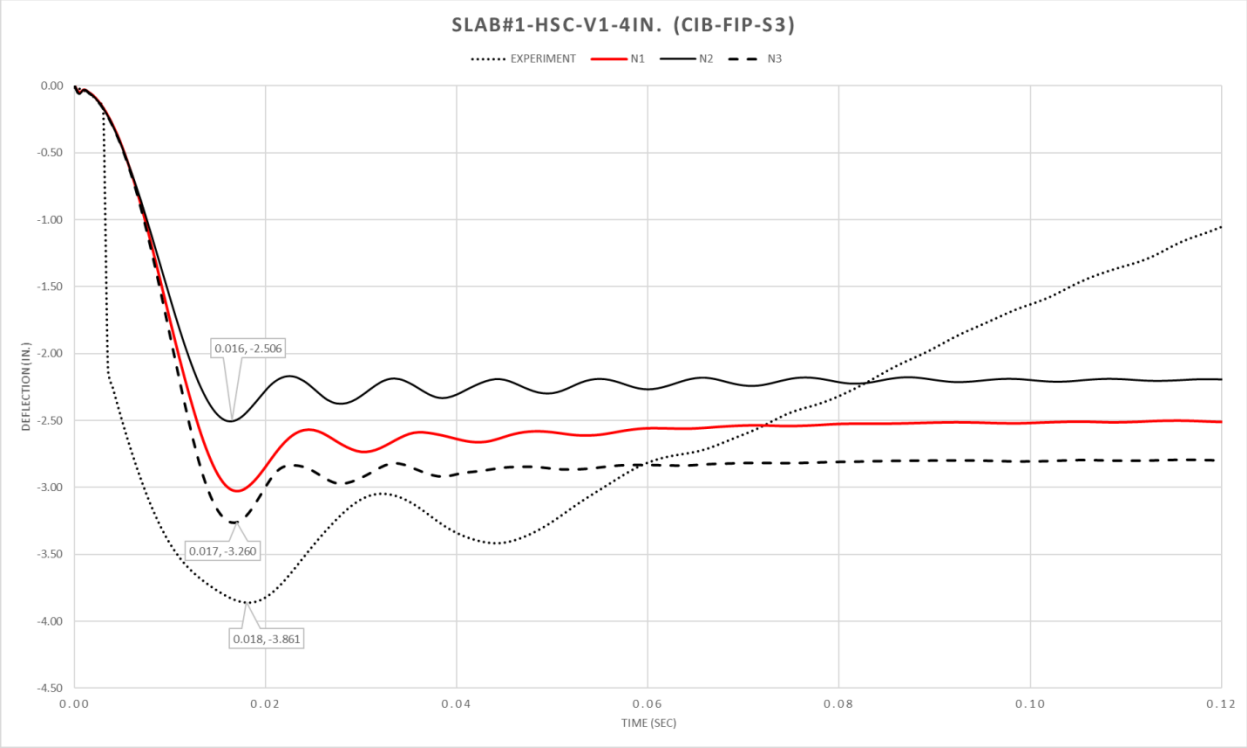

Figure 6.1-10: Deflection Comparison between NCOUP parameter of Beam-Bond Parameter with CIP-FIP-S3 function for CDR3 concrete model of 1 in. (24.4 mm.) mesh model with Experimental Deflection for Slab#1-HSC-V2-4in.

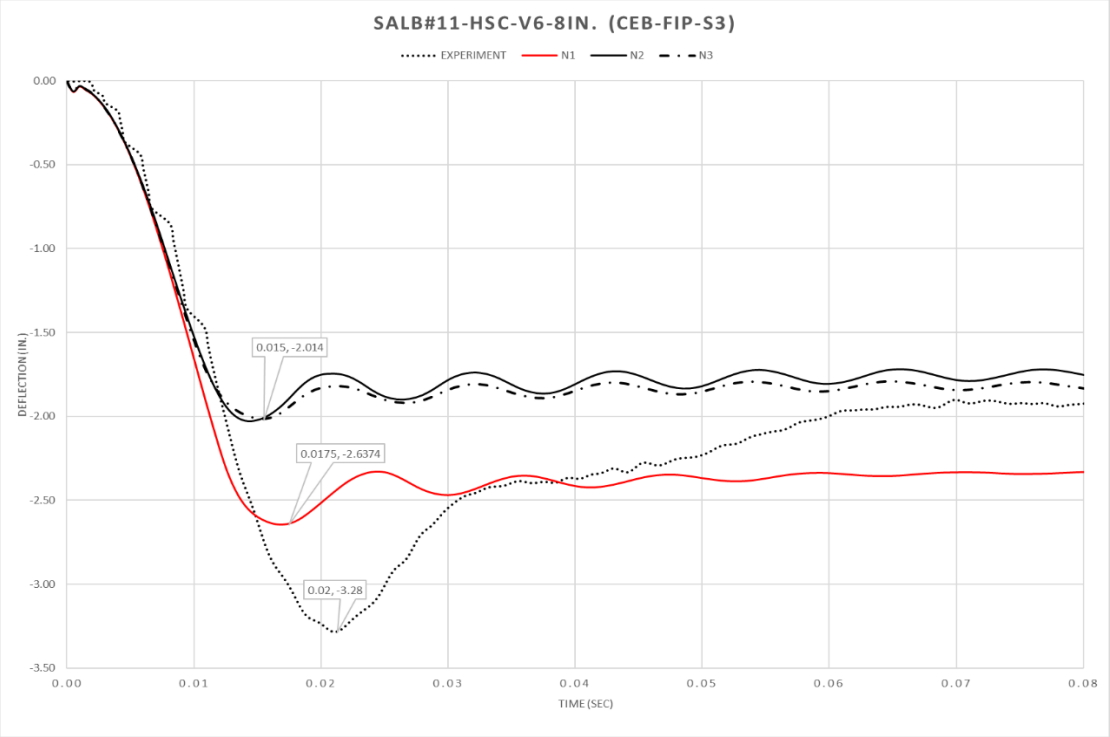

Figure 6.1-11: Deflection Comparison between NCOUP parameter of Constrained Beam-Bond Parameter with CEB-FIP-S3 function for CDR3 concrete model of 1 in. (24.4 mm.) mesh model with Experimental Deflection forSlab#11-HSC-V6-4in.

6.2 High Strength Concrete with High Strength Steel Slabs (HSC-V)

The first set of slabs studied here are the ones having combination of high strength concrete reinforced with regular strength steel (HSC-V). The deflection-time histories for each of the 6 slabs are represented in this section. The comparison is made between two mesh sizes i.e. 1" and 0.5" for each of the two constrains and their functions with experimental peak deflection are given in this section.

6.2.1 Mesh size effect on Slab # 1 (HSC-V1-4in.)

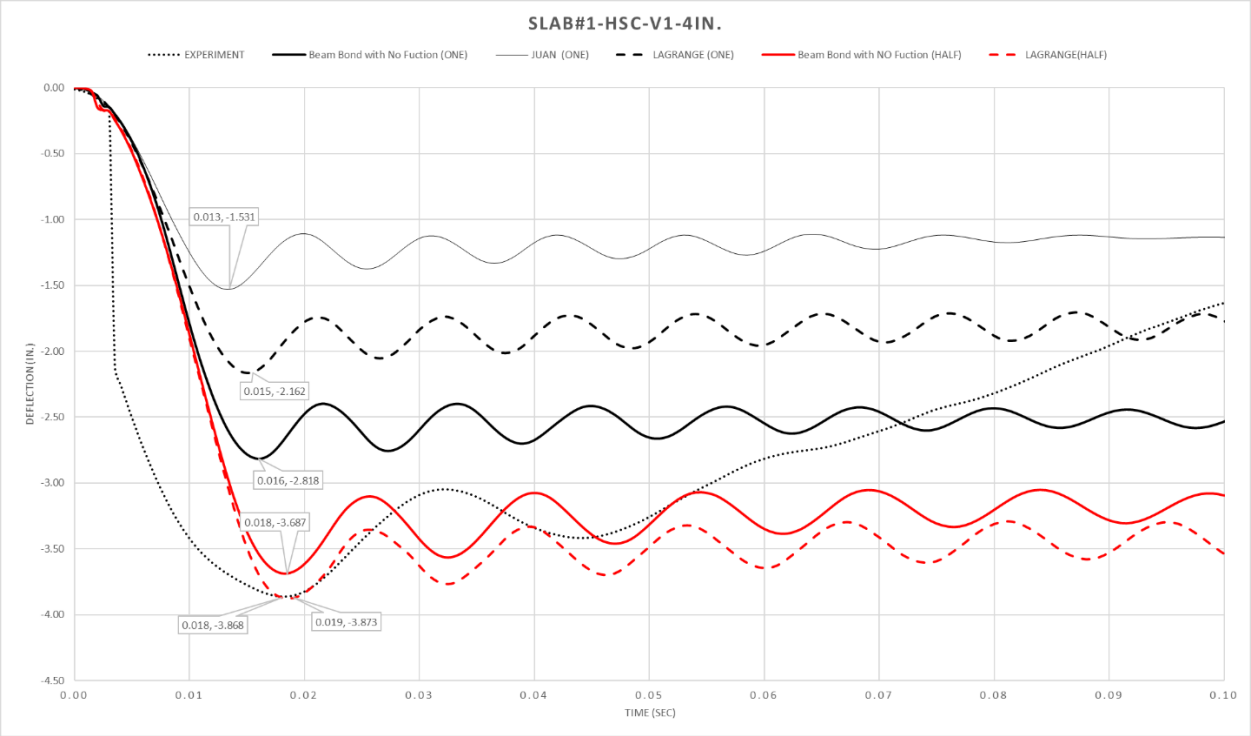

Figure 6.2-1 : Deflection Comparison between 1 in. (25.4 mm.) and 0.5 in. (12.7 mm.) for Constrained Lagrange and Beam in solid with no defined function and Juan function with Experimental Deflection for Slab#1– HSC-V1-4in.

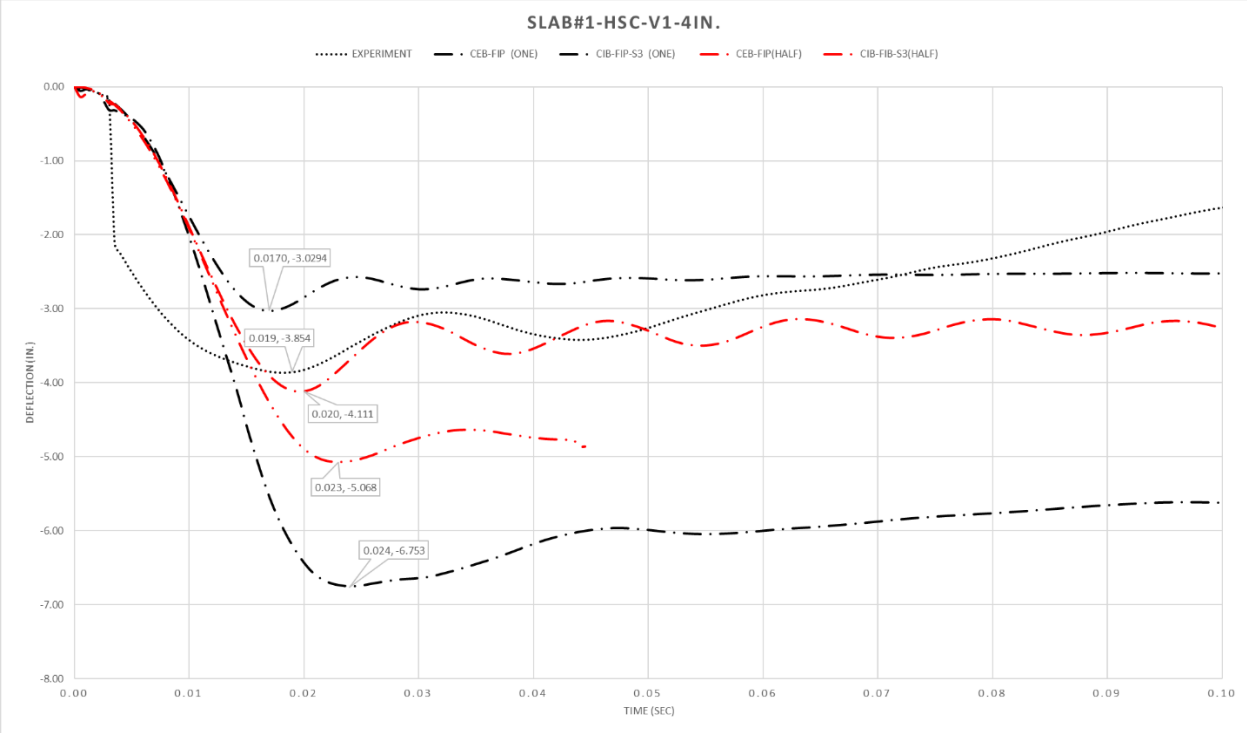

Figure 6.2-2: Deflection Comparison between 1 in. (25.4 mm.) and 0.5 in. (12.7 mm.) for CEB-FIP and CEB-FIP-S3 functions and Experimental Deflection for Slab#1– HSC-V1-4in.

SLAB#1 HSC-V1-4IN	Peak Deflection			% Change Compared to Experimental		% Change for Mesh Size reduction form 1in. to 1/2in.
	1in.	1/2in.	Experiment	1in.	1/2in.	
Lagrange_IN_Solid	2.16	3.87	3.85	↓44%	↑0.5%	↑79%
Beam_IN_Solid						
No User Function	2.81	3.68	3.85	↓27%	↓4.4%	↑31%
Juan	1.53	**	3.85	↓60%	**	**
CEB-FIP	6.75	4.11	3.85	↑75%	↑6.7%	↓39%
CEB-FIP-S3	3.02	5.06	3.85	↓21.5%	↑31.5%	↑67.54%

Table 6-4: Numerical Simulation Results for Slab#1 HSC-V1-4IN.

6.2.2 Mesh size effect on Slab # 3 (HSC-V2-4in.)

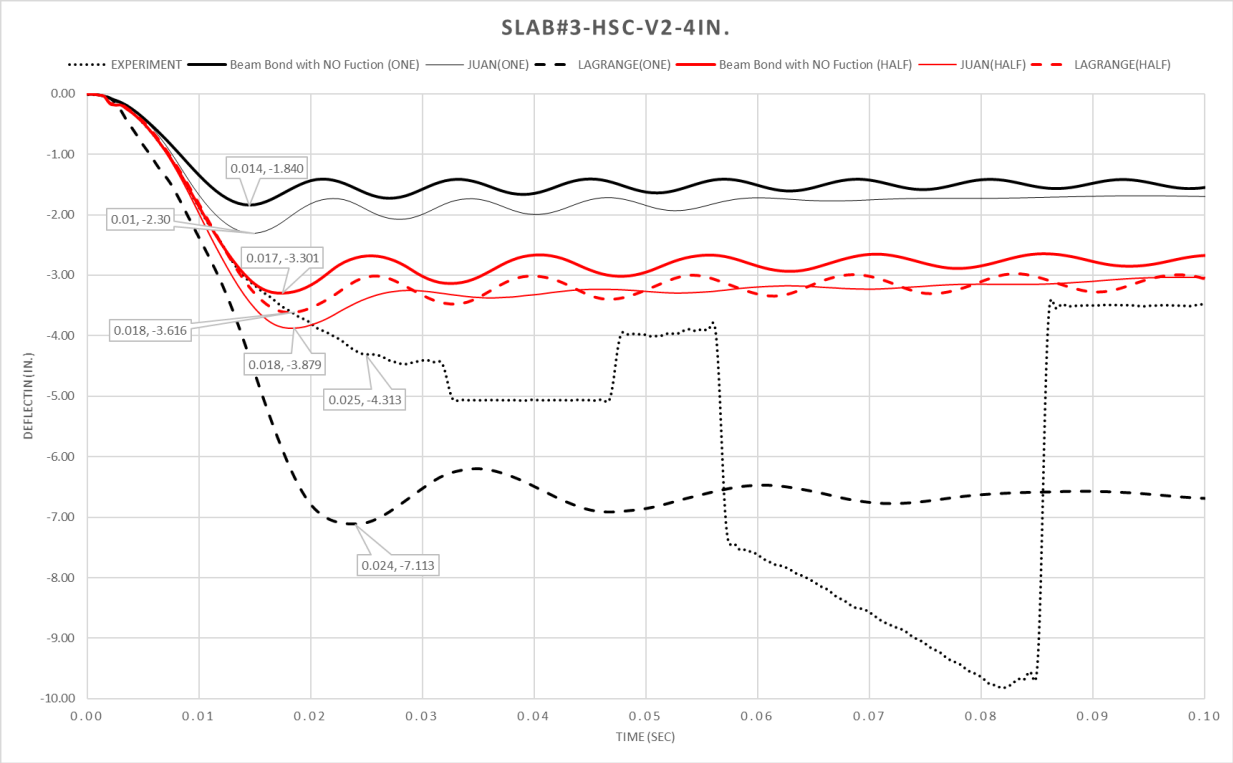

Figure 6.2-3: Deflection Comparison between 1 in. (25.4 mm.) and 0.5 in. (12.7 mm.) for Constrained Lagrange and Beam in solid with no defined function and Juan function with Experimental Deflection for Slab#3– HSC-V2-4in.

SLAB#3 HSC-V2-4IN	Peak Deflection			% Change Compared to Experimental		% Change for Mesh Size reduction form 1in. to 1/2in.
	1in.	1/2in.	Experiment	1in.	1/2in.	
Lagrange_IN_Solid	7.11	3.87	4.31	↑65%	↑0.5%	↑79%
Beam_IN_Solid						
No User Function	1.84	3.3	4.31	↓57%	↓23%	↑79%
Juan	2.3	3.87	4.31	↓46%	↓10%	↑68%
CEB-FIP	1.78	4.10	4.31	↓59%	↓5%	↑130%
CEB-FIP-S3	1.97	4.6	4.31	↓54%	↑6.7%	↑133.5%

Table 6-5: Numerical Simulation Results for Slab#3, HSC-V2-4IN.

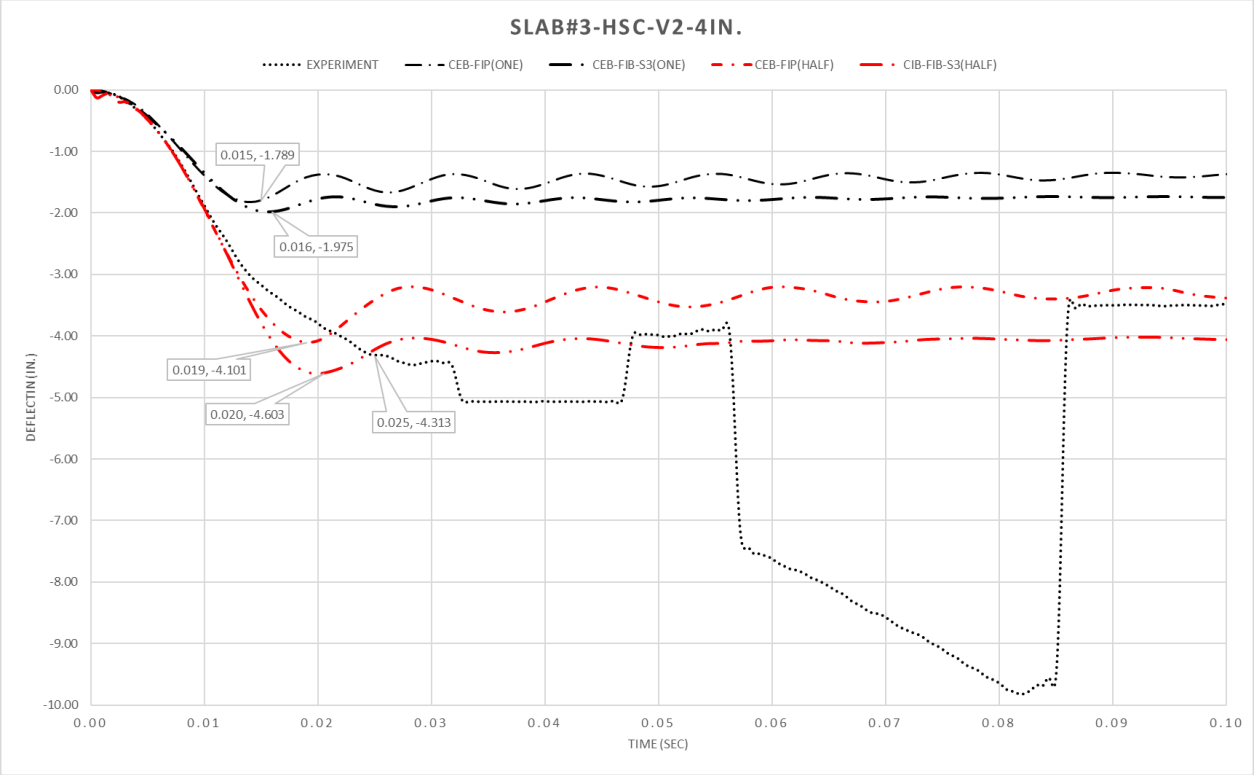

Figure 6.2-4: Deflection Comparison between 1 in. (25.4 mm.) and 0.5 in. (12.7 mm.) for CEB-FIP and CEB-FIP-S3 functions and Experimental Deflection for Slab#3– HSC-V2-4in.

6.2.3 Mesh size effect on Slab # 5 (HSC-V3-4in.)

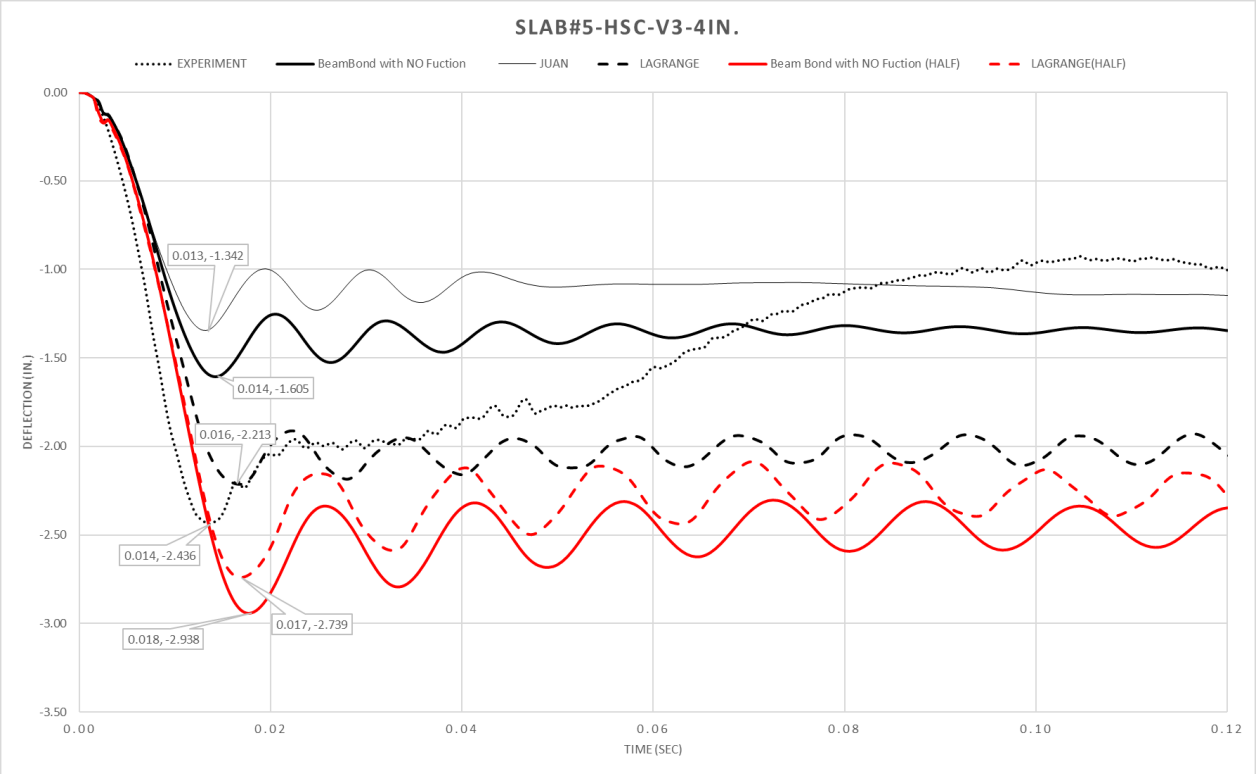

Figure 6.2-5: Deflection Comparison between 1 in. (25.4 mm.) and 0.5 in. (12.7 mm.) for Constrained Lagrange and Beam in solid with no defined function and Juan function with Experimental Deflection for Slab#5– HSC-V3-4in.

SLAB#5 HSC-V3-4IN	Peak Deflection			% Change Compared to Experimental		% Change for Mesh Size reduction form 1in. to 1/2in.
	1in.	1/2in.	Experiment	1in.	1/2in.	
Lagrange_IN_Solid	2.21	2.73	2.43	↓9%	↑23.5%	↑23.5%
Beam_IN_Solid						
No User Function	1.6	2.93	2.43	↓34%	↑20.5%	↑83%
Juan	1.34	**	2.43	↓44%	**	**
CEB-FIP	1.31	3.22	2.43	↓46%	↑32.5%	↑146%
CEB-FIP-S3	1.77	3.77	2.43	↓27%	↑55%	↑123%

** Negative volume in elements terminated the analysis

Table 6-6: Numerical Simulation Results for Slab#5, HSC-V3-4IN.

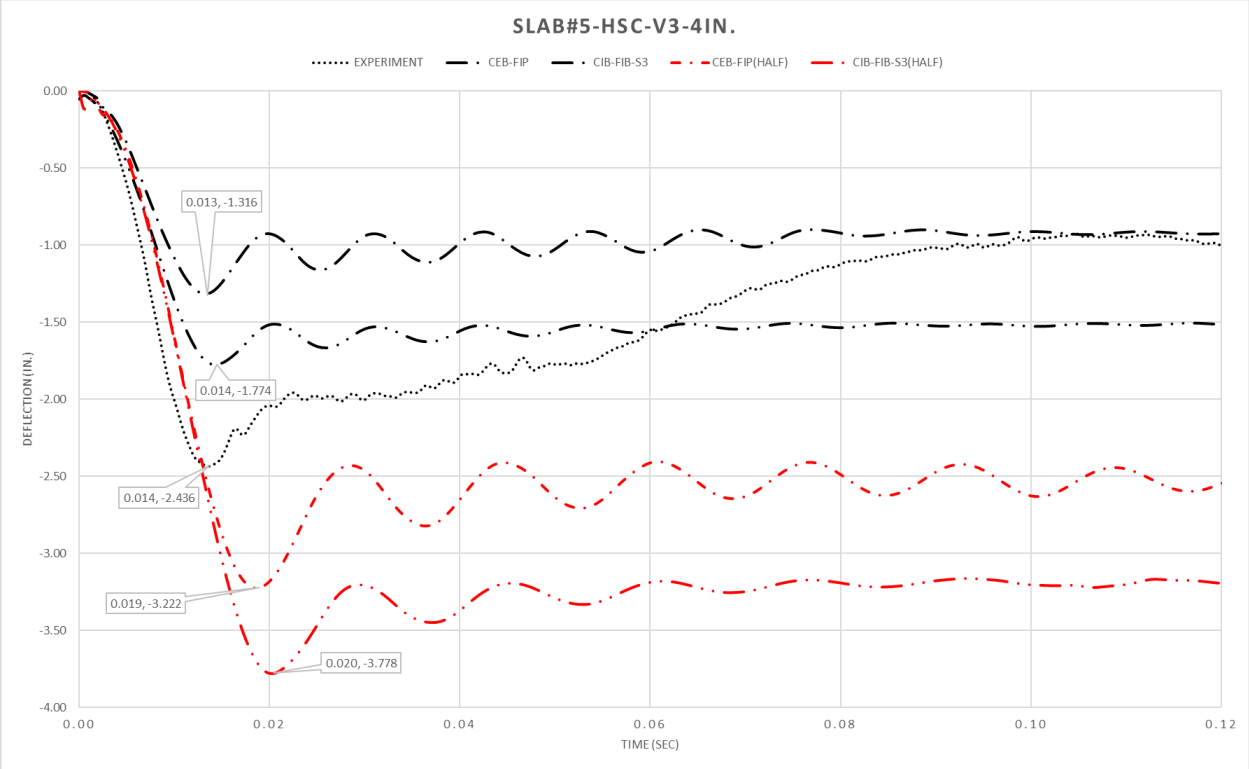

Figure 6.2-6: Deflection Comparison between 1 in. (25.4 mm.) and 0.5 in. (12.7 mm.) for CEB-FIP and CEB-FIP-S3 functions and Experimental Deflection for Slab#5– HSC-V3-4in.

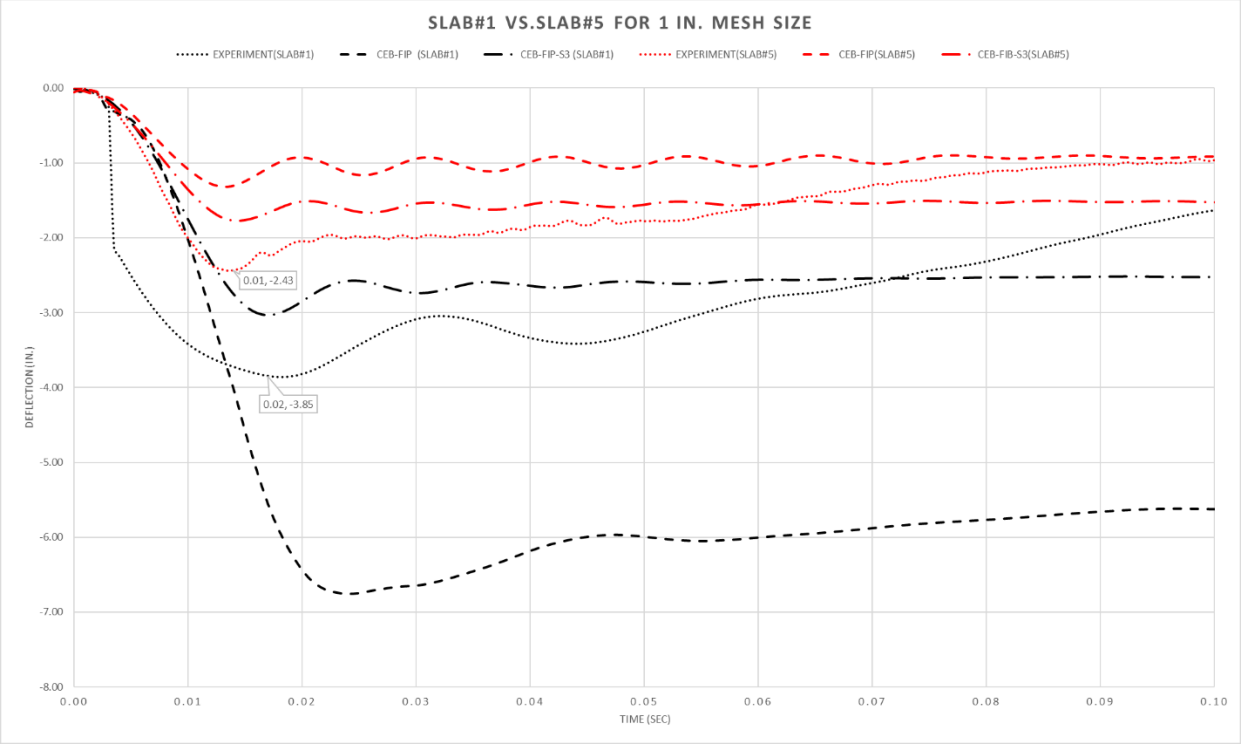

Figure 6.2-7: Comparison between Slab#1 vs. Slab#5 for CEB-FIP and CEB-FIP-S3 functions and Experimental Deflection for 1in. (25.4 mm) Mesh Size.

6.2.4 Mesh size effect on Slab # 7 (HSC-V4-8in.)

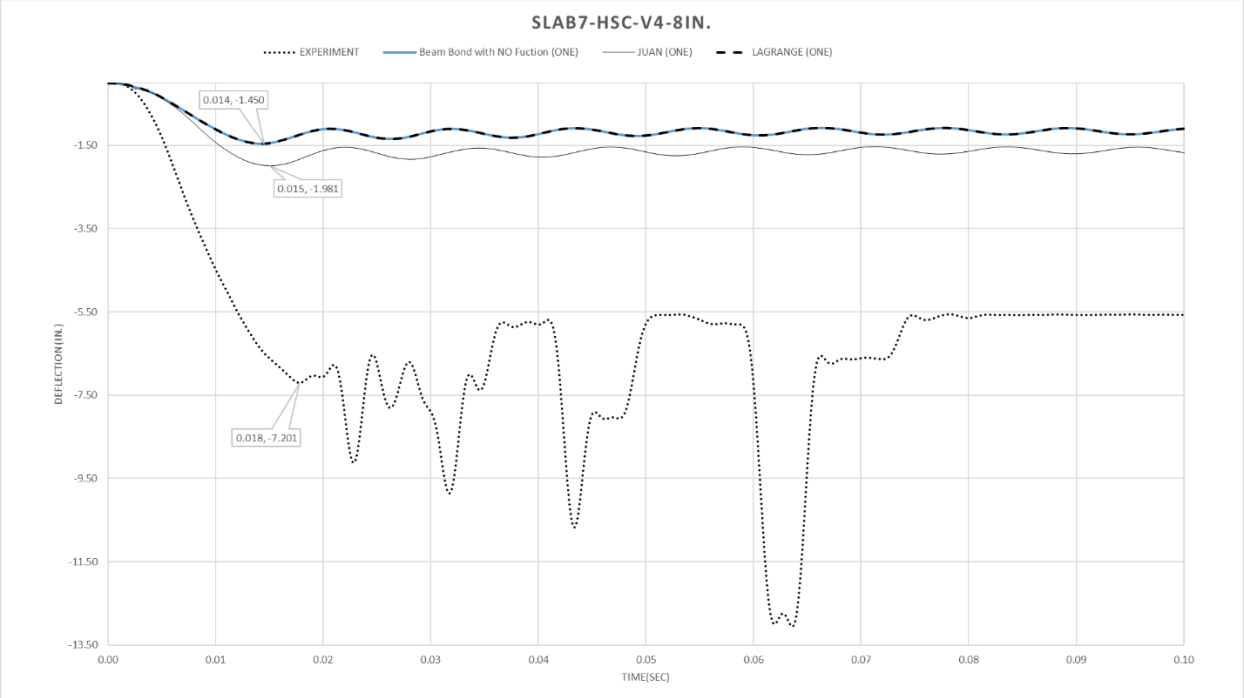

Figure 6.2-8: Deflection Comparison between 1 in. (25.4 mm.) and 0.5 in. (12.7 mm.) for Constrained Lagrange and Beam in solid with no defined function and Juan function with Experimental Deflection for Slab#7– HSC-V4-8in.

SLAB#7 HSC-V4-8IN	Peak Deflection			% Change Compared to Experimental		% Change for Mesh Size reduction form 1in. to 1/2in.
	1in.	1/2in.	Experiment	1in.	1/2in.	
Lagrange_IN_Solid	1.45	**	7.20	↓80%	**	**
Beam_IN_Solid						
No User Function	1.45	**	7.20	↓80%	**	**
Juan	1.98	**	7.20	↓72.5%	**	**
CEB-FIP	1.71	3.79	7.20	↓76%	↓47%	↑121%
CEB-FIP-S3	3.13	4.50	7.20	↓56.5%	↓37.5%	↑44%

** Negative volume in elements terminated the analysis

Table 6-7: Numerical Simulation Results for Slab#7, HSC-V4-8IN.

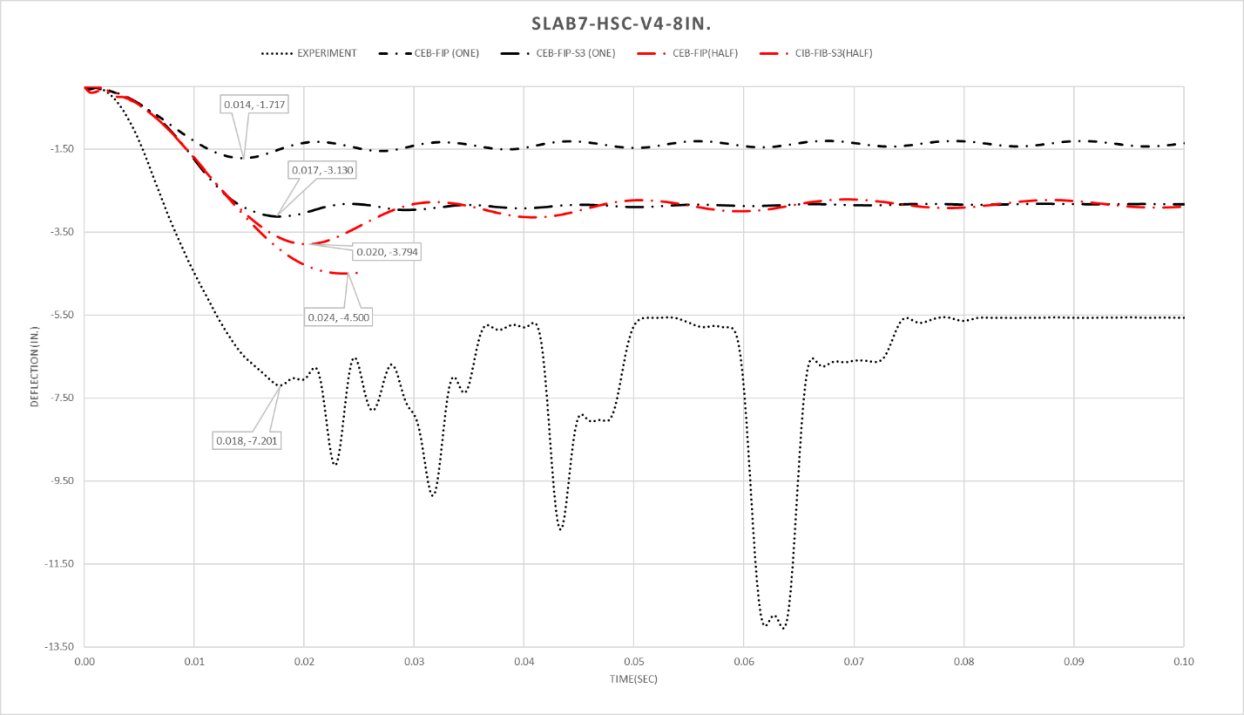

Figure 6.2-9: Deflection Comparison between 1 in. (25.4 mm.) and 0.5 in. (12.7 mm.) for CEB-FIP and CEB-FIP-S3 functions and Experimental Deflection for Slab#7– HSC-V4-8in.

6.2.5 Mesh size effect on Slab # 9 (HSC-V5-8in.)

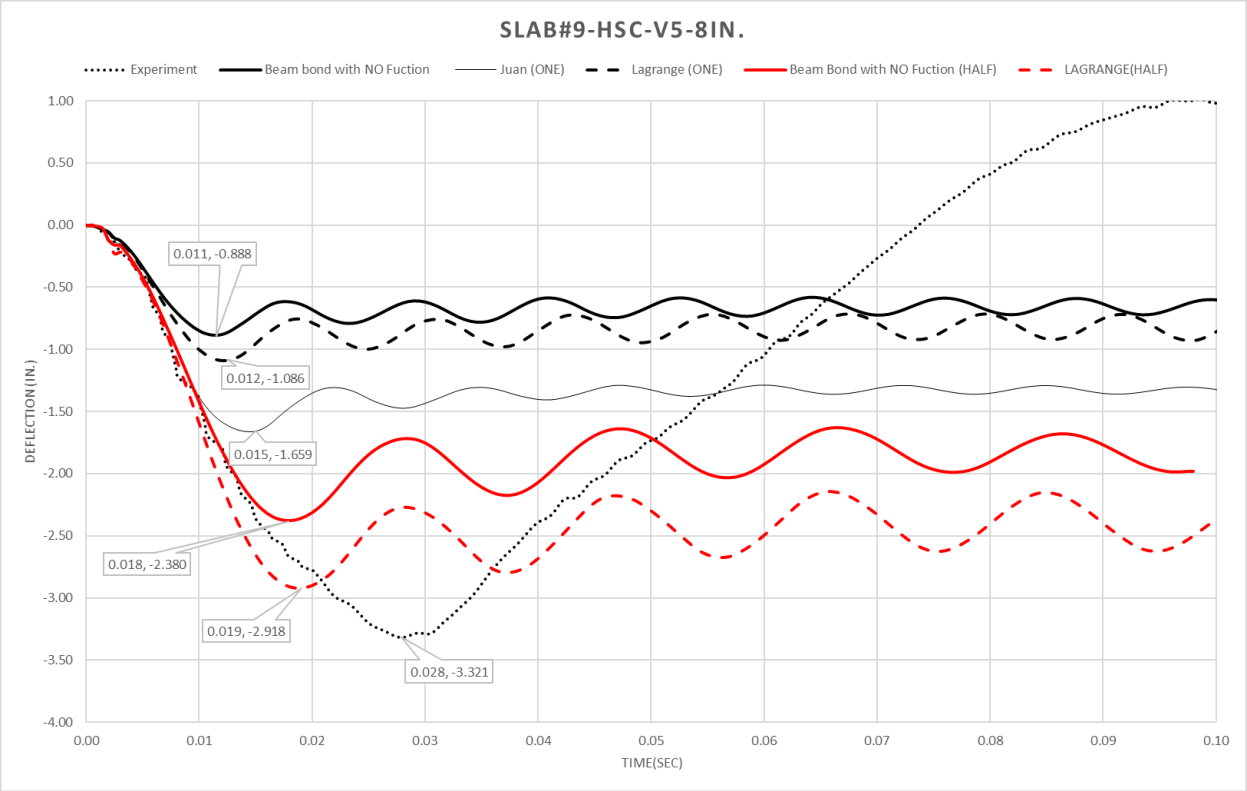

Figure 6.2-10: Deflection Comparison between 1 in. (25.4 mm.) and 0.5 in. (12.7 mm.) for Constrained Lagrange and Beam in solid with no defined function and Juan function with Experimental Deflection for Slab#9– HSC-V5-8in.

SLAB#9 HSC-V5-8IN	Peak Deflection			% Change Compared to Experimental		% Change for Mesh Size reduction form 1in. to 1/2in.
	1in.	1/2in.	Experiment	1in.	1/2in.	
Lagrange_IN_Solid	1.24	2.91	3.32	↓67.5%	↓12.5%	↑169.4%
Beam_IN_Solid						
No User Function	1.27	2.38	3.32	↓73%	↓28%	↑170.5%
Juan	1.84	**	3.32	↓50%	**	**
CEB-FIP	1.0	2.66	3.32	↓45.5%	↓20%	↑46%
CEB-FIP-S3	2.96	2.66	3.32	↓32.5%	↓19.87%	↑18.75%

** Negative volume in elements terminated the analysis

Table 6-8: Numerical Simulation Results for Slab#9, HSC-V5-8IN.

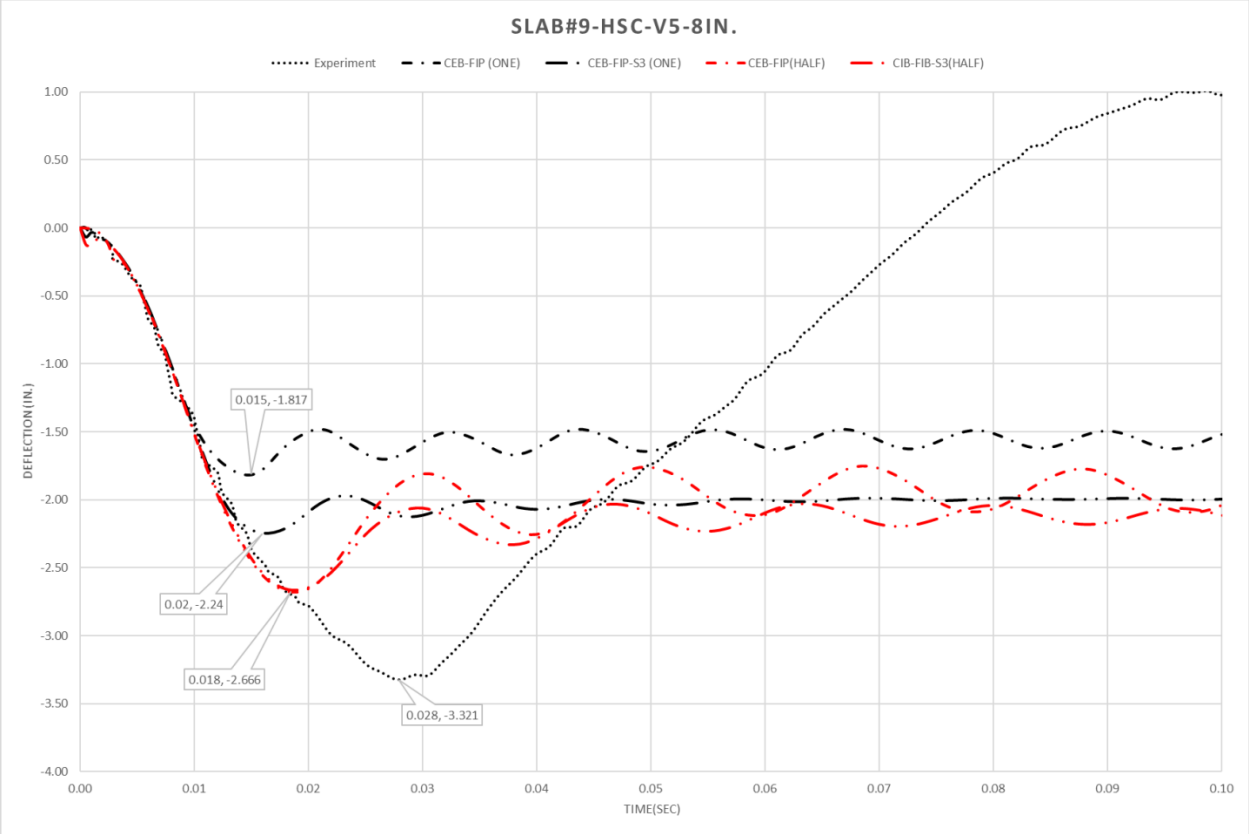

Figure 6.2-11: Deflection Comparison between 1 in. (25.4 mm.) and 0.5 in. (12.7 mm.) for CEB-FIP and CEB-FIP-S3 functions and Experimental Deflection for Slab#9– HSC-V5-8in.

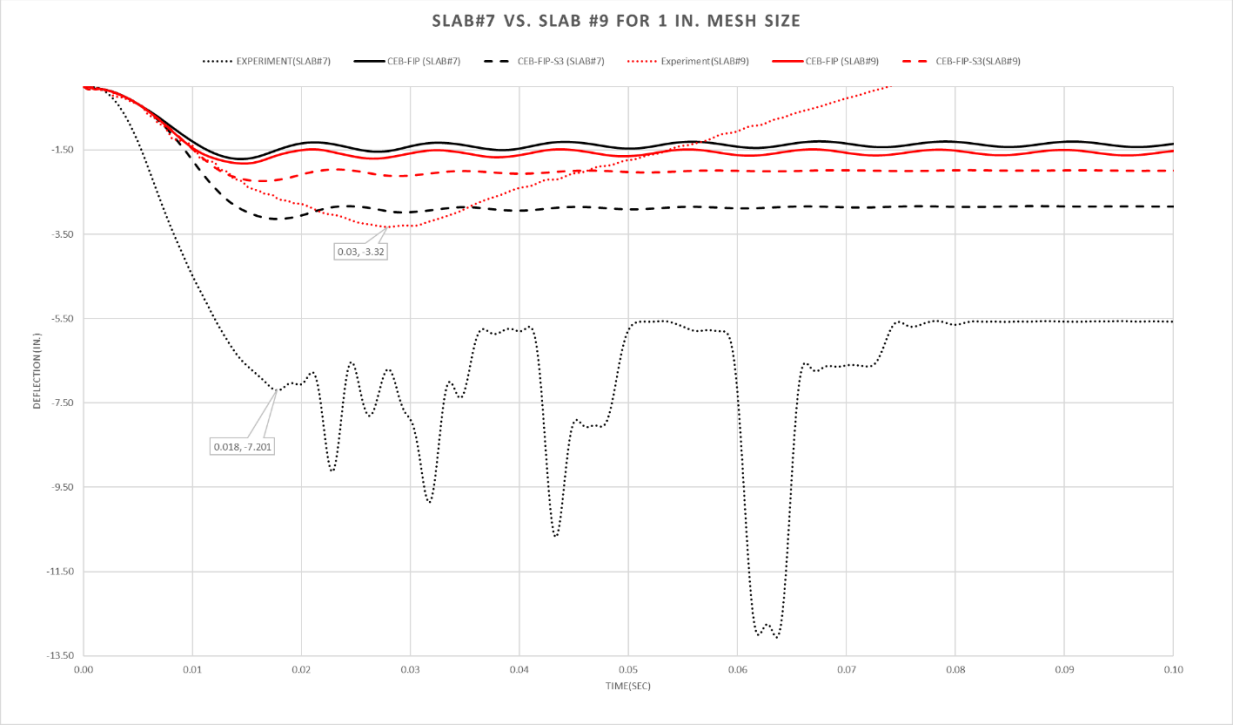

Figure 6.2-12: Comparison between Slab#7 vs. Slab#9 for CEB-FIP and CEB-FIP-S3 functions and Experimental Deflection for 1in. (25.4 mm) Mesh Size.

6.2.6 Mesh Size Effect for Slab # 11 (HSC-V6-8in.)

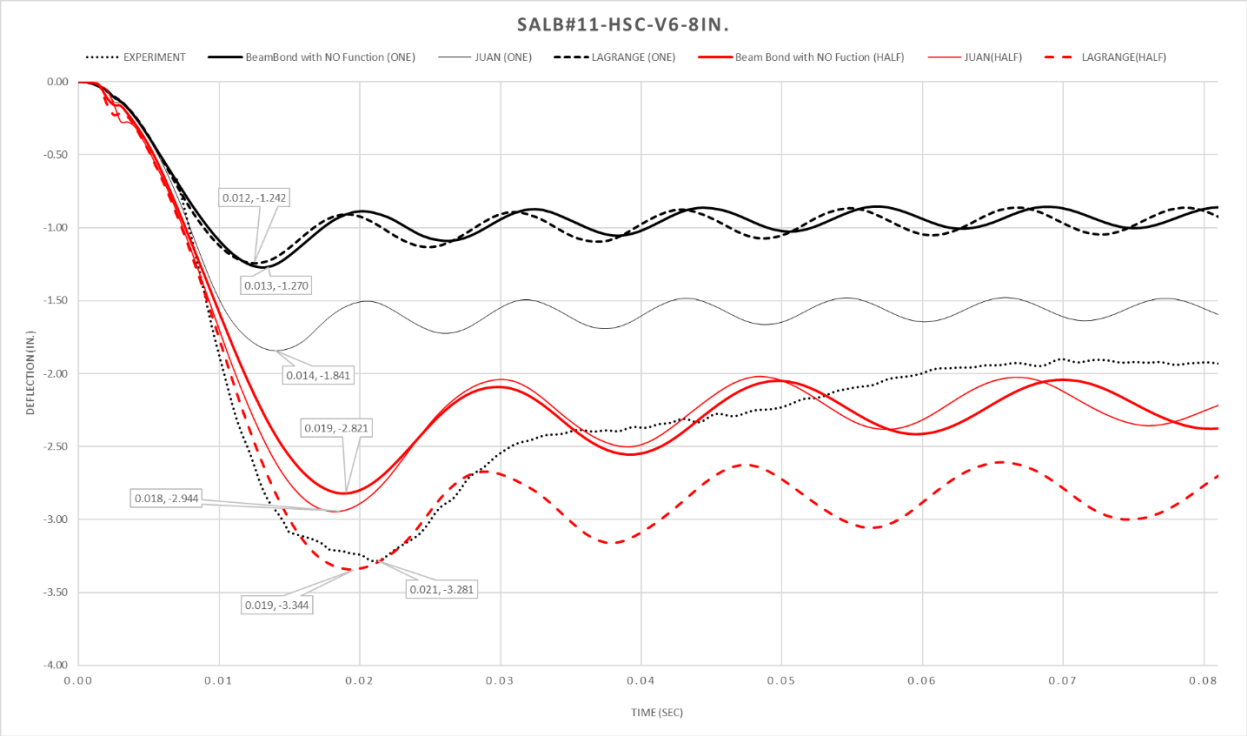

Figure 6.2-13: Deflection Comparison between 1 in. (25.4 mm.) and 0.5 in. (12.7 mm.) for Constrained Lagrange and Beam in solid with no defined function and Juan function with Experimental Deflection for Slab#11– HSC-V6-8in.

SLAB#11 HSC-V6-8IN	Peak Deflection			% Change Compared to Experimental		% Change for Mesh Size reduction form 1in. to 1/2in.
	1in.	1/2in.	Experiment	1in.	1/2in.	
Lagrange_IN_Solid	1.24	3.34	3.28	↓62%	↑1.8%	↑169.3%
Beam_IN_Solid						
No User Function	1.27	2.82	3.28	↓61%	↓14%	↑122%
Juan	1.84	2.94	3.28	↓44%	↓10.5%	↑60%
CEB-FIP	1.0	2.63	3.28	↓69.5%	↓20%	↑163%
CEB-FIP-S3	2.96	3.39	3.28	↓10%	↑3.35%	↑14.5%

Table 6-9: Numerical Simulation Results for Slab#11, HSC-V6-8IN.

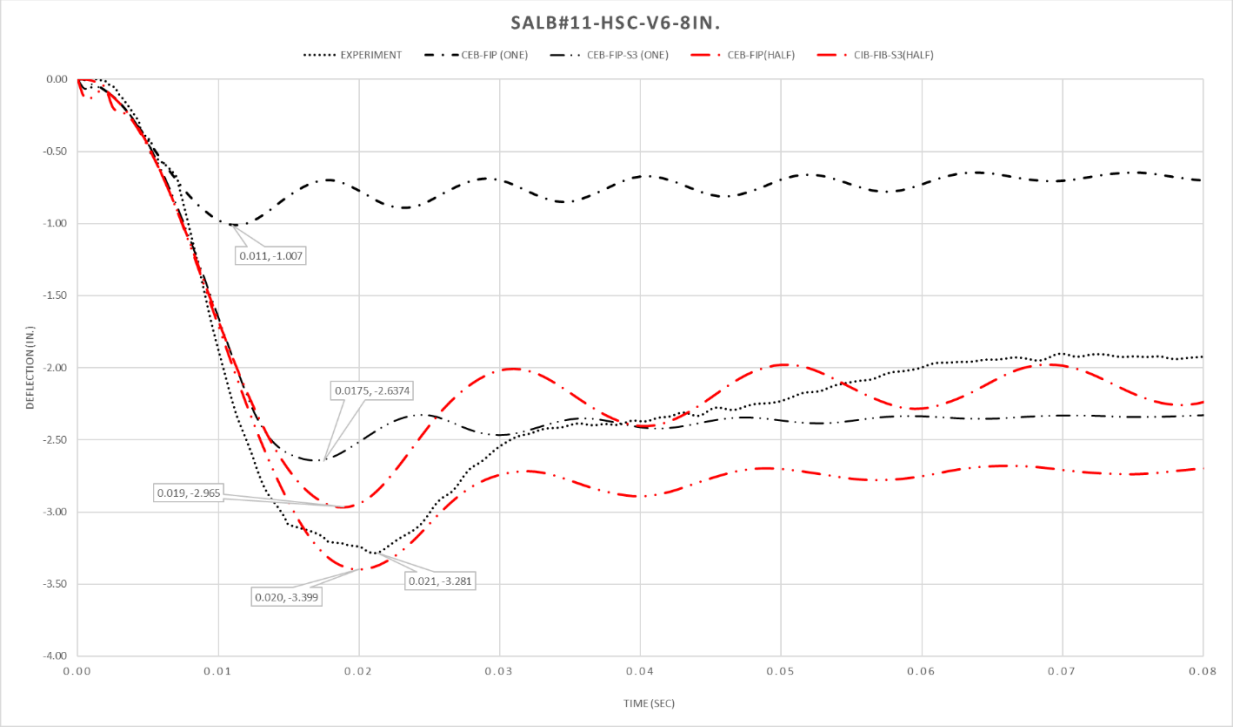

Figure 6.2-14: Deflection Comparison between 1 in. (25.4 mm.) and 0.5 in. (12.7 mm.) for CEB-FIP and CEB-FIP-S3 functions and Experimental Deflection for Slab#11– HSC-V6-8in.

6.3 Normal Strength Concrete with Normal Strength Steel Slabs (RSC-R)

The second set of slabs studied here are the ones having combination of normal strength concrete reinforced with regular strength steel (RSC-R). The deflection-time histories for each of the 6 slabs are represented in this section. The comparison is made between two mesh sizes i.e. 1" and 0.5" for each of the two constrains and their functions with experimental peak deflection for all beam bond formulations are given for regular strength materials.

6.3.1 Mesh size effect on Slab # 2 (RSC-R1-4in.)

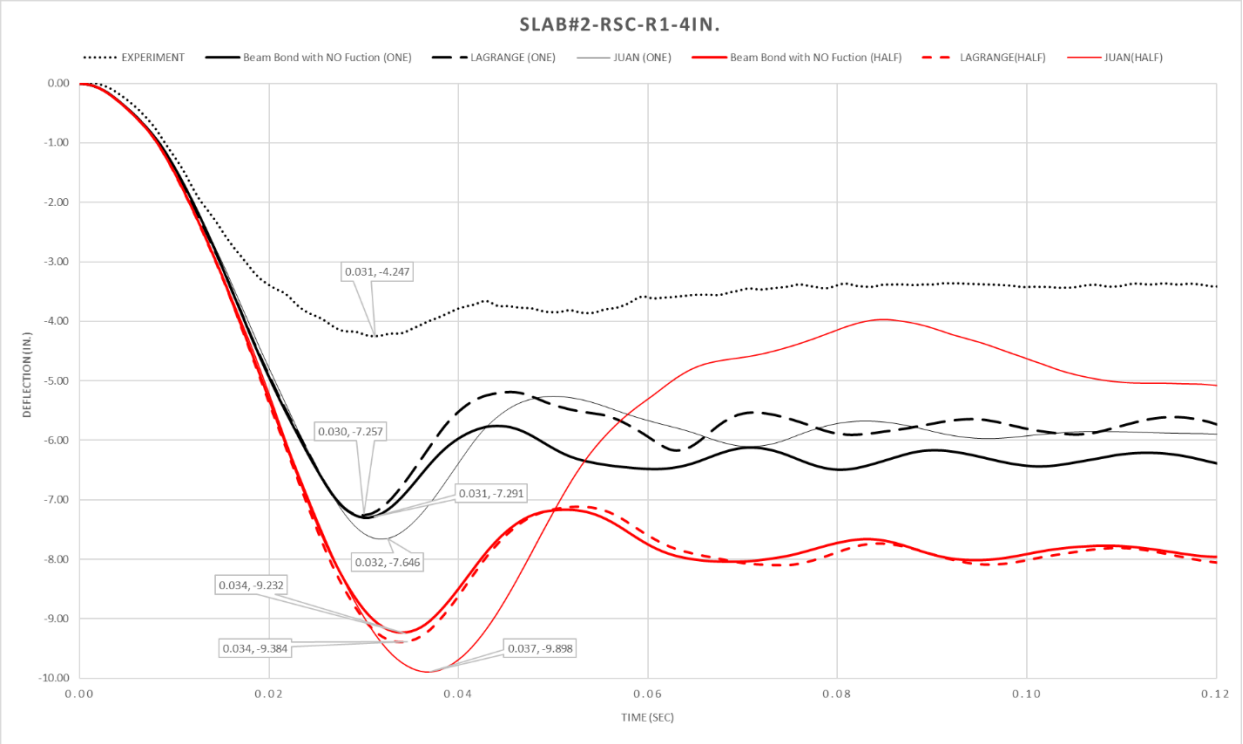

Figure 6.3-1: Deflection Comparison between 1 in. (25.4 mm.) and 0.5 in. (12.7 mm.) for Constrained Lagrange and Beam in solid with no defined function and Juan function with Experimental Deflection for Slab#2– RSC-R1-4in.

SLAB#2 RSC-R1-4IN	Peak Deflection			% Change Compared to Experimental		% Change for Mesh Size reduction form 1in. to 1/2in.
	1in.	1/2in.	Experiment	1in.	1/2in.	
Lagrange_IN_Solid	7.25	9.38	4.24	↑70%	↑121%	↑29%
Beam_IN_Solid						
No User Function	7.29	9.23	4.24	↑71.94%	↑117%	↑26.5%
Juan	7.64	9.89	4.24	↑80.1%	↑133%	↑29.5%
CEB-FIP	12.24	15.14	4.24	↑188%	↑257%	↑24%
CEB-FIP-S3	16.52	18.49	4.24	↑289%	↑336%	↑12%

Table 6-10: Numerical Simulation Results for Slab#2, RSC-R1-4IN.

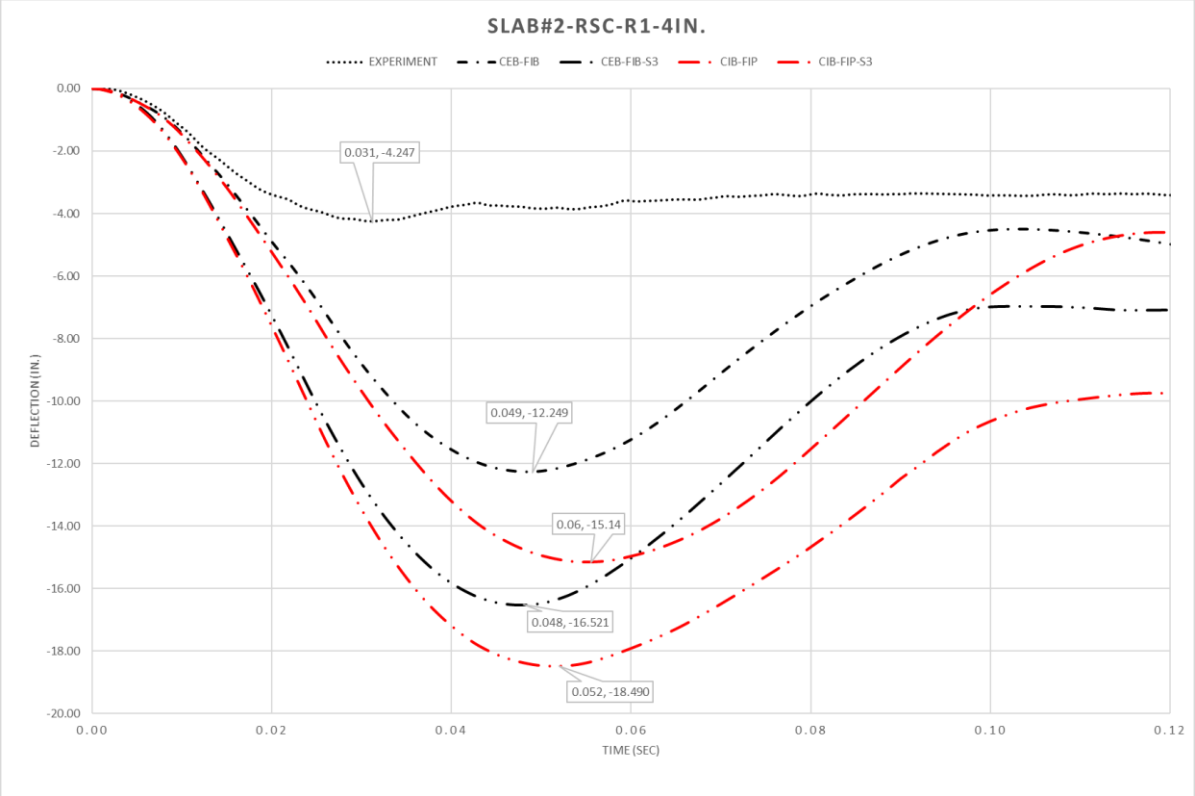

Figure 6.3-2: Deflection Comparison between 1 in. (25.4 mm.) and 0.5 in. (12.7 mm.) for CEB-FIP and CEB-FIP-S3 functions and Experimental Deflection for Slab#1– RSC-R1-4in.

6.3.2 Mesh Size Effect for Slab # 4 (RSC-R2-4in.)

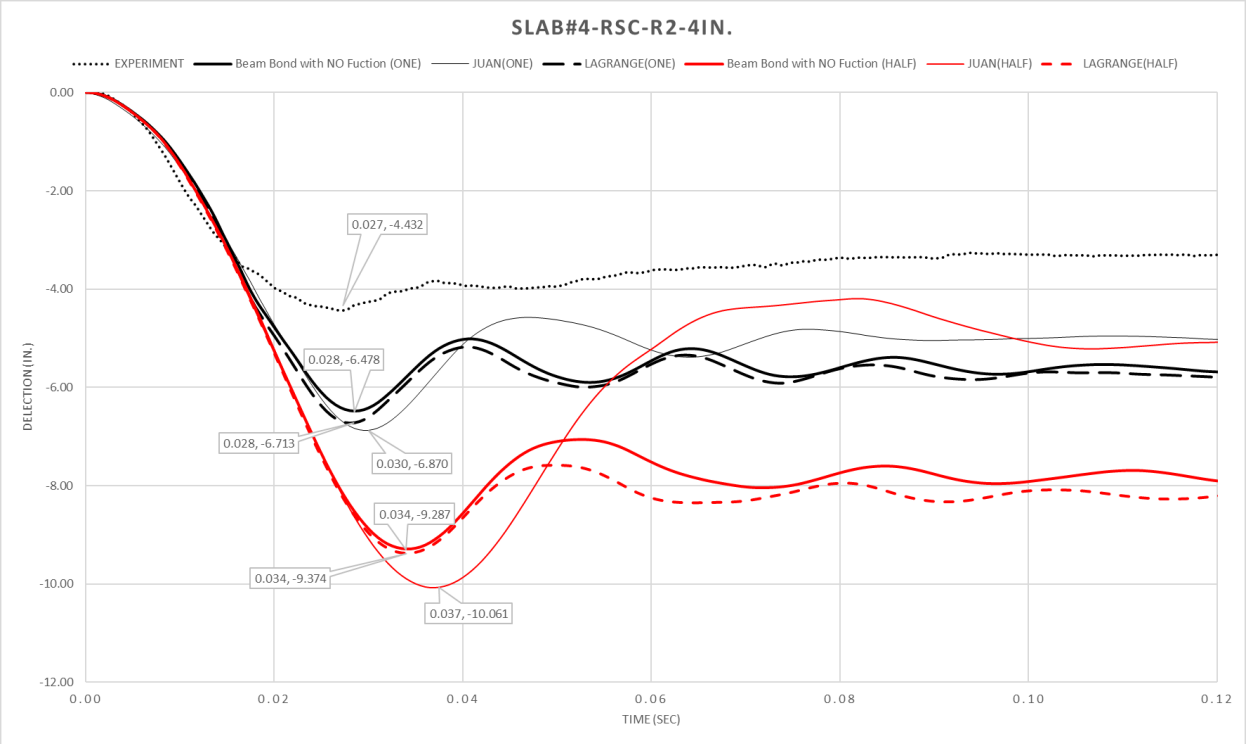

Figure 6.3-3: Deflection Comparison between 1 in. (25.4 mm.) and 0.5 in. (12.7 mm.) for Constrained Lagrange and Beam in solid with no defined function and Juan function with Experimental Deflection for Slab#4– RSC-R2-4in.

SLAB#4 RSC-R2-4IN	Peak Deflection			% Change Compared to Experimental		% Change for Mesh Size reduction form 1in. to 1/2in.
	1in.	1/2in.	Experiment	1in.	1/2in.	
Lagrange_IN_Solid	6.71	9.37	4.43	↑51.4%	↑111%	↑39.5%
Beam_IN_Solid						
No User Function	6.47	9.28	4.43	↑46.05%	↑111%	↑43.5%
Juan	6.87	10.06	4.43	↑55.08%	↑127%	↑46.5%
CEB-FIP	10.77	15.53	4.43	↑143%	↑250%	↑44%
CEB-FIP-S3	14.89	17.63	4.43	↑236%	↑298%	↑18.5%

Table 6-11: Numerical Simulation Results for Slab#4, RSC-R2-4IN.

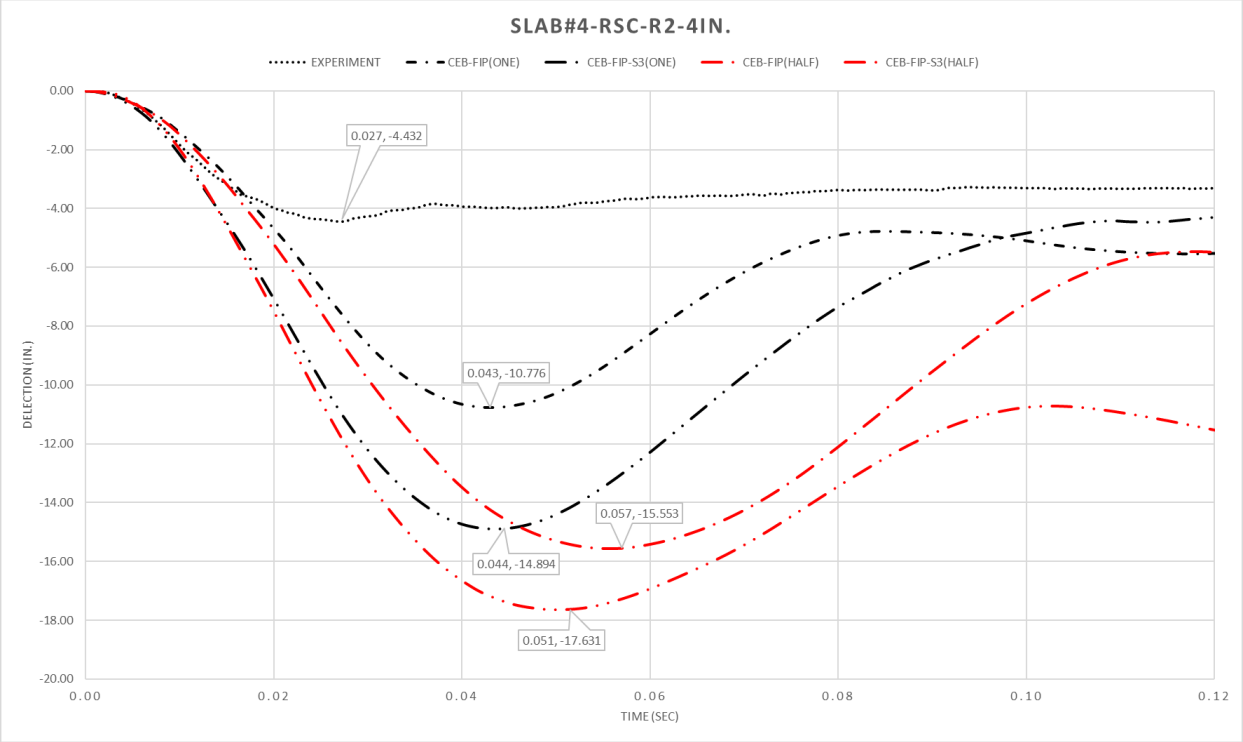

Figure 6.3-4: Deflection Comparison between 1 in. (25.4 mm.) and 0.5 in. (12.7 mm.) for CEB-FIP and CEB-FIP-S3 functions and Experimental Deflection for Slab#4– RSC-R2-4in.

6.3.3 Mesh Size Effect for Slab # 6 (RSC-R3-4in.)

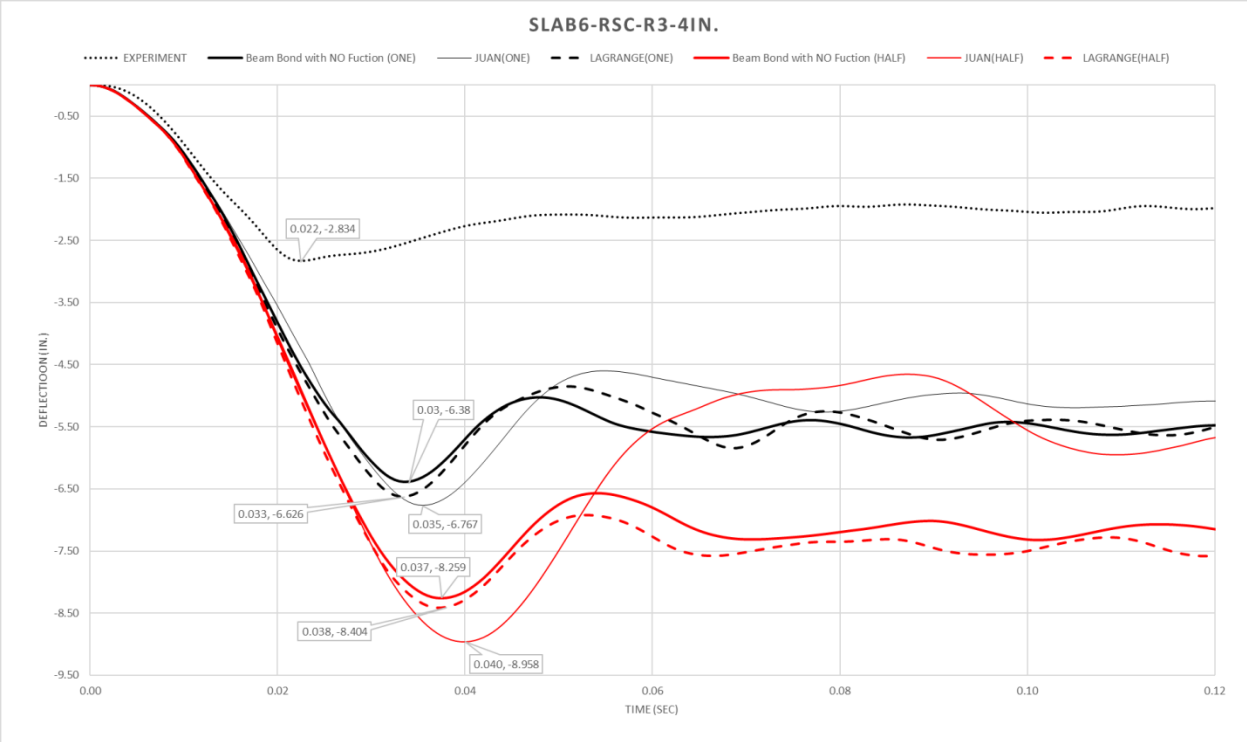

Figure 6.3-5: Deflection Comparison between 1 in. (25.4 mm.) and 0.5 in. (12.7 mm.) for Constrained Lagrange and Beam in solid with no defined function and Juan function with Experimental Deflection for Slab#6– RSC-R3-4in.

SLAB#6 RSC-R3-4IN	Peak Deflection			% Change Compared to Experimental		% Change for Mesh Size reduction form 1in. to 1/2in.
	1in.	1/2in.	Experiment	1in.	1/2in.	
Lagrange_IN_Solid	6.62	8.40	2.83	↑133.9%	↑196%	↑27%
Beam_IN_Solid						
No User Function	6.38	8.25	2.83	↑125.4%	↑191%	↑29.5%
Juan	6.76	8.95	2.83	↑138.86%	↑216%	↑32.5
CEB-FIP	10.58	14.02	2.83	↑273%	↑396%	↑32.5%
CEB-FIP-S3	15.90	17.65	2.83	↑462%	↑524%	↑11%

Table 6-12: Numerical Simulation Results for Slab#6, RSC-R3-4IN.

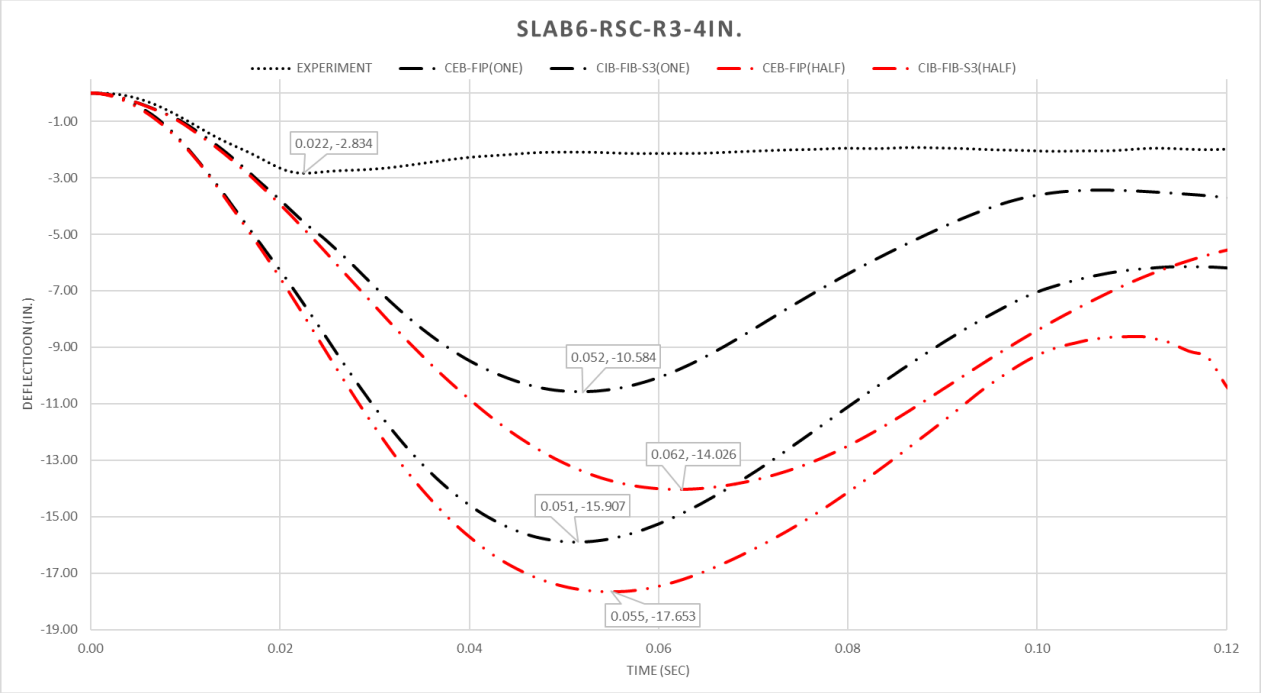

Figure 6.3-6: Deflection Comparison between 1 in. (25.4 mm.) and 0.5 in. (12.7 mm.) for CEB-FIP and CEB-FIP-S3 functions and Experimental Deflection for Slab#6– RSC-R3-4in.

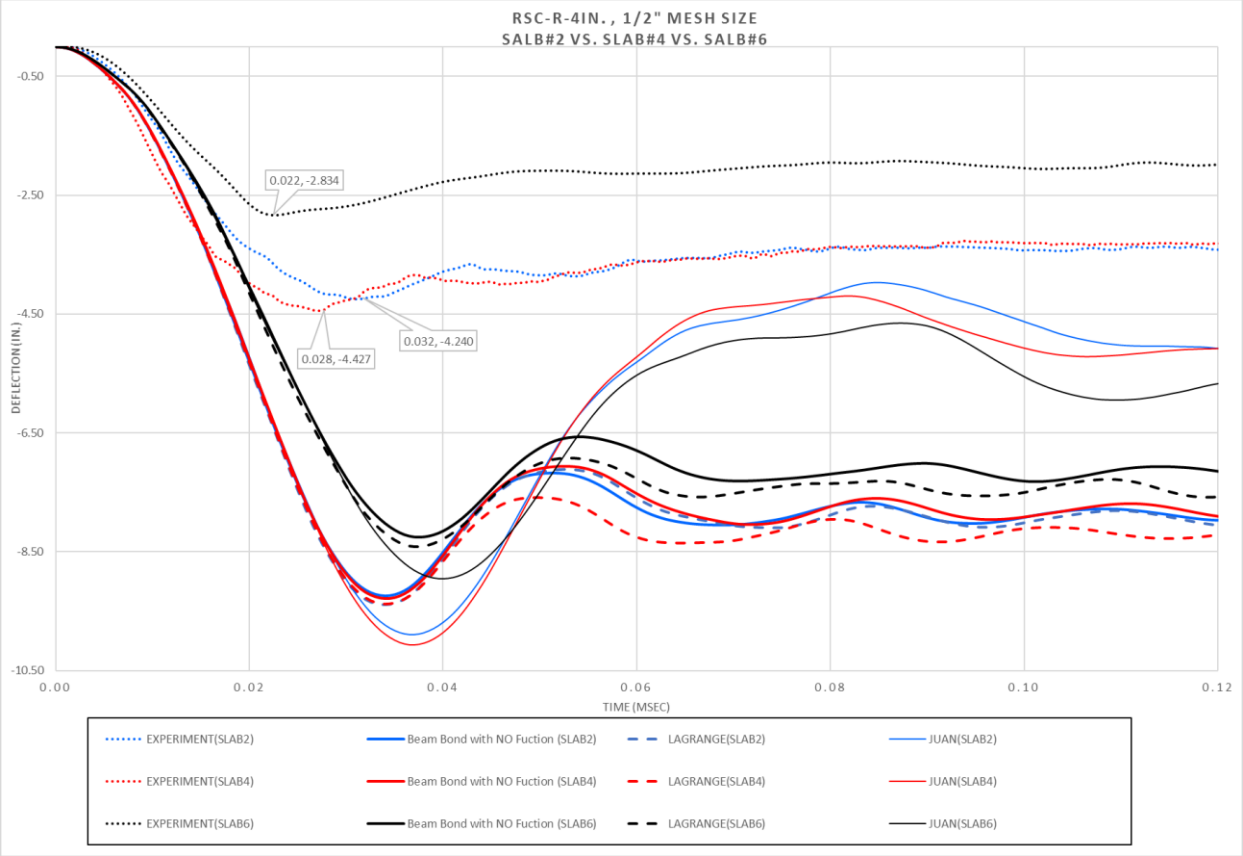

Figure 6.3-7: Comparison between Slab#2 vs. Slab#4 vs. Slab#6 for Constrained Lagrange and Beam in solid with no defined function and Juan function with Experimental Deflection for0.5 in. (12.7 mm.) Mesh Size.

Figure 6.4-7 shows for the RSC-R-4IN models generates deflection history curves for Beam In Solid formulation with Juan function with distinct rebounds. For Lagrange In Solid formulation and Beam In Solid formulation with no user function shows similar deflection history curves for all three RSC-R-4IN models.

6.3.4 Mesh Size Effect for Slab # 8 (RSC-R4-8in.)

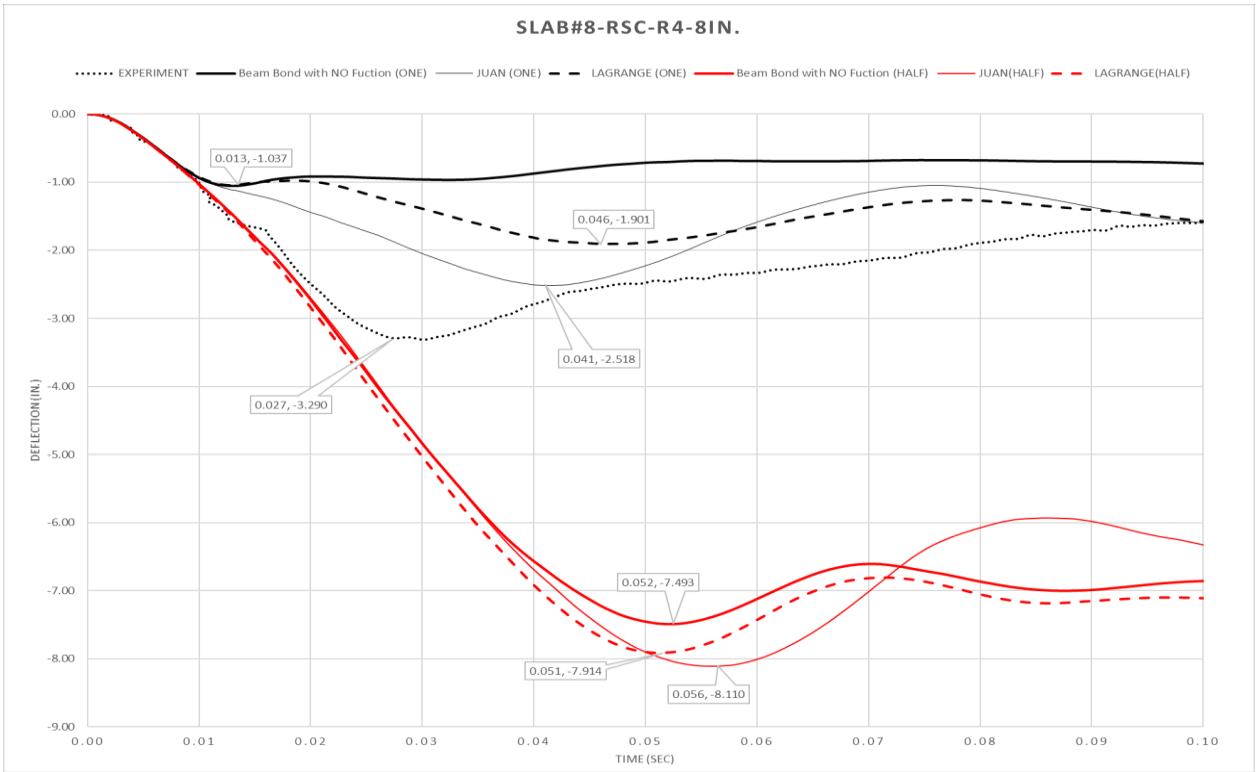

Figure 6.3-8 : Deflection Comparison between 1 in. (25.4 mm.) and 0.5 in. (12.7 mm.) for Constrained Lagrange and Beam in solid with no defined function and Juan function with Experimental Deflection for Slab#8– RSC-R4-8in.

SLAB#8 RSC-R4-8IN	Peak Deflection			% Change Compared to Experimental		% Change for Mesh Size reduction form 1in. to 1/2in.
	1in.	1/2in.	Experiment	1in.	1/2in.	
Lagrange_IN_Solid	1.90	7.91	3.29	↓42.2%	↑140%	↑316%
Beam_IN_Solid						
No User Function	1.03	7.49	3.29	↓68.7%	↑127%	↑627%
Juan	2.51	8.11	3.29	↓23.70%	↑223%	↑160.5%
CEB-FIP	4.28	11.15	3.29	↑30%	↑238%	↑160.5%
CEB-FIP-S3	18.28	17.91	3.29	↑455%	↓2%	↓3.5%

Table 6-13: Numerical Simulation Results for Slab#8, RSC-R4-8IN.

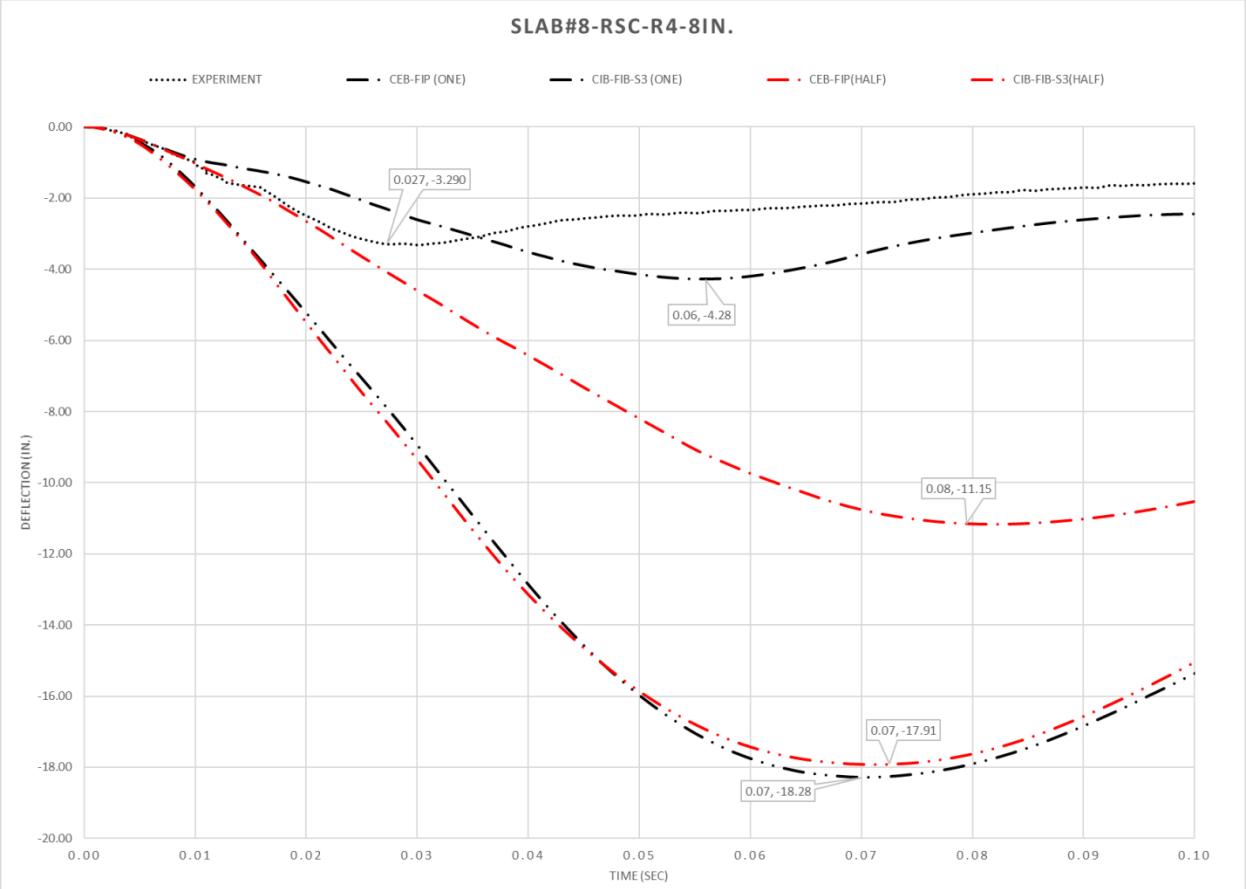

Figure 6.3-9 : Deflection Comparison between 1 in. (25.4 mm.) and 0.5 in. (12.7 mm.) for CEB-FIP and CEB-FIP-S3 functions and Experimental Deflection for Slab#8– RSC-R4-8in.

6.3.5 Mesh Size Effect for Slab # 10 (RSC-R5-8in.)

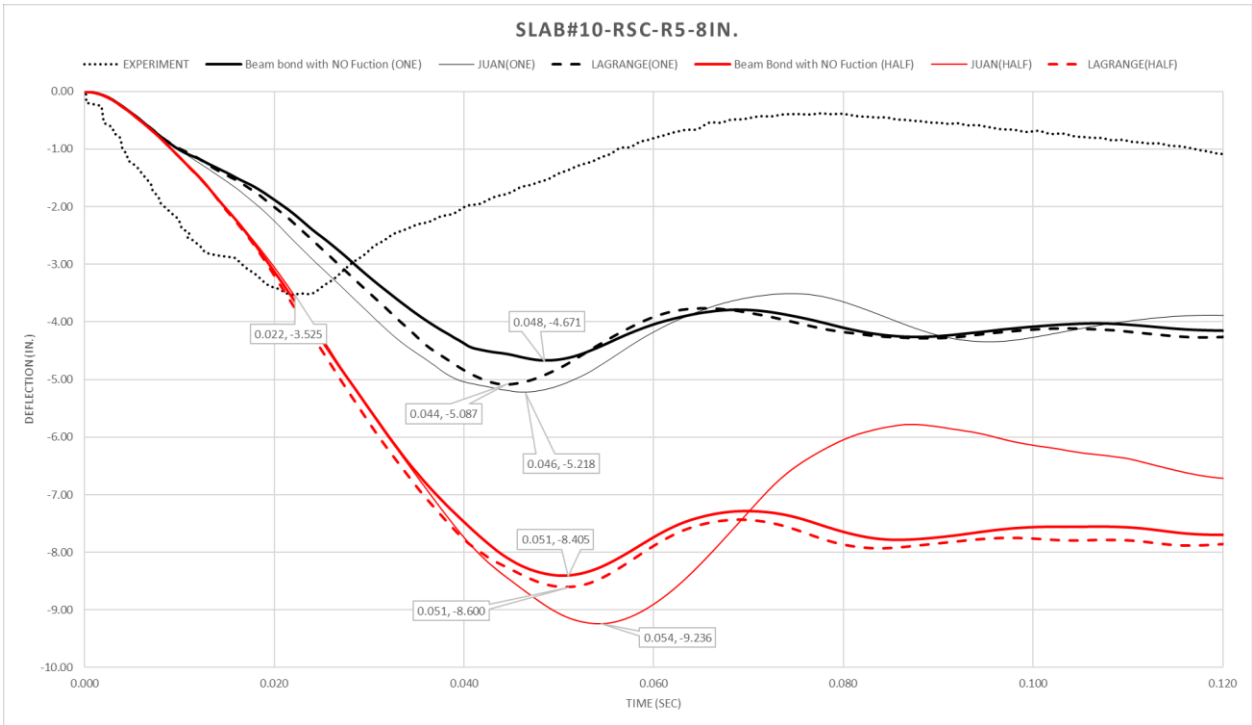

Figure 6.3-10: Deflection Comparison between 1 in. (25.4 mm.) and 0.5 in. (12.7 mm.) for Constrained Lagrange and Beam in solid with no defined function and Juan function with Experimental Deflection for Slab#10– RSC-R5-8in.

SLAB#10 RSC-R5-8IN	Peak Deflection			% Change Compared to Experimental		% Change for Mesh Size reduction form 1in. to 1/2in.
	1in.	1/2in.	Experiment	1in.	1/2in.	
Lagrange_IN_Solid	5.08	8.6	3.52	↑44.3%	↑144%	↑69%
Beam_IN_Solid						
No User Function	4.67	8.4	3.52	↑32.67%	↑138%	↑79.8%
Juan	5.21	9.23	3.52	↑48.02%	↑162%	↑77%
CEB-FIP	7.07	13.20	3.52	↑100%	↑275%	↑86.7%
CEB-FIP-S3	18.82	18.46	3.52	↑434%	↑424%	↓1.91%

Table 6-14: Numerical Simulation Results for Slab#10, RSC-R5-8IN.

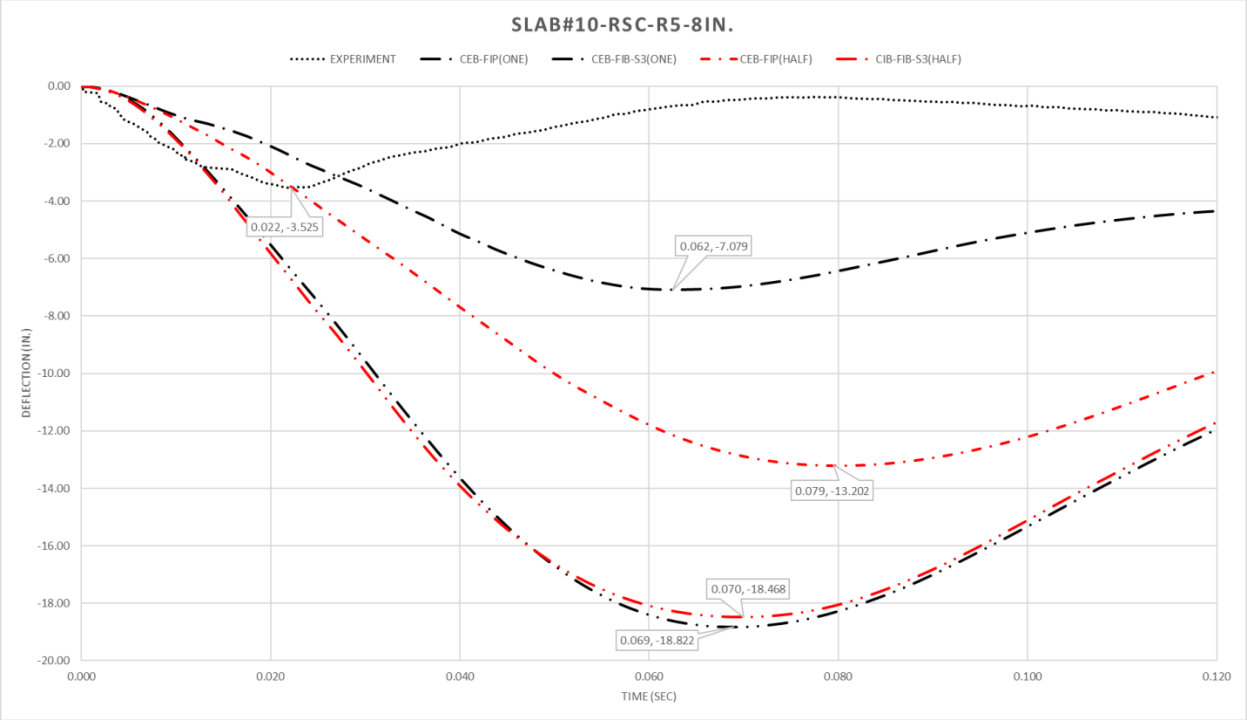

Figure 6.3-11 : Deflection Comparison between 1 in. (25.4 mm.) and 0.5 in. (12.7 mm.) for CEB-FIP and CEB-FIP-S3 functions and Experimental Deflection for Slab#10– RSC-R5-8in.

6.3.6 Mesh Size Effect for Slab # 12 (RSC-R6-8in.)

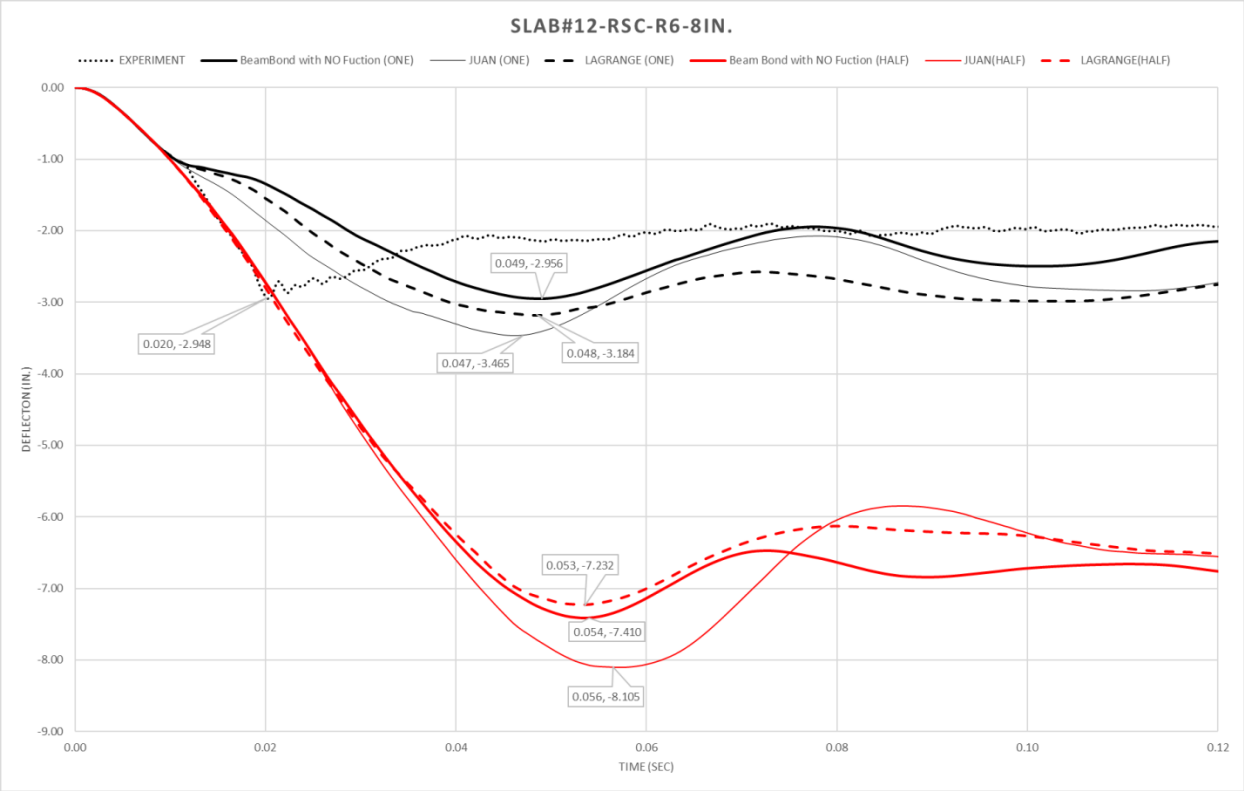

Figure 6.3-12: Deflection Comparison between 1 in. (25.4 mm.) and 0.5 in. (12.7 mm.) for Constrained Lagrange and Beam in solid with no defined function and Juan function with Experimental Deflection for Slab#12– RSC-R6-8in.

SLAB#12 RSC-R6-8IN	Peak Deflection			% Change Compared to Experimental		% Change for Mesh Size reduction form 1in. to 1/2in.
	1in.	1/2in.	Experiment	1in.	1/2in.	
Lagrange_IN_Solid	3.18	7.23	2.94	↑8.1%	↑145%	↑127%
Beam_IN_Solid						
No User Function	2.95	7.41	2.94	↑0.34%	↑152%	↑151%
Juan	3.46	8.10	2.94	↑17.68%	↑175%	↑151%
CEB-FIP	4.20	11.96	2.94	↑42%	↑307%	↑184.7%
CEB-FIP-S3	18.70	18.04	2.94	↑536%	↑513%	↓3.5%

Table 6-15: Numerical Simulation Results for Slab#12, RSC-R6-8IN.

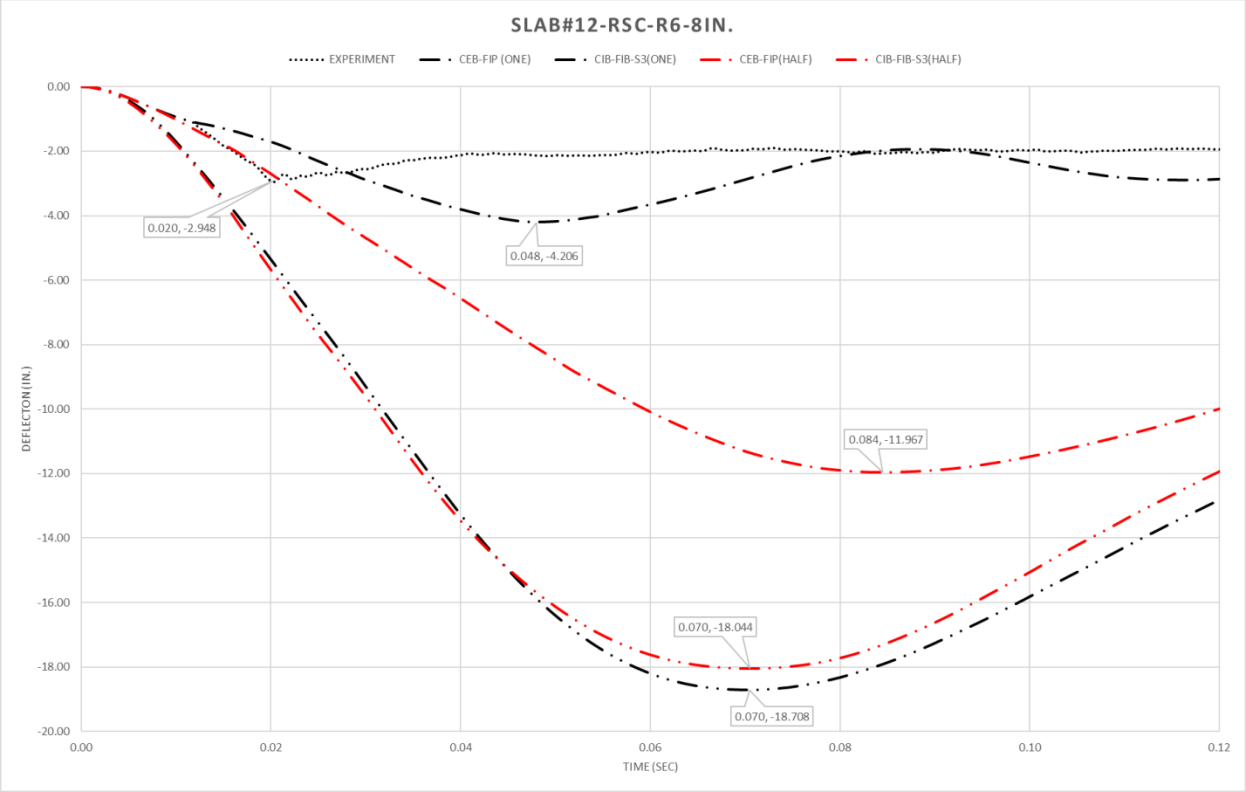

Figure 6.3-13: Deflection Comparison between 1 in. (25.4 mm.) and 0.5 in. (12.7 mm.) for CEB-FIP and CEB-FIP-S3 functions and Experimental Deflection for Slab#12– RSC-R6-8in.

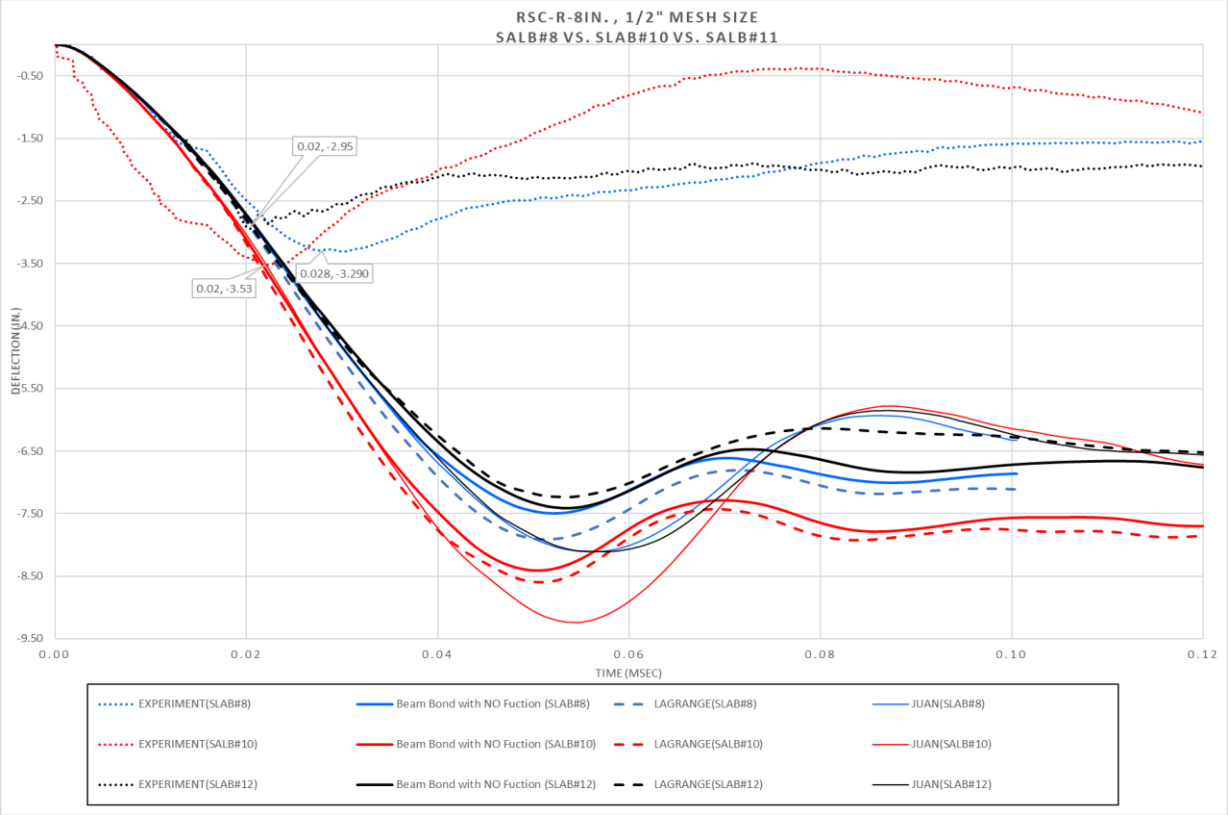

Figure 6.3-14: Comparison between Slab#2 vs. Slab#4 vs. Slab#6 for Constrained Lagrange and Beam in solid with no defined function and Juan function with Experimental Deflection for0.5 in. (12.7 mm.) Mesh Size.

Figure 6.4-14 shows for the RSC-R-8IN models also Beam In Solid formulation with Juan function gives distinct rebound for deflection history curves. For Lagrange In Solid formulation and Beam In Solid formulation with no user function shows similar deflection history curves for all three RSC-R-8IN models.

CHAPTER 7. DISCUSSION OF RESULTS

Comparison of all the twelve slabs is carried out between numerical simulation results and experimental data. Normal-strength concrete with normal-strength steel (RSC-R) and high-strength concrete with high-strength steel (HSC-V) are the two material combinations used for this comparison. These are discussed in detail in this chapter with the comparison criterion of the deflection response of both the experimental and numerical analysis. High-Strength Concrete – Comparison of Model with 1 in. (25.4 mm.) Mesh to ½ in. (12.7 mm.) Mesh Model.

The custom defined function for beam bond formulation also has similar change in peak deflection when compared to experimental peak deflection. Whereas residual defection of Juan function and CEB-FIP-S3 shows results of rhythm of the defection history curve which dies once peak deflection is reached for most cases.

For ½ in. (12.7 mm.) mesh size is accurately able to predict peak deflection history value for high strength material than1 in. (25.4 mm.). But the number of simulations runs terminated are also more in comparison with 1 in. (25.4 mm.), mesh size. Juan function for beam-bond formulation produced only two out of six results, whereas both CEB-FIP gave all six slabs results. Both CEB-FIP functions tend to give more variation for 4in slabs in comparison to the 8in slabs. Perfect bond formulation and beam-bond formulation generated by this program tended to give more accurate results than all the three user defined functions for beam-bond formulation.

7.1 High-Strength Concrete – Comparison of Model with 1 in. (25.4 mm.) Mesh to ½ in. (12.7 mm.) Mesh Model.

Table 7-1: Analytical and Experimental Peak Slab Deflection Summary for High Strength Slabs for 1 in. mesh size.

Slab No.	Description	Deflection					
		For 1 in. Mesh Size					
		Experimental	LAGRANGE_IN_SOID	BEAM_IN_SOLID			
				No Function	Juan	CEBFIP	CEBFIP-S3
Slab1	HSC-V1-4IN	3.85	2.16	2.81	1.53	6.75	3.02
Slab3	HSC-V2-4IN	4.31	7.11	1.84	2.3	1.78	1.97
Slab5	HSC-V3-4IN	2.43	2.21	1.6	1.34	1.31	1.77
Slab7	HSC-V4-8IN	7.20	1.45	1.45	1.98	1.71	3.13
Slab9	HSC-V5-8IN	3.32	1.08	0.88	1.65	1.81	2.24
Slab11	HSC-V6-8IN	3.28	1.24	1.27	1.84	1.0	2.96

Table 7-2: Analytical and Experimental Peak Slab Deflection Summary for High Strength Slabs for 1/2 in. mesh size**.**

Slab No.	Description	Deflection					
		For 1/2 in. Mesh Size					
		Experimental	LAGRANGE_IN_SOID	BEAM_IN_SOLID			
				No Function	Juan	CEBFIP	CEBFIP-S3
Slab1	HSC-V1-4IN	3.85	3.87	3.68	**	4.11	5.06
Slab3	HSC-V2-4IN	4.31	3.61	3.3	3.87	4.10	4.6
Slab5	HSC-V3-4IN	2.43	2.73	2.93	**	3.22	3.77
Slab7	HSC-V4-8IN	7.20	**	**	**	3.79	4.50
Slab9	HSC-V5-8IN	3.32	2.91	2.38	**	2.66	2.66
Slab11	HSC-V6-8IN	3.28	3.34	2.82	2.94	2.63	3.39

** Negative volume in elements terminated the analysis

Table 7-3: Percentage Comparison of Peak Slab Deflections with the Experimental Value for High Strength Slabs for 1in. mesh size.

Slab No.	Description	Percentage Change in Deflection	
		For 1 in. Mesh Size	
		LAGRANGE_IN_SOILD	BEAM_IN_SOLID

			No Function	Juan	CEBFIP	CEBFIP-S3
Slab1	HSC-V1-4IN	↓44%	↓27%	↓60%	↑75%	↓21.5%
Slab3	HSC-V2-4IN	↑65%	↓57%	↓46%	↓59%	↓54%
Slab5	HSC-V3-4IN	↓9%	↓34%	↓44%	↓46%	↓27%
Slab7	HSC-V4-8IN	↓80%	↓80%	↓72.5%	↓76%	↓56.5%
Slab9	HSC-V5-8IN	↓67.5%	↓73%	↓50%	↓45.5%	↓32.5%
Slab11	HSC-V6-8IN	↓62%	↓61%	↓44%	↓69.5%	↓10%

Table 7-4: Percentage Comparison of Peak Slab Deflections with the Experimental Value for High Strength Slabs for ½ in. mesh size.

Slab No.	**Description**	**Percentage Change in Deflection**				
		For 1/2 in. Mesh Size				
		LAGRANGE_IN_SOILD	BEAM_IN_SOLID			
			No Function	Juan	CEBFIP	CEBFIP-S3
Slab1	HSC-V1-4IN	↑0.5%	↓4.4%	**	↑6.7%	↑31.5%
Slab3	HSC-V2-4IN	↓16%	↓23%	↓10%	↓5%	↑6.7%
Slab5	HSC-V3-4IN	↑12%	↑20.5%	**	↑32.5%	↑55%
Slab7	HSC-V4-8IN	**	**	**	↓47%	↓37.5%
Slab9	HSC-V5-8IN	↓12.5%	↓28%	**	↓20%	↓19.87%
Slab11	HSC-V6-8IN	↑1.8%	↓14%	↓10.5%	↓20%	↑3.35%

7.2 Normal-Strength Concrete – Comparison of Model with 1 in. (25.4 mm.) Mesh to ½ in. (12.7 mm.) Mesh Model.

Normal strength material slabs have far more variation in their results compared to high strength material slabs. Both CEB-FIP functions give variation on results up to 462% with 1 in. (25.4mm.) mesh size and 524% with ½ in. (12.7 mm.) mesh Model. Whereas beam-bond formulation for Jaun function and program generated faction has maximum variation of results up to 125% and the majority of its variation is less than 50% for 1 in. (25.4mm.) mesh size. Perfect bond relation and Beam bond relation generated by the program LS-DYNA give identical

deflection history curves in their results, in most cases, for both mesh sizes, and have less variation between them.

The nature of residual deflection history curve for Juan function is similar for most of the twelve slabs, which is not affected by reinforcement ratio. For 1 in. (25.4mm.) mesh size all the residual deflection curve are similar and for all ½ in. (12.7 mm.) mesh size all the residual deflection curve are also similar. In the case of both CEB-FIP functions there is no chance to comment on residual deflection.

For the reduction of the mesh size form 1 in. (25.4mm.) to ½ in. (12.7 mm.) peak deflection tends to increase. CIB-FIP-S3 function for beam-bond formulation give less reduction when mesh size is decreased than other bond functions.

The overall mesh analysis results for all six slabs of regular material strength are tabulated in the Table 7.2-1 to Table 7.2-4. The Table 7.2-1 and Table 7.2-2 gives peak deflection for 1 in. (25.4 mm) and ½ in. (12.7 mm) mesh size respectively. Table 7.2-3 and Table 7.2-4 gives percentage change in peck deflection for same with respect to the experimental peak deflections.

Table 7-5: Analytical and Experimental Peak Slab Deflection Summary for Regular Strength Slabs for 1 in. mesh size.

Slab No.	Description	Deflection					
		For 1 in. Mesh Size					
		Experimental	LAGRANGE_IN_SOID	BEAM_IN_SOLID			
				No Function	Juan	CEBFIP	CEBFIP-S3
Slab2	RSC-R1-4IN	4.24	7.25	7.29	7.64	12.24	16.52
Slab4	RSC-R2-4IN	4.43	6.71	6.47	6.87	10.77	14.89
Slab6	RSC-R3-4IN	2.83	6.62	6.38	6.76	10.58	15.90
Slab8	RSC-R4-8IN	3.29	1.90	1.03	2.51	4.28	18.28
Slab10	RSC-R5-8IN	3.52	5.08	4.67	5.21	7.07	18.82
Slab12	RSC-R6-8IN	2.94	3.18	2.95	3.46	4.20	18.70

Table 7-6: Analytical and Experimental Peak Slab Deflection Summary for Regular Strength Slabs for 1/2 in. mesh size.

Slab No.	Description	Deflection					
		For 1/2 in. Mesh Size					
		Experimental	LAGRANGE_IN_SOILD	BEAM_IN_SOLID			
				No Function	Juan	CEBFIP	CEBFIP-S3
Slab2	RSC-R1-4IN	4.24	9.38	9.23	9.89	15.14	18.49
Slab4	RSC-R2-4IN	4.43	9.37	9.28	10.06	15.53	17.63
Slab6	RSC-R3-4IN	2.83	8.40	8.25	8.95	14.02	17.65
Slab8	RSC-R4-8IN	3.29	7.91	7.49	8.11	11.15	17.91
Slab10	RSC-R5-8IN	3.52	8.6	8.4	9.23	13.20	18.46
Slab12	RSC-R6-8IN	2.94	7.23	7.41	8.10	11.96	18.04

Table 7-7: Percentage Change in Peak Slab Deflection when the Mesh Size was reduced from 1 in. (25.4mm.) to ½ in. (12.7 mm.) for R Strength Slabs.

Slab No.	Description	Percentage Change in Deflection				
		For 1 in. Mesh Size				
		LAGRANGE_IN_SOILD	BEAM_IN_SOLID			
			No Function	Juan	CIBFIP	CIBFIP-S3
Slab2	RSC-R1-4IN	↑70%	↑71.94%	↑80.1%	↑188%	↑289%
Slab4	RSC-R2-4IN	↑51.4%	↑46.05%	↑55.08%	↑143%	↑236%
Slab6	RSC-R3-4IN	↑133.9%	↑125.4%	↑138.86%	↑273%	↑462%
Slab8	RSC-R4-8IN	↓42.2%	↓68.7%	↓23.70%	↑30%	↑455%
Slab10	RSC-R5-8IN	↑44.3%	↑32.67%	↑48.02%	↑100%	↑434%
Slab12	RSC-R6-8IN	↑8.1%	↑0.34%	↑17.68%	↑42%	↑536%

Table 7-8: Percentage Comparison of Peak Slab Deflections with the Experimental Value for Regular Strength Slabs for ½ in. mesh size

Slab No.	Description	Deflection				
		For 1/2 in. Mesh Size				
		LAGRANGE_IN_SOILD	BEAM_IN_SOLID			
			No Function	Juan	CIBFIP	CIBFIP-S3
Slab2	RSC-R1-4IN	↑121%	↑117%	↑133%	↑257%	↑336%
Slab4	RSC-R2-4IN	↑111%	↑111%	↑127%	↑250%	↑298%
Slab6	RSC-R3-4IN	↑196%	↑191%	↑216%	↑396%	↑524%
Slab8	RSC-R4-8IN	↑140%	↑127%	↑146%	↑238%	↑444%
Slab10	RSC-R5-8IN	↑144%	↑138%	↑162%	↑275%	↑424%
Slab12	RSC-R6-8IN	↑145%	↑152%	↑175%	↑307%	↑513%

7.3 Mesh Size Effects

With reduction in mesh size from 1 in. (25.4mm.) to 1/2in. (12.7 mm.) it was expected to have increase in peak deflection history, which was observed in most of the cases. For High Strength concrete material Lagrange In Solid Formulation shows minimum increase in peak deflection for some 4 IN reinforcement ratio models. For 8 IN reinforcement ratio models these difference increases up to 169%. Similar result pattern is shown by Beam In Solid formulation with no user defined function. But with both CEB-FIP functions no constant pattern has been observed for both 8IN and 4IN models.

For normal strength materials change in deflection with respect to reduction in mesh size has shown constant change in peak deflections for 4 in. models with maximum increase in deflection of 46.5%. For 8 in. models also with few exceptions, constant variation like 4 in. models is observed. Table 7.3-1 and 7.3-2 shows details for all 12 slabs for percentage change in peak slab deflections.

Table 7-9 Percentage Change in Peak Slab Deflection when the Mesh Size was reduced from 1 in. (25.4mm.) to ½ in. (12.7 mm.) for High Strength Slabs.

Slab No.	Description	Deflection				
		For 1 in. to 1/2 in. Mesh Size				
		LAGRANGE_IN_SOILD	BEAM_IN_SOLID			
			No Function	Juan	CEBFIP	CEBFIP-S3
Slab1	HSC-V1-4IN	↑79%	↑31%	**	↓39%	↑67.54%
Slab3	HSC-V2-4IN	↓49%	↑79%	↑68%	↑130%	↑133.5%
Slab5	HSC-V3-4IN	↑23.5%	↑83%	**	↑146%	↑123%
Slab7	HSC-V4-8IN	**	**	**	↑121%	↑44%
Slab9	HSC-V5-8IN	↑169.4%	↑170.5%	**	↑46%	↑18.75%
Slab11	HSC-V6-8IN	↑169.3%	↑122%	↑60%	↑163%	↑14.5%

Table 7-10: Percentage Change in Peak Slab Deflection when the Mesh Size was reduced from 1 in. (25.4mm.) to ½ in. (12.7 mm.) for Regular Strength Slabs.

Slab No.	Description	Percentage change in Deflection				
		For 1 in. to 1/2 in. Mesh Size				
		LAGRANGE_IN_SOILD	BEAM_IN_SOLID			
			No Function	Juan	CEBFIP	CEBFIP-S3
Slab2	RSC-R1-4IN	↑29%	↑26.5%	↑29.5%	↑24%	↑12%
Slab4	RSC-R2-4IN	↑39.5%	↑43.5%	↑46.5%	↑44%	↑18.5%
Slab6	RSC-R3-4IN	↑27%	↑29.5%	↑32.5	↑32.5%	↑11%
Slab8	RSC-R4-8IN	↑316%	↑627%	↑223%	↑160.5%	↓2%
Slab10	RSC-R5-8IN	↑69%	↑79.8%	↑77%	↑86.7%	↓1.91%
Slab12	RSC-R6-8IN	↑127%	↑151%	↑151%	↑184.7%	↓3.5%

CHAPTER 8. CONCLUSION AND FUTURE WORK

This chapter discusses conclusions and observations of the results of comparison of numerical simulation experimental records of all twelve single-mat reinforced concrete slabs, which were subjected to blast loading. Further results obtained were compared to experimental data in order to validate bond interactions between concrete and steel. Further, in this chapter, the scope for future work is also outlined based on the results and conclusions of this study.

1. Prefect bond formulation using Lagrange In solid Formulation gives most accurate results for peak deflection when compared to experimental records. Beam In Solid formulation fails to give accurate results for blast loading,
2. If Beam In solid formulation is to be used than CEB-FIP-S3 function is most appropriate function for high strength material and bond-slip function defined by Juan for regular strength concrete is most appropriate.
3. Modification of CEB-FIP function by inclusion of new parameter can control free vibration of slab after peak deflection is reached.
4. Winfrith concrete Model is unable to produces results which can be compared to experimental records, hence its use for bond-slip analysis is not recommended.
5. ¼ inch (6.23 mm.) mesh size is unable to generate deflection history curves with normal termination for analysis.

8.1 Future Scope of Work

The suggestions for future work are obtained from studies conducted in this thesis and are given below.

1. The scope of improvement of beam-bond formulation functions which can address material strength of concrete used to predict response more accurately in comparison of experiment records for normal strength-concrete.
2. Based on experimental data available for single–mat slabs pressure- impulse diagrams can be developed.
3. Use of hourglass control needs to be studied as it influences peak deflection history of numerical simulation and developing relation between its parameters and the strength of concrete used.

APPENDIX A - PRESSURE AND IMPULSE DATA FOR 12 SLABS

Summary of Peak Pressures and Impulse for twelve RC slabs recorded at six locations on each slab:

Slab #1	P+ (psi)	I+ (psi-msec)
P1	48.97	994.16
P2	54.72	1142.59
P3	52.39	998.72
P4	53.1	966.49
P5	53.48	978.36
P6	53.04	996.94
PD	53.2	986.16
PE	53.65	1042.8
Sum	422.55	8106.22
Avg	52.82	1013.28
	Deflection (in)	
L1	3.89	
A1	3.97	
	Strain	
S1		
S2		

Slab #2	P+ (psi)	I+ (psi-msec)
P1	52.55	971.56
P2	56.73	1089.44
P3	51.72	972.04
P4	53.3	889.41
P5	51.87	974.37
P6	53.67	985.68
PD	49.98	967.83
PE	55	959
Sum	424.82	7809.33
Avg	53.10	976.17
	Deflection (in)	
L1	4.29	
A1	5.37	
	Strain	
S1		
S2		

Slab #3	P+ (psi)	I+ (psi-msec)
P1	47.43	973.95
P2	52.74	1140.11
P3	48.68	984.34
P4	48.55	923
P5	48.45	971.28
P6	50.74	1011.77
PD	47.6	976.78
PE	50.02	999.73
Sum	394.21	7980.96
Avg	49.28	997.62
	Deflection (in)	
L1	4.53	
A1	4.69	
	Strain	
S1		
S2		

Slab #4	P+ (psi)	I+ (psi-msec)
P1	48.25	986.22
P2	54	1073.28
P3	50.49	988.37
P4	55.83	1014.28
P5	52.1	974.33
P6	51.65	993.69
PD	49.58	992.68
PE	57.2	980.16
Sum	419.1	8003.01
Avg	52.39	1000.38
	Deflection (in)	
L1	4.45	
A1	NG	
	Strain	
S1		
S2		

Slab #5	P+ (psi)	I+ (psi-msec)
P1	42.4	756.33
P2	44.62	805.45
P3	42.1	754.03
P4	43.19	806.8
P5	41.05	744.67
P6	41.47	778.9
PD	39.81	758.61
PE	41.67	786.8
Sum	336.31	6191.59
Avg	42.04	773.95
	Deflection (in)	
L1	2.46	
A1	NG	
	Strain	
S1		
S2		

Slab #6	P+ (psi)	I+ (psi-msec)
P1	43.97	778.53
P2	43.63	789.51
P3	44.57	772.82
P4	45.65	800.56
P5	43.19	771.71
P6	44.84	799.05
PD	44.46	773.35
PE	43.28	797.28
Sum	353.59	6282.81
Avg	44.20	785.35
	Deflection (in)	
L1	3.17	
A1	NA	
	Strain	
S1		
S2		

Slab #7	P+ (psi)	I+ (psi-msec)
P1	41.89	755.87
P2	45.87	743.29
P3	44.92	757.07
P4	50.61	766.41
P5	46.83	744.18
P6	42.18	753.33
PD	40.22	749.39
PE	42.87	761.35
Sum	355.39	6030.89
Avg	44.42	753.86
	Deflection (in)	
L1	7.2	
A1	5.44, 7.28, 8.61	
	Strain	
S1		
S2		

Slab #8	P+ (psi)	I+ (psi-msec)
P1	32.38	493.5
P2	32.91	532.02
P3	35	494.99
P4	34.41	401.28
P5	33.9	488.51
P6	34.32	534.79
PD	31.73	498.04
PE	32.57	511.95
Sum	267.22	3955.08
Avg	33.40	494.39
	Deflection (in)	
L1	3.36	
A1	3.38	
	Strain	
S1		
S2		

Slab #9	P+ (psi)	I+ (psi-msec)
P1	32.65	490.44
P2	35.09	553.94
P3	36.25	492.39
P4	35.69	535.85
P5	32.34	488.46
P6	33.69	515.66
PD	33.81	501.71
PE	32.57	515.72
Sum	272.09	4094.17
Avg	34.01	511.77
	Deflection (in)	
L1	3.4	
A1	1.78, 3.57	
	Strain	
S1		
S2		

Slab #10	P+ (psi)	I+ (psi-msec)
P1	34.94	518.32
P2	36.43	549.86
P3	37	519.8
P4	34.94	582.35
P5	33.4	511.01
P6	33.94	615.82
PD	33.24	529.24
PE	34.37	569.58
Sum	278.26	4395.98
Avg	34.78	549.50
	Deflection (in)	
L1	3.6	
A1	3.75	
	Strain	
S1		
S2		

Slab #11	P+ (psi)	I+ (psi-msec)
P1	37.91	565.13
P2	37.18	571.36
P3	37.19	578.71
P4	37.45	586.54
P5	37.47	569.86
P6	37.76	582.16
PD	35.79	571.33
PE	35.65	583.47
Sum	296.4	4608.56
Avg	37.05	576.07
	Deflection (in)	
L1	3.38	
A1	3.96	
	Strain	
S1		
S2		

Slab #12	P+ (psi)	I+ (psi-msec)
P1	34.17	484.64
P2	33.4	400.48
P3	36.91	485.62
P4	32.6	592.56
P5	33.43	499.28
P6	32.24	558.79
PD	32.73	519.73
PE	34.4	531
Sum	269.88	4072.1
Avg	33.74	509.01
	Deflection (in)	
L1	3.17	
A1	2.12, 2.85	
	Strain	
S1		
S2		

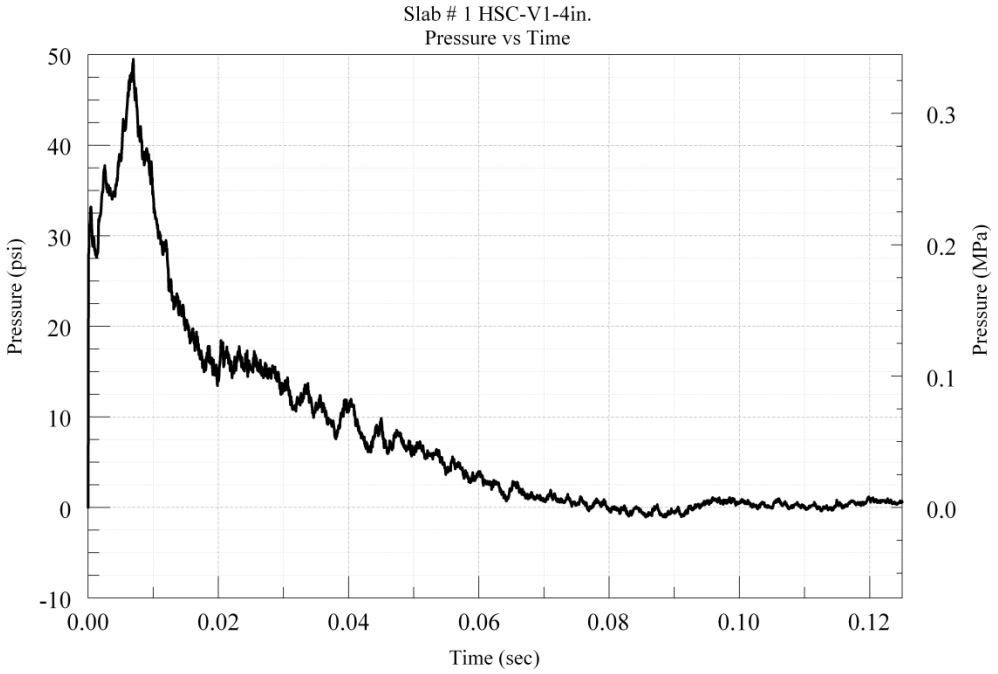

Figure B-8.1-1 : Average Pressure-time History for Slab # 1.

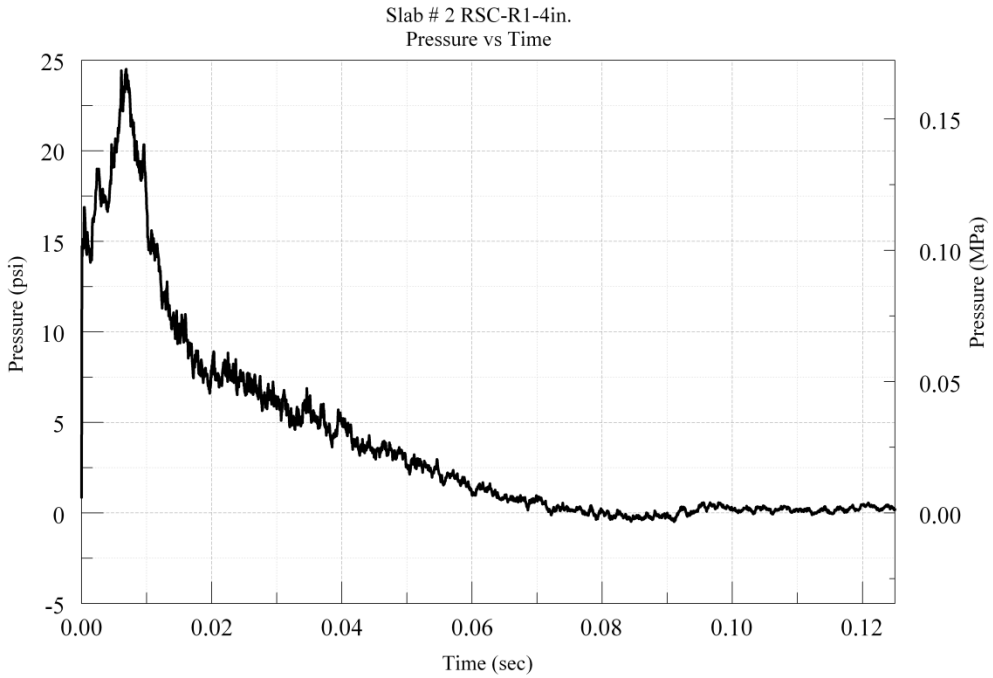

Figure B-8.1-2**:** Average Pressure-time History for Slab # 2.

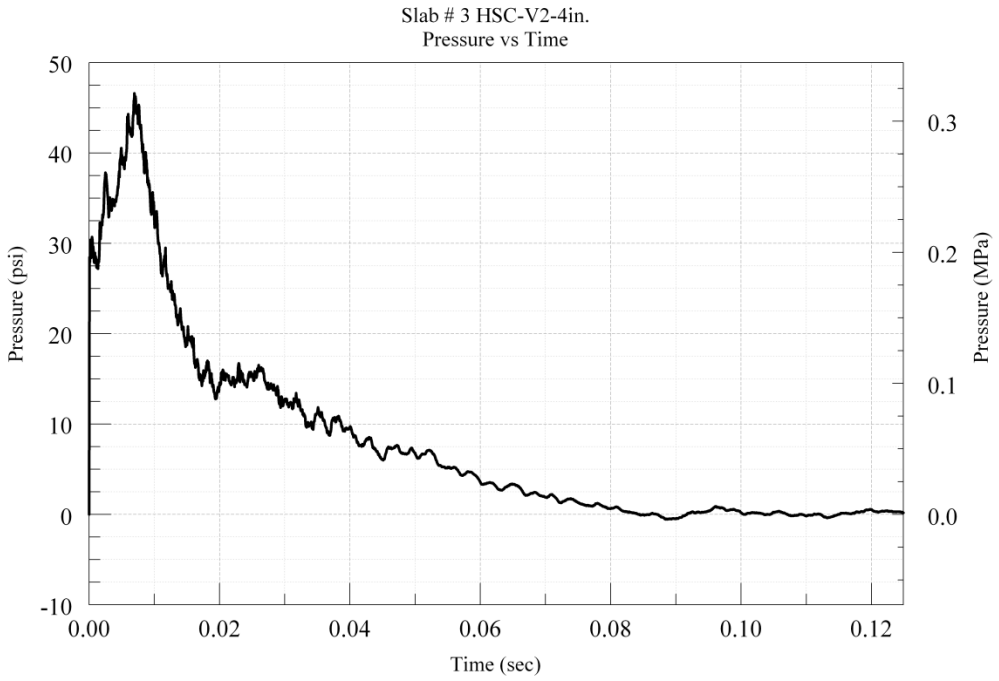

Figure B-8.1-3: Average Pressure-time History for Slab # 3.

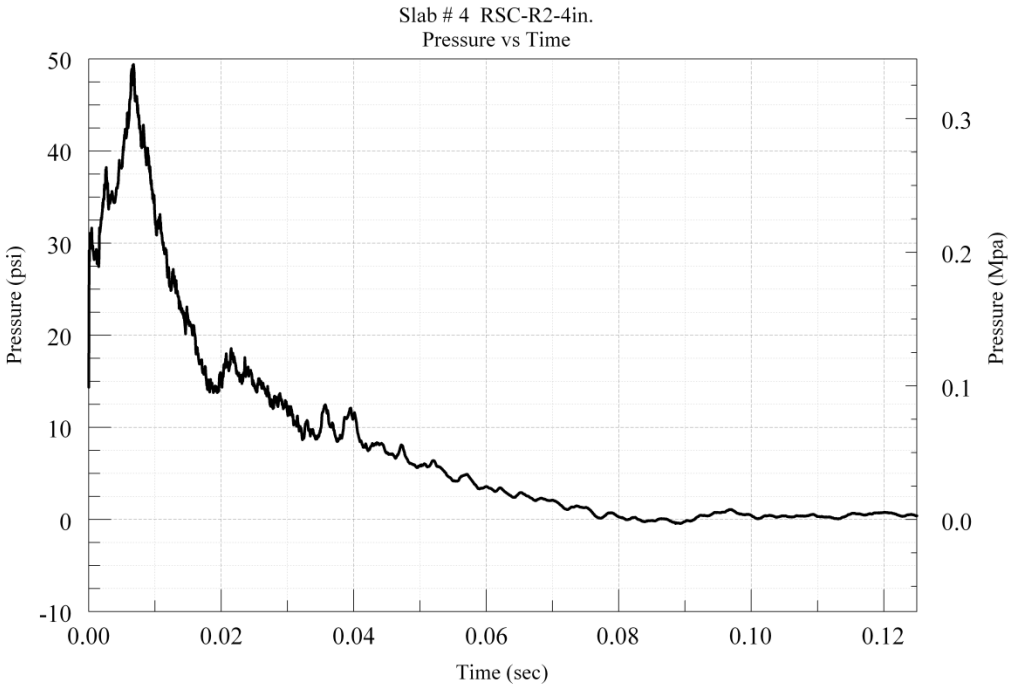

Figure B-8.1-4: Average Pressure-time History for Slab # 4.

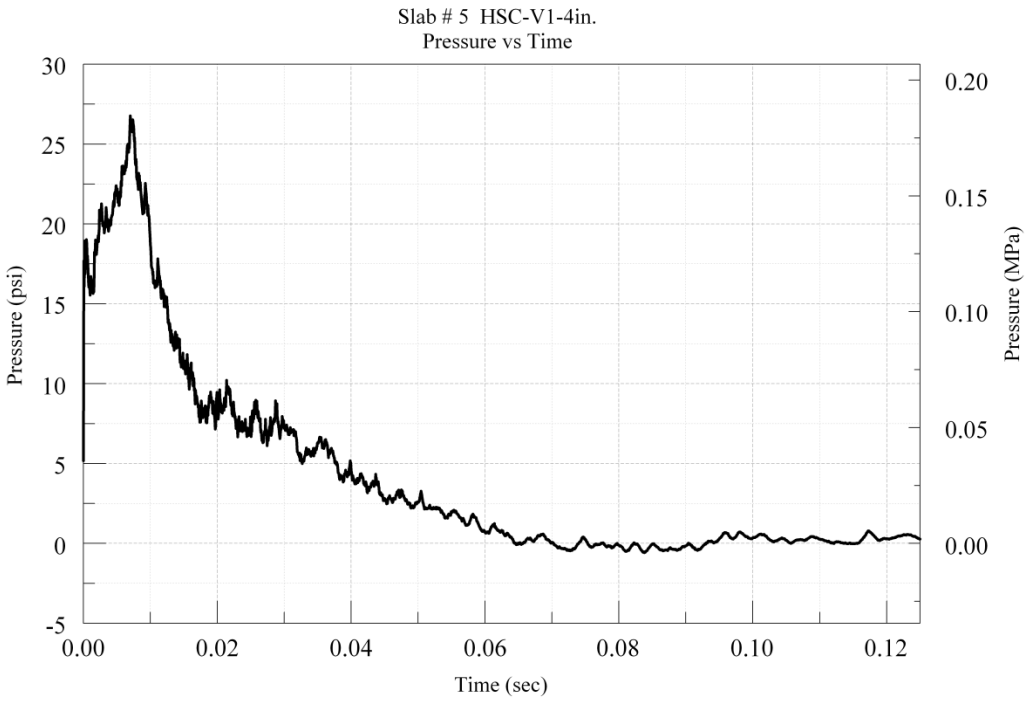

Figure B-8.1-5: Average Pressure-time History for Slab # 5.

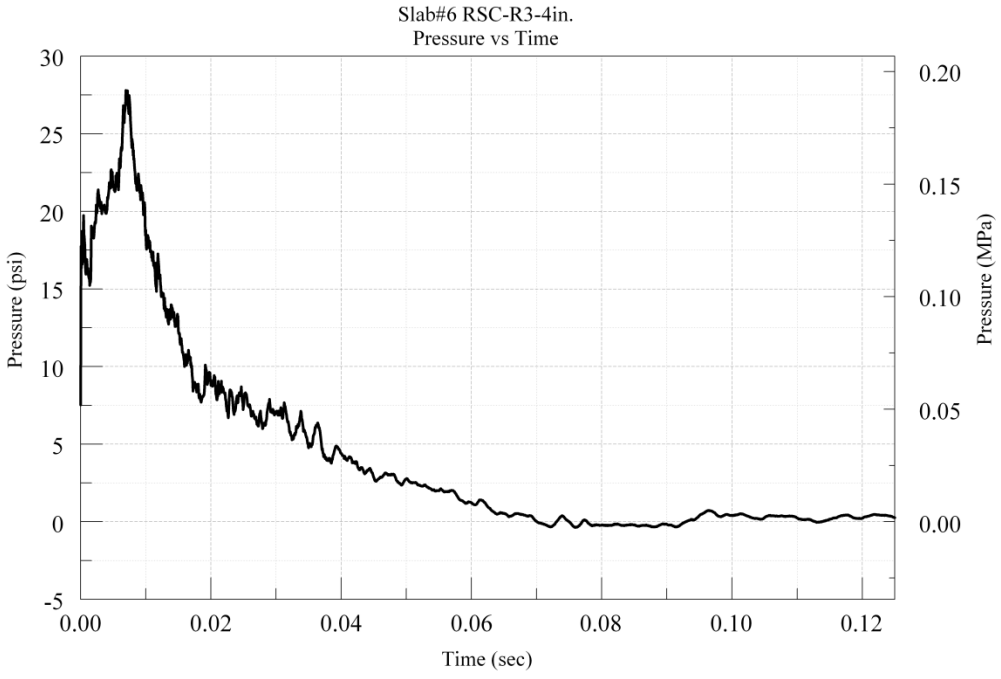

Figure B-8.1-6: Average Pressure-time History for Slab # 6.

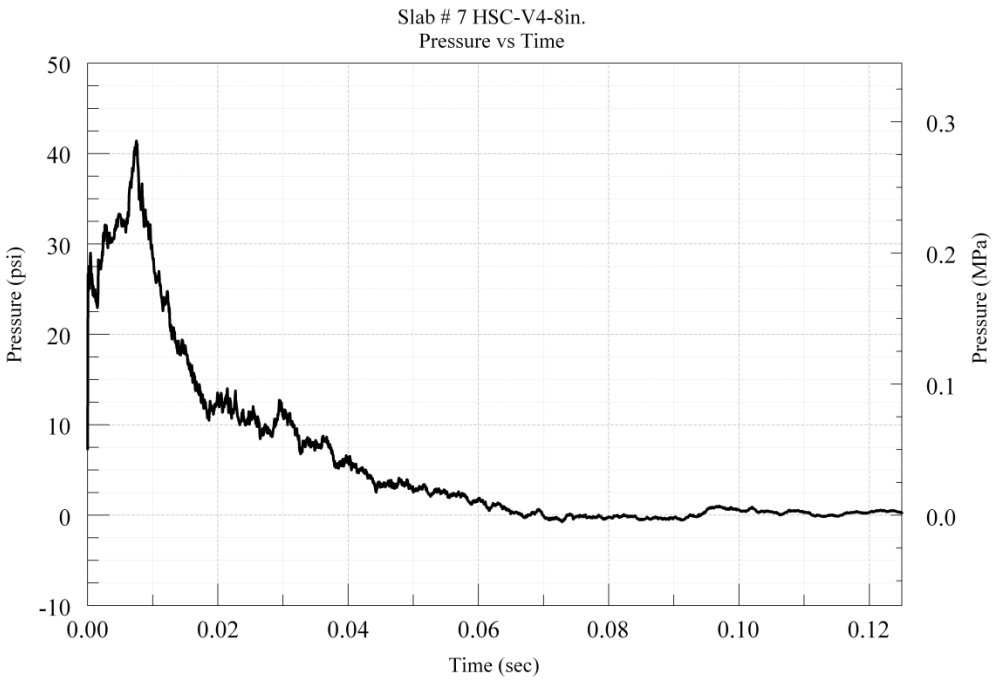

Figure B-8.1-7: Average Pressure-time History for Slab # 7.

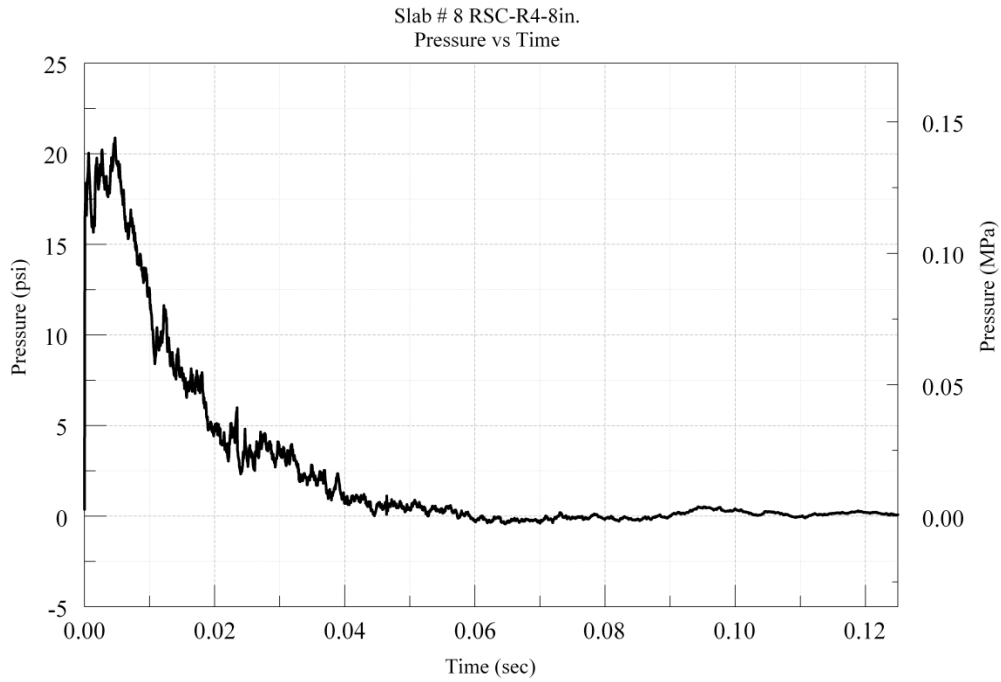

Figure B-8.1-8**:** Average Pressure-time History for Slab # 8.

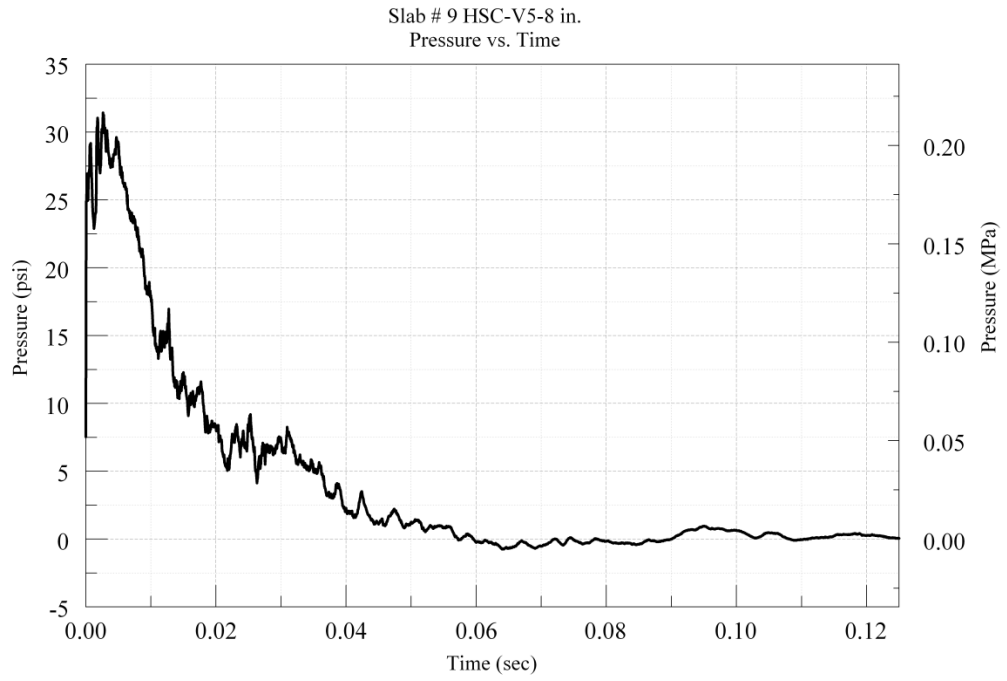

Figure B-8.1-9**:** Average Pressure-time History for Slab # 9.

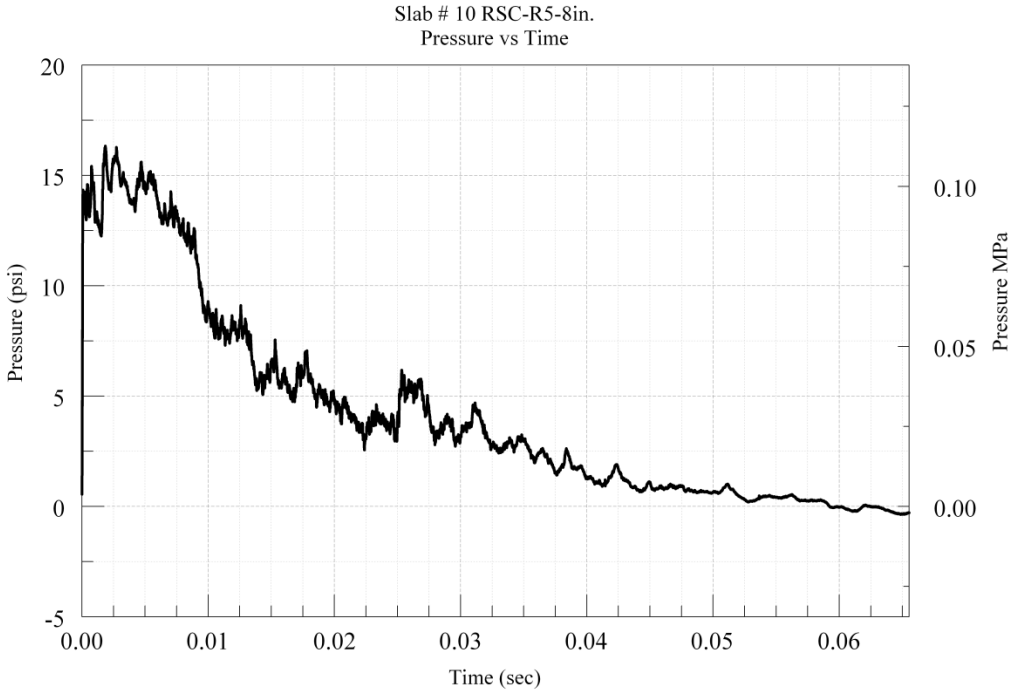

Figure B-8.1-10**:** Average Pressure-time History for Slab # 10.

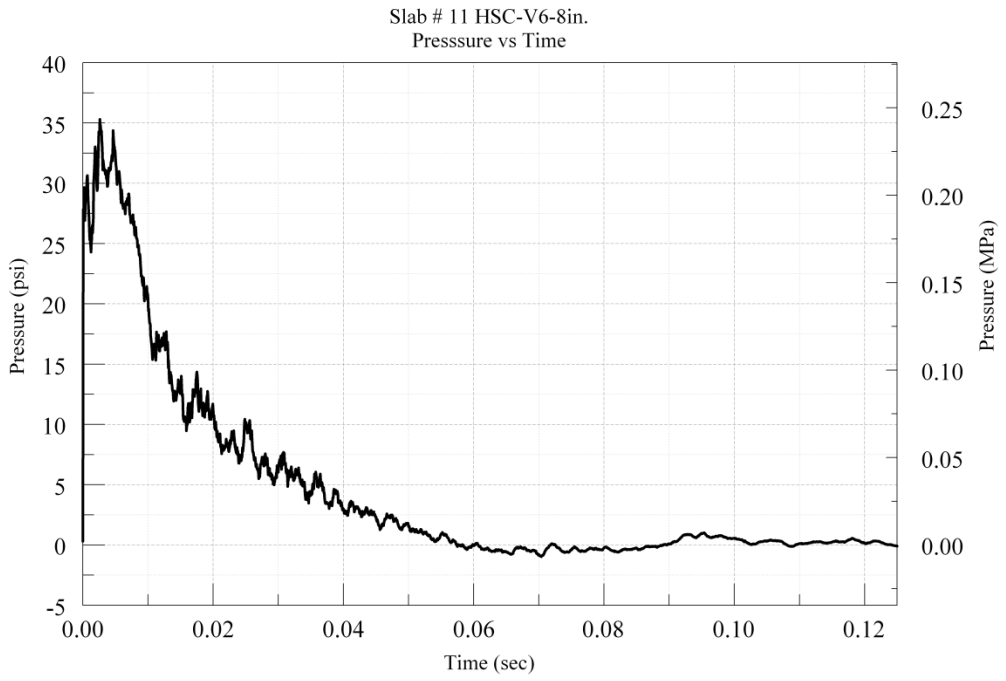

Figure B-8.1-11: Average Pressure-time History for Slab # 11.

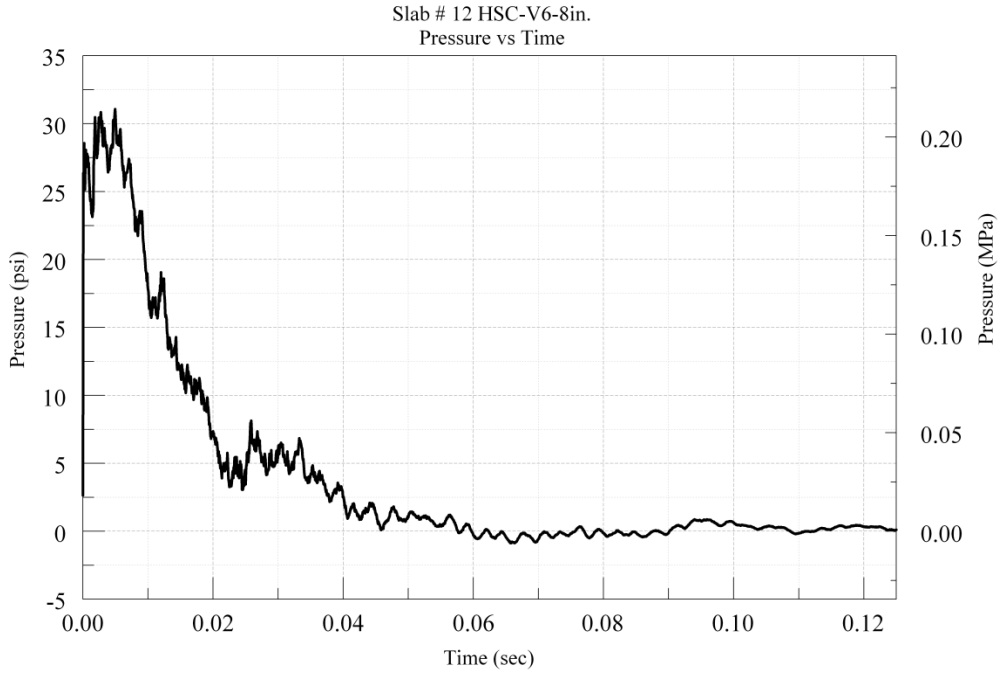

Figure B-8.1-12: Average Pressure-time History for Slab # 12.

APPENDIX C - SUMMARY TABLES

Table C- 0-1: Input parameters for Concrete Damage Model Release 3

Variable	Description	Input value for High strength concrete	Input value for Normal strength concrete
RHO	Mass Density	2.24E-04 lb-s/in^3	2.24E-04 lb-s/in^3
PR	Poisson's Ratio	0.18	0.18
FT	Uniaxial Tensile Strength	928 psi	462psi
A0/-fc'	Uniaxial Compressive Strength	4700	3200
A1	Maximum shear surface parameter	0.55	0.60
A2	Maximum shear failure parameter	0.0000082	0.00000152
B1	Damage Scaling Parameter	1.6	1.6
OMEGA	Fractional dilatancy	0.5	0.5
A1F	Residual Failure Coefficient	0.4417	0.4417
Sλ	Stretch factor	100	100
NOUT	Output selector for effective plastic strain	2	2
RSIZE	Unit Conversion factor for length	1	1
UCF	Unit Conversion factor for stress	1	1
LCRATE	Load Curve for strain rate effects	0	0
LOCWID	Maximum aggregate diameter	1	1
λ01-λ13	Damage Functions	default	default
B3	Damage scaling coefficient for tri-axial tension	1.15	1.15
A0Y	Initial yield surface cohesion	3460	1500
A1Y	Initial yield surface coefficient	0.625	0.625
η01-η13	Scale factor	default	default

B2	Tensile Damage scaling coefficient	1.35	1.35
A2F	Residual failure surface coefficient	0.00000763	0.0000177
A2Y	Initial yield surface coefficient	0.0000166	0.0000384

Table C- 0-2: Input Parameters for Plastic Kinematic Model for Steel Rebar

Variable	**Description**	**Input value for High strength steel**	**Input value for Normal strength steel**
RO	Mass Density	7.30E-04 lb-s/in^3	7.30E-04 lb-s/in^3
E	Young's Modulus of Rebar	2.90E+07 psi	2.90E+07 psi
PR	Poisson's Ratio	3.00E-01 psi	3.00E-01 psi
SIGY	Yield strength of Rebar	83000 psi	60000 psi
ETAN	Tangent Modulus	Default	Default
BETA	Hardening Parameter	Default	Default
SRC	Strain Rate Parameter	Default	Default
SRP	Strain Rate Parameter	Default	Default
FS	Failure Strain for Eroding Elements	Default	Default

```
$# LS-DYNA Keyword file created by LS-PREPOST 3.0 - 30May2010(20:48)
$# Created on Jul-25-2012 (11:21:13)
*KEYWORD
*TITLE
$# title
LS-DYNA keyword deck by LS-Prepost
*CONTROL_ACCURACY
$ cleaned up (eliminated unused commands, parts)
$#     osu       inn    pidosu
         1         0         0
*CONTROL_ENERGY
$  reduce tssf
$#    hgen      rwen    slnten     rylen
         2         2         2         2
*CONTROL_HOURGLASS
$         1       0.0
$#     ihq        qh
         4  1.400000
*CONTROL_TERMINATION
$#  endtim    endcyc     dtmin    endeng    endmas
  0.145000         0     0.000     0.000     0.000
*CONTROL_TIMESTEP
$       0.0       0.0         0       0.0       0.0
$#  dtinit    tssfac      isdo    tslimt     dt2ms      lctm     erode     ms1st
     0.000  0.600000         0     0.000     0.000         0         0         0
$#  dt2msf   dt2mslc     imscl
     0.000         0         0
*DATABASE_BNDOUT
$#      dt    binary      lcur     ioopt
  0.001000         0         0         1
*DATABASE_GLSTAT
$#      dt    binary      lcur     ioopt
  0.001000         0         0         1
*DATABASE_MATSUM
$#      dt    binary      lcur     ioopt
  0.001000         0         0         1
*DATABASE_BINARY_D3PLOT
$#      dt      lcdt      beam     npltc    psetid
 5.0000E-4         0         0         0         0
$#   ioopt
         0
*DATABASE_BINARY_D3THDT
$#      dt      lcdt      beam     npltc    psetid
  0.004000         0         0         0         0
*DATABASE_EXTENT_BINARY
$#   neiph     neips    maxint    strflg    sigflg    epsflg    rltflg    engflg
         0         0         0         1         0         0         0         0
$#  cmpflg    ieverp    beamip     dcomp      shge     stssz    n3thdt   ialemat
         0         0         1         0         0         0         0         0
$# nintsld   pkp_sen      sclp    unused     msscl     therm    iniout    iniout
         0         0  1.000000         0         0         0   OSTRESS    STRESS
```

Figure D - 8.1-1 : Input and Output Control Parameters

```
*MAT_Concrete_Damage_Rel3
$     MATID        RO        PR
          1 2.120E-04 1.500E-01
$      f't        A0        A1        A2        B1     OMEGA       A1F
 9.280E+02 4.700E+03 5.500E-01 8.200E-06 1.600E+00 5.000E-01 4.417E-01
$  sLambda      NOUT     EDROP     RSIZE       UCF    LCRate  LocWidth      NPTS
 1.000E+02 2.000E+00 1.000E+00 1.000E+00 1.000E+00 0.000E+00 1.000E+00 1.300E+01
$ Lambda01  Lambda02  Lambda03  Lambda04  Lambda05  Lambda06  Lambda07  Lambda08
 0.000E+00 8.000E-06 2.400E-05 4.000E-05 5.600E-05 7.200E-05 8.800E-05 3.200E-04
$ Lambda09  Lambda10  Lambda11  Lambda12  Lambda13        B3       A0Y       A1Y
 5.200E-04 5.700E-04 1.000E+00 1.000E+01 1.000E+10 1.150E+00 3.460E+03 6.250E-01
$     Eta01     Eta02     Eta03     Eta04     Eta05     Eta06     Eta07     Eta08
 0.000E+00 8.500E-01 9.700E-01 9.900E-01 1.000E+00 9.900E-01 9.700E-01 5.000E-01
$     Eta09     Eta10     Eta11    Eta012     Eta13        B2       A2F       A2Y
 1.000E-01 0.000E+00 0.000E+00 0.000E+00 0.000E+00 1.350E+00 7.632E-06 1.661E-05
$---------------------------  EOS-8 CARDS  -------------------------------------
$ Generated EOS 8 (Tabulated Compaction)
*EOS_TABULATED_COMPACTION
$     EOSID     Gamma        E0      Vol0
8,0.000E+00,0.000E+00,1.00
$    VolStrain01     VolStrain02     VolStrain03     VolStrain04     VolStrain05
0.00000000E+00,-3.6177502,-2.9239512,-2.5180457, -2.2306366
$    VolStrain06     VolStrain07     VolStrain08     VolStrain09     VolStrain10
-1.6709091,-0.1381511,-0.0255410,-0.6941716,-1.1001311
$     Pressure01      Pressure02      Pressure03      Pressure04      Pressure05
0.00000000E+00,958.16,2107.87,3353.33,4311.49
$     Pressure06      Pressure07      Pressure08      Pressure09      Pressure10
7664.83,23382.41,25717.49,35323.02,42915.07
$            Multipliers of Gamma*E
0.000000000E+00,0.000000000E+00,0.000000000E+00,0.000000000E+00,0.000000000E+00
0.000000000E+00,0.000000000E+00,0.000000000E+00,0.000000000E+00,0.000000000E+00
$     BulkUnld01      BulkUnld02      BulkUnld03      BulkUnld04      BulkUnld05
3.37925846E+06,3.37925846E+06,3.42656808E+06,3.59891026E+06,4.28152047E+06
$     BulkUnld06      BulkUnld07      BulkUnld08      BulkUnld09      BulkUnld10
4.96750994E+06,5.65012015E+06,6.16714669E+06,1.38752352E+07,1.68962923E+07
$-------------------------------------------------------------------------------
```

Figure D - 8.1-2: Input Parameters for Concrete Damage Model Release 3 for High-Strength Concrete

```
-----------------------------------------
 Automatic version f3dm16_b21.f
 by K&C/Javier Malvar (9/99 updated 5/03)
 based on LRDA/K&C f3dm16w.f (8/7/95)
   LS-DYNA® Release III of Mat 72 by
       Len Schwer (May 04)
-----------------------------------------
 pressure phi     0.00000E+00    5.00000E-01
 pressure phi     3.68212E+03    6.26014E-01
 pressure phi     8.46889E+03    6.91461E-01
 pressure phi     3.31391E+04    7.53000E-01
 pressure phi     9.33419E+04    1.00000E+00
 a0  a1  a2  =   4.70000E+03    5.50000E-01    8.20000E-06
 a0f a1f a2f =   0.00000E+00    4.41700E-01    7.63200E-06
 a0y a1y a2y =   3.46000E+03    6.25000E-01    1.66100E-05
 nu  w   ucf =   1.50000E-01    5.00000E-01    1.00000E+00
 f c  fyc    ft   =   1.10464E+04    6.95321E+03    9.28000E+02
 Ec         =   7.09644E+06
 rls taurus edrop =    1.00000E+02    2.00000E+00    1.00000E+00
 b1  b2  b3  =    1.60000E+00    1.35000E+00    1.15000E+00
 npt RateCurve localiz.width =    1.30000E+01    0.00000E+00    1.00000E+00
 lambdas  0.000E+00 8.000E-06 2.400E-05 4.000E-05 5.600E-05 7.200E-05 8.800E-05
 etas     0.000E+00 8.500E-01 9.700E-01 9.900E-01 1.000E+00 9.900E-01 9.700E-01
 lambdas  3.200E-04 5.200E-04 5.700E-04 1.000E+00 1.000E+01 1.000E+10
 etas     5.000E-01 1.000E-01 0.000E+00 0.000E+00 0.000E+00 0.000E+00
-----------------------------------------
equation of state 8
 lnv   0.0000E+00 -3.6178E+00 -2.9240E+00 -2.5180E+00 -2.2306E+00
 lnv  -1.6709E+00 -1.3815E-01 -2.5541E-02 -6.9417E-01 -1.1001E+00
 p     0.0000E+00  9.5816E+02  2.1079E+03  3.3533E+03  4.3115E+03
 p     7.6648E+03  2.3382E+04  2.5717E+04  3.5323E+04  4.2915E+04
uk    3.3793E+06  3.3793E+06  3.4266E+06  3.5989E+06  4.2815E+06
uk    4.9675E+06  5.6501E+06  6.1671E+06  1.3875E+07  1.6896E+07
$
$---------- MATERIAL CARDS ----------
$ LS-DYNA® Keyword Generated Input for Release III
$    [Default values = K&C generic f'c=6580 psi concrete]
$  *** Users need to change/check: MatID & RO & Rsize & LocWidth for units ***
*MAT_Concrete_Damage_Rel3
$    MATID       RO       PR
        72 2.120E-04 1.500E-01
$       ft       A0       A1       A2       B1    OMEGA      A1F
 9.280E+02 4.700E+03 5.500E-01 8.200E-06 1.600E+00 5.000E-01 4.417E-01
$  sLambda     NOUT    EDROP    RSIZE      UCF   LCRate  LocWidth     NPTS
 1.000E+02 2.000E+00 1.000E+00 1.000E+00 1.000E+00 0.000E+00 1.000E+00 1.300E+01
$ Lambda01  Lambda02  Lambda03  Lambda04  Lambda05  Lambda06  Lambda07  Lambda08
 0.000E+00 8.000E-06 2.400E-05 4.000E-05 5.600E-05 7.200E-05 8.800E-05 3.200E-04
$ Lambda09  Lambda10  Lambda11  Lambda12  Lambda13       B3      A0Y      A1Y
 5.200E-04 5.700E-04 1.000E+00 1.000E+01 1.000E+10 1.150E+00 3.460E+03 6.250E-01
$    Eta01     Eta02     Eta03     Eta04     Eta05     Eta06     Eta07     Eta08
 0.000E+00 8.500E-01 9.700E-01 9.900E-01 1.000E+00 9.900E-01 9.700E-01 5.000E-01
$    Eta09     Eta10     Eta11    Eta012     Eta13       B2      A2F      A2Y
 1.000E-01 0.000E+00 0.000E+00 0.000E+00 0.000E+00 1.350E+00 7.632E-06 1.661E-05
$
$---------- EOS-8 CARDS ----------
$ Generated EOS 8 (Tabulated Compaction)
*EOS_Tabulated_Compaction
$    EOSID     Gamma        E0      Vol0
        8 0.000E+00 0.000E+00 1.000E+00
$    VolStrain01     VolStrain02     VolStrain03     VolStrain04     VolStrain05
  0.00000000E+00 -3.61775020E+00 -2.92395120E+00 -2.51804570E+00 -2.23063660E+00
```

Figure D - 8.1-3: Input Parameters Generated by Concrete Damage Model Release 3 for High- Strength Concrete.

```
*MAT_CONCRETE_DAMAGE_REL3
$     MATID         RO         PR
$#      mid         ro         pr
          1 2.2460E-4  0.180000
$       f't         A0         A1         A2         B1      OMEGA       A1F
 4.620E+02 3.200E+03  0.600000 1.5200E-5  1.600000  0.500000  0.441700
$   sLambda       NOUT      EDROP      RSIZE        UCF     LCRate  LocWidth       NPTS
 1.000E+02 2.000E+00 1.000E+00 1.000E+00 1.000E+00 0.000E+00 1.000E+00 1.300E+01
$ Lambda01   Lambda02  Lambda03  Lambda04  Lambda05  Lambda06  Lambda07  Lambda08
 0.000E+00 8.000E-06 2.400E-05 4.000E-05 5.600E-05 7.200E-05 8.800E-05 3.200E-04
$ Lambda09   Lambda10  Lambda11  Lambda12  Lambda13         B3        A0Y        A1Y
 5.200E-04 5.700E-04 1.000E+00 1.000E+01 1.000E+10 1.150E+00 1.500E+03 6.250E-01
$     Eta01      Eta02      Eta03      Eta04      Eta05      Eta06      Eta07      Eta08
 0.000E+00 8.500E-01 9.700E-01 9.900E-01 1.000E+00 9.900E-01 9.700E-01 5.000E-01
$     Eta09      Eta10      Eta11     Eta012      Eta13         B2        A2F        A2Y
 1.000E-01 0.000E+00 0.000E+00 0.000E+00 0.000E+00 1.350E+00 1.770E-05 3.840E-05
*EOS_TABULATED_COMPACTION
$     EOSID      Gamma         E0       Vol0
8,0.000E+00,0.000E+00,1.00
0,-0.0324,-0.2631,-0.5325,-0.7445
-0.9612,-1.3212,-1.5405,-1.7649,-1.9093
0,12729.521,14807.69,18020.745,21425.635
25776.94,37439.29,48455.81,66252.24,86958.24
$             Multipliers of Gamma*E
$#             t1              t2              t3              t4              t5
           0.000           0.000           0.000           0.000           0.000
$#             t6              t7              t8              t9             t10
           0.000           0.000           0.000           0.000           0.000
$      BulkUnld01      BulkUnld02      BulkUnld03      BulkUnld04      BulkUnld05
  2.22173861E+06  2.22173861E+06  2.25284295E+06  2.36615162E+06  2.81494282E+06
$      BulkUnld06      BulkUnld07      BulkUnld08      BulkUnld09      BulkUnld10
  3.26595576E+06  3.71474696E+06  4.05467296E+06  9.12245873E+06  1.11086930E+07
```

Figure D - 8.1-4 : Input Parameters for Concrete Damage Model Release 3for Normal-Strength Concrete

```
Automatic version f3dm16_b21.f
 by K&C/Javier Malvar (9/99 updated 5/03)
 based on LRDA/K&C f3dm16w.f (8/7/95)
   LS-DYNA Release III of Mat 72 by
        Len Schwer (May 04)
pressure phi      0.00000E+00    5.00000E-01
 pressure phi      2.23333E+03    6.25716E-01
 pressure phi      5.13667E+03    6.37453E-01
 pressure phi      2.01000E+04    7.53000E-01
 pressure phi      5.66150E+04    1.00000E+00
 a0  a1  a2  =    1.98052E+03    4.46300E-01    1.20597E-05
 a0f a1f a2f =    0.00000E+00    4.41700E-01    1.76567E-05
 a0y a1y a2y =    1.49544E+03    6.25000E-01    3.84328E-05
 pu  w   ucf =    1.50000E-01    5.00000E-01    1.00000E+00
 f'c  fyc    ft    =    6.70000E+03    3.00522E+03    5.61531E+02
 Ec          =    4.66565E+06
 rla taurus edrop =    1.00000E+02    2.00000E+00    1.00000E+00
 b1  b2  b3  =    1.60000E+00    1.35000E+00    1.15000E+00
 npt RateCurve localiz.width =    1.30000E+01    0.00000E+00    1.00000E+00
 lambdas  0.000E+00 8.000E-06 2.400E-05 4.000E-05 5.600E-05 7.200E-05 8.800E-05
 etas     0.000E+00 8.500E-01 9.700E-01 9.900E-01 1.000E+00 9.900E-01 9.700E-01
 lambdas  3.200E-04 5.200E-04 5.700E-04 1.000E+00 1.000E+01 1.000E+10
 etas     5.000E-01 1.000E-01 0.000E+00 0.000E+00 0.000E+00 0.000E+00

equation of state 8
 lnv   0.0000E+00 -1.5000E-03 -4.3000E-03 -1.0100E-02 -3.0500E-02
 lnv  -5.1300E-02 -7.2600E-02 -9.4300E-02 -1.7400E-01 -2.0800E-01
 p     0.0000E+00  3.3326E+03  7.2651E+03  1.1664E+04  2.2162E+04
 p     3.3426E+04  4.7423E+04  7.2551E+04  4.2357E+05  6.4786E+05
uk    2.2217E+06  2.2217E+06  2.2528E+06  2.3662E+06  2.8149E+06
uk    3.2660E+06  3.7147E+06  4.0547E+06  9.1225E+06  1.1109E+07
$---------------------------  MATERIAL CARDS ---------------------------------------
$ LS-DYNA Keyword Generated Input for Release III
$    [Default values = K&C generic f'c=6580 psi concrete]
$ *** Users need to change/check: MatID & RO & Rsize & LocWidth for units ***
*MAT_Concrete_Damage_Rel3
$    MATID        RO        PR
        72 2.120E-04 1.500E-01
$       ft        A0        A1        A2        B1     OMEGA       A1F
 5.615E+02 1.981E+03 4.463E-01 1.206E-05 1.600E+00 5.000E-01 4.417E-01
$  sLambda      NOUT     EDROP     RSIZE       UCF    LCRate  LocWidth      NPTS
 1.000E+02 2.000E+00 1.000E+00 1.000E+00 1.000E+00 0.000E+00 1.000E+00 1.300E+01
$ Lambda01  Lambda02  Lambda03  Lambda04  Lambda05  Lambda06  Lambda07  Lambda08
 0.000E+00 8.000E-06 2.400E-05 4.000E-05 5.600E-05 7.200E-05 8.800E-05 3.200E-04
$ Lambda09  Lambda10  Lambda11  Lambda12  Lambda13        B3       A0Y       A1Y
 5.200E-04 5.700E-04 1.000E+00 1.000E+01 1.000E+10 1.150E+00 1.495E+03 6.250E-01
$    Eta01     Eta02     Eta03     Eta04     Eta05     Eta06     Eta07     Eta08
 0.000E+00 8.500E-01 9.700E-01 9.900E-01 1.000E+00 9.900E-01 9.700E-01 5.000E-01
$    Eta09     Eta10     Eta11     Eta012    Eta13        B2       A2F       A2Y
 1.000E-01 0.000E+00 0.000E+00 0.000E+00 0.000E+00 1.350E+00 1.766E-05 3.843E-05
$---------------------------  EOS-8 CARDS  -----------------------------------------
$ Generated EOS 8 (Tabulated Compaction)
*EOS_Tabulated_Compaction
$    EOSID     Gamma        E0      Vol0
         8 0.000E+00 0.000E+00 1.000E+00
$    VolStrain01     VolStrain02     VolStrain03     VolStrain04     VolStrain05
  0.00000000E+00 -1.50000000E-03 -4.30000000E-03 -1.01000000E-02 -3.05000000E-02
$    VolStrain06     VolStrain07     VolStrain08     VolStrain09     VolStrain10
 -5.13000000E-02 -7.26000000E-02 -9.43000000E-02 -1.74000000E-01 -2.08000000E-01
$     Pressure01      Pressure02      Pressure03      Pressure04      Pressure05
  0.00000000E+00  3.33260791E+03  7.26508525E+03  1.16641277E+04  2.21618426E+04
$     Pressure06      Pressure07      Pressure08      Pressure09      Pressure10
  3.34260574E+04  4.74230106E+04  7.25508743E+04  4.23574466E+05  6.47858979E+05
$           Multipliers of Gamma*E
  .000000000E+00  .000000000E+00  .000000000E+00
  .000000000E+00  .000000000E+00  .000000000E+00
$     BulkUnld01      BulkUnld02      BulkUnld03      BulkUnld04      BulkUnld05
  2.22173861E+06  2.22173861E+06  2.25284295E+06  2.36615162E+06  2.81494282E+06
$     BulkUnld06      BulkUnld07      BulkUnld08      BulkUnld09      BulkUnld10
```

Figure D - 8.1-5: Input Parameters Generated by Concrete Damage Model Release 3 for High-Strength Concrete

```
*MAT_PLASTIC_KINEMATIC
$#     mid        ro         e        pr      sigy      etan      beta
         2 7.3000E-4 2.9000E+7  0.300000 83000.000     0.000     0.000
$#     src       srp        fs        vp
     0.000     0.000     0.000     0.000
```

Figure D - 8.1-6: Input Parameters for Plastic-Kinematic Model for High-Strength Concrete

```
*MAT_PLASTIC_KINEMATIC
$#     mid        ro         e        pr      sigy      etan      beta
         2 7.3000E-4 2.9000E+7  0.300000 60000.000 2.9000E+6     0.000
$#     src       srp        fs        vp
     0.000     0.000     0.000     0.000
```

Figure D - 8.1-7: Input Parameters for Plastic-Kinematic Model for Normal-Strength Concrete

```
*CONSTRAINED_LAGRANGE_IN_SOLID
         2         1         1         1         0         2         0         0
$         2         1         1         1         0         4
     0.000     0.000     0.000     0.000     0.000         0         0     0.000
     0.000     0.000     0.000         0     0.000         0         0         0
         0         0         0         0     0.000         0     0.000
```

Figure D - 8.1-8: Input Parameters for Constrained Lagrange in Solid Formulation

```
*CONSTRAINED_BEAM_IN_SOLID_ID
$#  coupid
title
         1
$#   slave    master     sstyp     mstyp
ncoup       cdir
         2         1         1         1         0         0
1         0
$#   start       end              axfor
       0.0       0.2         0         0
```

Figure D - 8.1-9: Input Parameters for Constrained Beam in Solid Formulation with no user defined function.

```
*CONSTRAINED_BEAM_IN_SOLID_ID
$#   coupid
title
          1
$#    slave     master      sstyp      mstyp
ncoup        cdir
          2          1          1          1          0          0
1          1
$#    start        end               axfor
        0.0        0.2          0         -10
```

Figure D - 8.1-10: Input Parameters for Constrained Beam in Solid Formulation with user defined function.

```
*DEFINE_FUNCTION
$#      fid
heading
         10
$#
function
float force(float slip,float leng)
{
float force,pi,d,area,shear,pf,s1,s2,s3,tmax,tf;
pi = 3.1415926;
d = 0.375;
area = pi*d*leng;
pf = 1.0;
s1=0.024;
s2=0.4;
tmax=2940;
if (slip < s1) {
shear = tmax*(slip/s1)**s2;
} else {
shear = tmax;
}
force = shear*area;
return force;
}
```

Figure D - 8.1-11: Input function for CEB-FIP Function for High-Strength Concrete.

```
*DEFINE_FUNCTION
$#     fid
heading
        10
$#
function
float force(float slip,float leng)
{
float force,pi,d,area,shear,pf,s1,s2,s3,tmax,tf;
pi = 3.1415926;
d = 0.375;
area = pi*d*leng;
pf = 1.0;
s1=0.024;
s2=0.4;
tmax=1700;
if (slip < s1) {
shear = tmax*(slip/s1)**s2;
} else {
shear = tmax;
}
force = shear*area;
return force;
}
```

Figure D - 8.1-12 : Input function for CEB-FIP Function for Normal-Strength Concrete.

```
*DEFINE_FUNCTION
$#     fid
heading
         10
$#
function
float force(float slip,float leng)
{
float force,pi,d,area,shear,pf,s1,s2,s3,tmax,tf;
pi = 3.1415926;
d = 0.375;
area = pi*d*leng;
pf = 1.0;
s1=0.024;
s2=0.4;
s3=5*s1;
tmax=2940;
if (0 < slip < s1) {
shear = tmax*(slip/s1)**s2;
} else if (s1 < slip < s3) {
shear = (tmax/(s3-s1))*(-slip+s3);
}
if (slip > s3) {
shear = 0;
}
force = shear*area;
return force;
}
```

Figure D - 8.1-13 : Input function for CEB-FIP-S3 Function for High-Strength Concrete.

```
*DEFINE_FUNCTION
$#     fid
heading
         10
$#
function
float force(float slip,float leng)
{
float force,pi,d,area,shear,pf,s1,s2,s3,tmax,tf;
pi = 3.1415926;
d = 0.375;
area = pi*d*leng;
pf = 1.0;
s1=0.024;
s2=0.4;
s3=5*s1;
tmax=1700;
if (0 < slip < s1) {
shear = tmax*(slip/s1)**s2;
} else if (s1 < slip < s3) {
shear = (tmax/(s3-s1))*(-slip+s3);
}
if (slip > s3) {
shear = 0;
}
force = shear*area;
return force;
}
```

Figure D - 8.1-14: Input function for CEB-FIP-S3 Function for Normal-Strength Concrete.

```
*DEFINE_FUNCTION
$#     fid
heading
        10
$#
function
float force(float slip,float leng)
{
float force,pi,d,area,shear,pf,s,tmax,tf;
pi = 3.1415926;
d = 0.5;
area = pi*d*leng;
pf = 1.0;
s=0.26e-01;
tmax=5470;
if (0 <= slip < 0.1*s) {
shear = ((tmax*slip)/s);
} else {if (0.1*s <= slip < s) {
shear = tmax*(0.25-0.15*(((slip-s)/0.9*s)**4));
} else{
shear = 0.25*tmax;
}
}
force = shear*area;
return force;
}
```

Figure D - 8.1-15: Input function for Juan Function for High-Strength Concrete.

```
*DEFINE_FUNCTION
$#     fid
heading
        10
$#
function
float force(float slip,float leng)
{
float force,pi,d,area,shear,pf,s,tmax,tf;
pi = 3.1415926;
d = 0.5;
area = pi*d*leng;
pf = 1.0;
s=0.02625;
tmax=2398;
if (0 <= slip < 0.1*s) {
shear = ((tmax*slip)/s);
} else {if (0.1*s <= slip < s) {
shear = tmax*(0.25-0.15*(((slip-s)/0.9*s)**4));
} else{
shear = 0.25*tmax;
}
}
force = shear*area;
return force;
}
```

Figure D - 8.1-16: Input function for Juan Function for Normal-Strength Concrete.

REFERENCES

1. LSDYNAV970, *971 Keyword manual Vol. 1 and Vol. 2, .* Livermore Software Technology Corporation, Livermore, CA.
2. Shetye, G. *Finite element analysis and experimental validation of reinforced concrete single-mat slabs subjected to blast loads*. 2013, University of Missouri-Kansas City, MO.
3. Grassl, P., Johansson, M. and Leppanen J. *On the numerical modelling of bond for the failure analysis of reinforced concrete*. 2017, University of Glasgow., doi:10.20944/preprints201704.0118.v2.
4. Murcia-Delso, J. and Shing, P. *Bond-Slip Model for Detailed Finite-Element Analysis of Reinforced Concrete Structure*, J. Struct Eng., 2015, 141(4):04014125.
5. Mlakar Sr, P., et al., *The Oklahoma City bombing: Analysis of Blast Damage to the Murrah Building.* Journal of Performance of Constructed Facilities, 1998.12: p.113-119.
6. Department of Defence (D.O.D), *Unified facilities criteria (UFC), DoD Minimum Antiterrorism Standards for Buildings.* Department of Defense, UFC 4-010-01, 2007. https://www.wbdg.org/ffc/dod/unified-facilities-criteria-ufc/ufc-4-010-01.
7. National Research Council. 1995. *Protecting Buildings from Bomb Damage : Transfer of Blast-Effects Mitigation Technologies from Military to Civilian Applications.* Washington, DC: National Academies Press. https://doi.org/10.17226/5021.
8. Crawford, J. and S. Lan, *Design and Implementation of Protective Technologies for Improving Blast Resistance of Buildings*, in *Enhancing Building Security Seminar Proceedings*. 2005: Singapore.
9. Du, H. and Li, Z. *Numerical Analysis of Dynamic Behavior of RC slabs Under Blast Loading.* Transactions of Tianjin University, 2008. 15(1): p.61-64.

10. Mosalam, K.M. and A.S. Mosallam, *Nonlinear Transient Analysis of Reinforced Concrete Slabs Subjected to Blast Loading and Retrofitted with CFRP Composites.* Composites Part B: Engineering, 2001. 32(8): p. 623-636.
11. Ågårdh, L., *Finite element modeling of fibre reinforced concrete slabs subjected to blast load.* Le Journal de Physique IV, 1997. **7**(C3): p. 3-3.
12. Kuang, X., et al., *Numerical Simulation for Responses of Reinforced Concrete Slabs under Blast Loads.* Computational Structural Engineering Journal, 2009: p. 691-698.
13. El-Dakhakhni, W.W., W.F. Mekky, and S.H.C. Rezaei, *Validity of SDOF Models for Analyzing Two-Way Reinforced Concrete Panels under Blast Loading.* Journal of Performance of Constructed Facilities, 2010. 24(4): p. 311-325.
14. Schwer, L. and L. Malvar, *Simplified Concrete Modeling with MAT_CONCRETE_DAMAGE_REL3*, in *JRI LS-DYNA User Week*. 2005: LS-DYNA Anwenderforum, Bamberg.
15. Tanapornraweekit, G., et al. *Modelling of a Reinforced Concrete Panel Subjected to Blast Load by Explicit Non-linear Finite Element Code*. in *Proceedings of the Earthquake Engineering* 2007. Australia.
16. Zhou, X., et al., *Numerical prediction of concrete slab response to blast loading.* International Journal of Impact Engineering, 2008. 35(10): p. 1186-1200.
17. Broadhouse, B., *The Winfrith Concrete Model in LS-DYNA3D.* Report: SPD/D (95), Impact, Fire and Blast Department, Winfrith Technology Center, Dorset, UK, 1993: p. 339-344.
18. Gebbeken, N. and M. Ruppert, *A new material model for concrete in high-dynamic hydrocode simulations.* Archive of Applied Mechanics, 2000. 70(7): p. 463-478.

19. Low, H.Y. and H. Hao, *Reliability analysis of reinforced concrete slabs under explosive loading.* Journal of Structural Safety, 2001. 23(2): p. 157-178.
20. Hallquist, J.O., Stillman, D.W. and Lin, T.L. *LS-DYNA3D users manual.* LSTC Report, Livermore, CA, 1994. Vol. 1007.
21. Vasudevan, A., *Finite element analysis and experimental comparison of doubly reinforced concrete slabs subjected to blast loads*. 2012, University of Missouri-Kansas City.
22. Hallquist, J.O., *LS-DYNA theory manual.* Livermore Software Technology Corporation, 2006. 3.
23. Kong, S., Remennikov, A. and B. Uy, *Numerical simulation of the response of non-composite steel-concrete-steel sandwich panels to impact loading.* Australian Journal of Structural Engineering. 12(3): p. 211-224.
24. Hibbitt, Karlsson, and Sorensen, *ABAQUS theory manual*. 1998: Hibbitt, Karlsson & Sorensen.
25. Kosloff, D. and Frazier, G.A. *Treatment of Hourglass Patterns in Low Order Finite Element Codes. International journal for numerical and analytical methods in geomechanics*, 2005. Vol. 2(1): p. 57-72.
26. Wilkins, M.L., *Use of artificial viscosity in multidimensional fluid dynamic calculations. Journal of Computational Physics*, 1980. 36(3): p. 281-303.
27. Magallanes, J.M., et al. *Recent Improvements to Release III of the K&C Concrete Model. in 11th International LS-DYNA Users Conference*. 2010.
28. Malvar, L.J., et al., *A Plasticity Concrete Material Model for DYNA3D*. International Journal of Impact Engineering, 1997. 19(9-10): p. 847-873.

29. Hallquist, J.O., *LS-DYNA theory manual. Livermore Software Technology Corporation, Livermore*, CA, 2006. Vol. 3.

VITA

Akash Ashok Iwalekar was born in Mumbai, in the state of Maharashtra, India on December 23rd, 1992. He joined University of Mumbai's G.V. Acharya Institute of Technology to pursue his Civil Engineering Studies. He was awarded a Bachelor of Engineering degree from the University of Mumbai in December 2014.

Akash joined the University of Missouri – Kansas City (UMKC) in the fall term of 2016 to pursue his Master's degree in Civil Engineering. He started working as a Graduate Research and Teaching Assistant in Civil and Mechanical Engineering Department in the Spring of 2017. He pursued his research interests in the field of finite-element analysis of reinforced concrete slabs subjected to blast loading in the Computational Mechanics Laboratory (UMKC) with Dr. Ganesh Thiagarajan. He is currently pursuing practical training as a Civil Engineer with Omega Concrete Systems Inc, in Kansas City, Kansas.

Upon completion of his degree requirements, Akash plans to continue his career in the field of Structural Engineering and to pursue research interests.